## Appendix F

## Isotherms Modeling: Case 4

In Appendix F, modeling efforts for case 4 are presented. Results from this case are summarized in Tables XVI through XXV in the main body of this report. The information for each data set is sequentially organized as follows:

1. A table with estimated constants and statistical parameters for each isotherm.
2. Curves of adsorbed concentration S [μmol(p+)/g] versus concentration in solution [μmol(p+)/mL] in a logarithmic scale. Both raw data and predictions by isotherms are included.
3. A graph with the calculated S-values versus observed S-values for all tested isotherms.

Tables and figures for the same data set are identified by the conditions defined in the table heading, which are also included in each figure in the same order but without units.

Units for constants are as follows: $K_d$ in mL/g; b in μmol(p+)/g and k in mL/μmol(p+); K, N, A, β, and $K_d$ have units corresponding to S in μmol(p+)/g and C in μmol(p+)/mL.

The following table of contents serves as a guide to locate the formation, e.g., Bullfrog, the particle sizes, e.g., all sizes, and the samples that belong to the same formation (or stratigraphic unit), e.g., YM-22, g1-1292, YM-30. This information identifies the set used for isotherm modeling.



92ϕ1ϕ9ϕ15ϕ - Part 2

Table of Contents - Appendix F

Printouts for Ce Isotherms (Topopah Spring, Tpt) . . . . . 273
Printouts for Eu Isotherms (Topopah Spring, Tpt) . . . . . 276
Printouts for Ba Isotherms (Topopah Spring, Tpt) . . . . . 279
Printouts for Cs Isotherms (Topopah Spring, Tpt) . . . . . 282
Printouts for Sr Isotherms (Topopah Spring, Tpt) . . . . . 285
Printouts for Ce Isotherms (Calico Hills, Tht) . . . . . 288
Printouts for Eu Isotherms (Calico Hills, Tht) . . . . . 291
Printouts for Ba Isotherms (Calico Hills, Tht) . . . . . 294
Printouts for Cs Isotherms (Calico Hills, Tht) . . . . . 297
Printouts for Sr Isotherms (Calico Hills, Tht) . . . . . 300
Printouts for Ce Isotherms (Prow Pass, Tcp). . . . . 303
Printouts for Eu Isotherms (Prow Pass, Tcp). . . . . 306
Printouts for Ba Isotherms (Prow Pass, Tcp). . . . . 309
Printouts for Cs Isotherms (Prow Pass, Tcp). . . . . 312
Printouts for Sr Isotherms (Prow Pass, Tcp). . . . . 315
Printouts for Eu Isotherms (Bullfrog Formation, Tcb) . . . . . 318
Printouts for Ba Isotherms (Bullfrog Formation, Tcb) . . . . . 321
Printouts for Cs Isotherms (Bullfrog Formation, Tcb) . . . . . 324
Printouts for Sr Isotherms (Bullfrog Formation, Tcb) . . . . . 327
Printouts for Ce Isotherms (Bullfrog Formation, Tcb) . . . . . 330
Printouts for Ce Isotherms (Tram, Tct) . . . . . 333
Printouts for Eu Isotherms (Tram, Tct) . . . . . 336
Printouts for Ba Isotherms (Tram, Tct) . . . . . 339
Printouts for Cs Isotherms (Tram, Tct) . . . . . 342
Printouts for Sr Isotherms (Tram, Tct) . . . . . 345

ELEMENT = Ce
FORMATION = Tpt
TIME = 21 days
ATMOS = Air
SIZE = All Sizes
SAMPLES = ym-22, gl-1292
ym-30, ja-18

| ISOTHERM | N | ALPHA | BETA | R**2 | SSE |
|---|---|---|---|---|---|
| LINEAR | 8 | 0.0000000 | 33.6963615 | 0.4522 | 0.02405391 |
| Kd = | 33.69636154 | | | | |
| LANGMUIR | 8 | 0.0046087 | 23.9077950 | 0.7676 | 0.00724519 |
| b = | 0.04182736 | | | | |
| k = | 5187.56201172 | | | | |
| FREUNDLICH | 8 | 0.9498262 | 0.7072785 | 0.9381 | 0.70275009 |
| K = | 8.90894413 | | | | |
| N = | 0.70727849 | | | | |

N = the number of experimental points
ALPHA and BETA are respectively the intercept and slope from the linear regression analysis
R = correlation coefficient
SSE = standard error
Kd in mL/g
b in micro mol(p+)/g and k in mL/micro mol(p+)
K and N in units corresponding to solute adsorbed S in micro mol(p+)/g and solute in solution C in micro mol(p+).

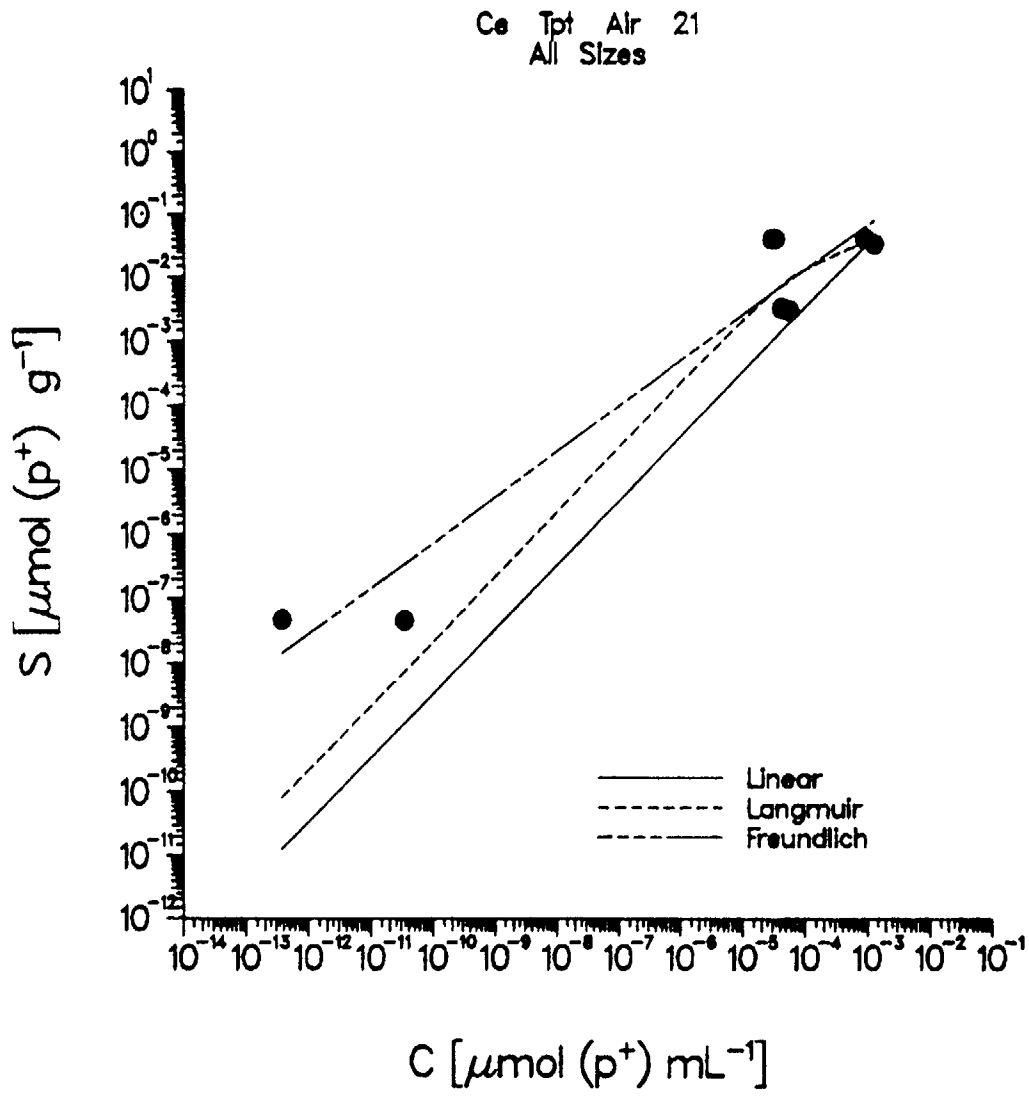
Ce Tpt Air 21
All Sizes
S [μmol (p+) g−1]
C [μmol (p+) mL−1]
Linear
Langmuir
Freundlich

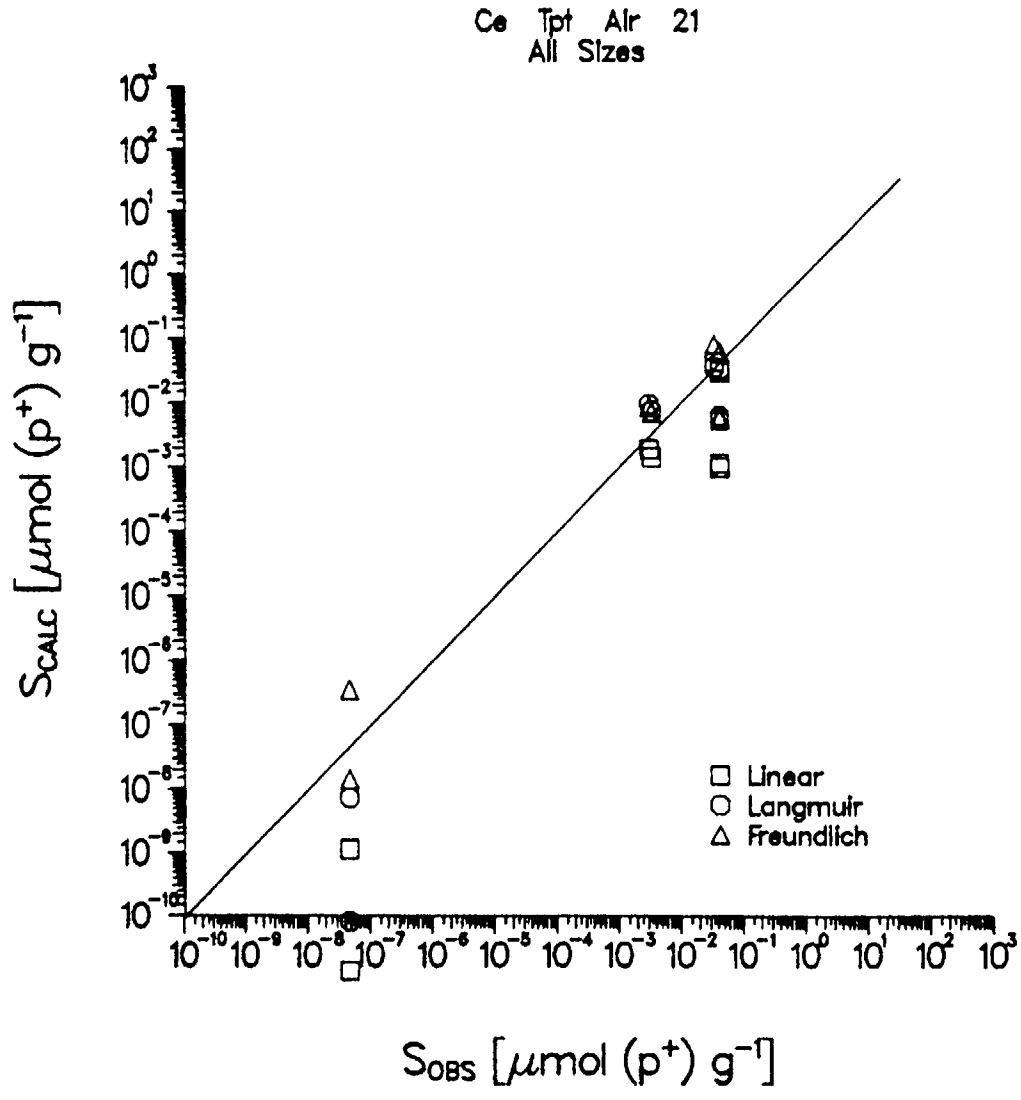
Ce Tpt Alr 21
All Sizes
$S_{CALC}$ [$\mu$mol ($p^+$) $g^{-1}$]
$S_{OBS}$ [$\mu$mol ($p^+$) $g^{-1}$]
Linear
Langmuir
Freundlich

ELEMENT = Eu
FORMATION = Tpt
TIME = 21 days
ATMOS = Air
SIZE = All Sizes
SAMPLES = ym-22, gl-1292
ym-30, ja-18

| ISOTHERM | N | ALPHA | BETA | R**2 | SSE |
|---|---|---|---|---|---|
| LINEAR | 18 | 0.0000000 | 233.8971863 | 0.1508 | 0.18331529 |
| Kd = | 233.89718628 | | | | |
| LANGMUIR | 18 | -0.0007740 | 45.8314972 | 0.7796 | 0.00703496 |
| b = | 0.02181906 | | | | |
| k = | -59216.08203125 | | | | |
| FREUNDLICH | 18 | 1.3947518 | 0.7126554 | 0.8611 | 0.60531002 |
| K = | 24.81714249 | | | | |
| N = | 0.71265537 | | | | |

N = the number of experimental points
ALPHA and BETA are respectively the intercept and slope from the linear regression analysis
R = correlation coefficient
SSE = standard error
Kd in mL/g
b in micromol(p+)/g and k in mL/micromol(p+)
K and N in units corresponding to solute adsorbed S in micromol(p+)/g and solute in solution C in micro mol(p+).

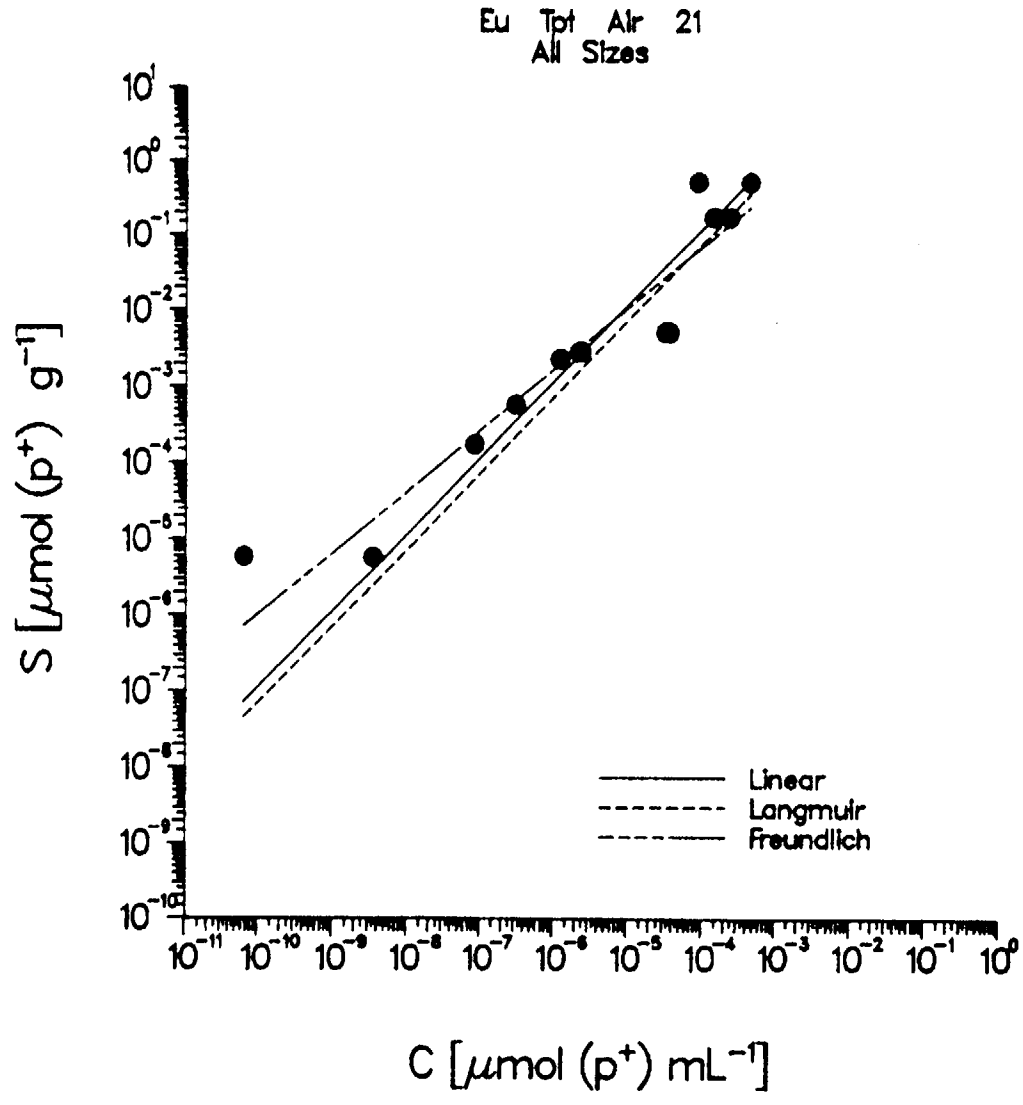
Eu Tpt Air 21
All Sizes
S [μmol (p+) g-1]
C [μmol (p+) mL-1]
Linear
Langmuir
Freundlich

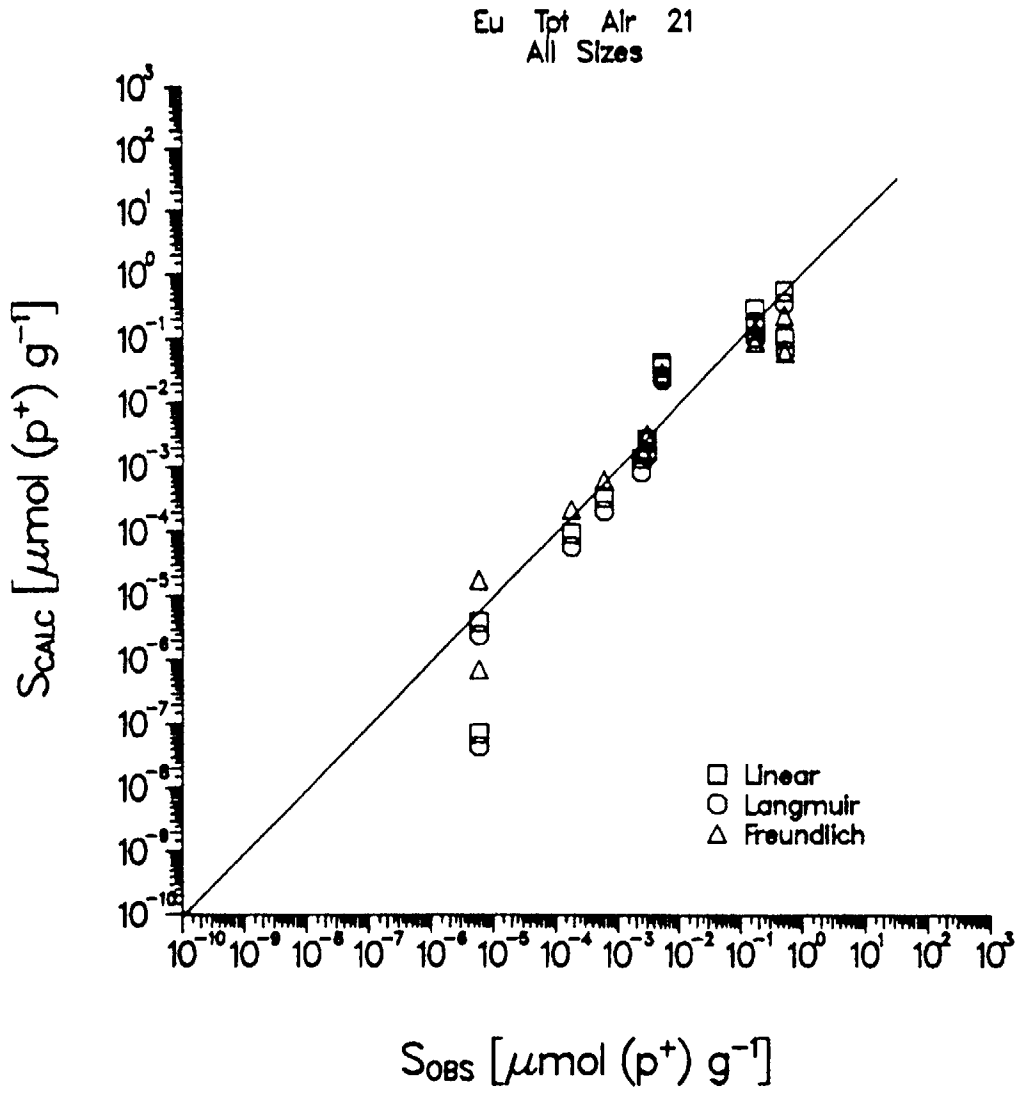
Eu Tpt Air 21
All Sizes
Linear
Langmuir
Freundlich
$S_{CALC}$ [$\mu$mol ($p^+$) $g^{-1}$]
$S_{OBS}$ [$\mu$mol ($p^+$) $g^{-1}$]

ELEMENT = Ba
FORMATION = Tpt
TIME = 21 days
ATMOS = Air
SIZE = All Sizes
SAMPLES = ym-22, gl-1292
ym-30, ja-18

| ISOTHERM | N | ALPHA | BETA | R**2 | SSE |
|---|---|---|---|---|---|
| LINEAR | 19 | 0.0000000 | 254.5225220 | 0.9030 | 0.40188855 |
| Kd = | 254.52252197 | | | | |
| LANGMUIR | 19 | 0.0008475 | 0.2159167 | 0.7601 | 0.00055132 |
| b = | 4.63141537 | | | | |
| k = | 254.76374817 | | | | |
| FREUNDLICH | 19 | 1.8705896 | 0.7339733 | 0.9475 | 0.31761172 |
| K = | 74.23173523 | | | | |
| N = | 0.73397326 | | | | |

N = the number of experimental points
ALPHA and BETA are respectively the intercept and slope from the linear regression analysis
R = correlation coefficient
SSE = standard error
Kd in mL/g
b in micro mol(p+)/g and k in mL/micro mol(p+)
K and N in units corresponding to solute adsorbed S in micro mol(p+)/g and solute in solution C in micro mol(p+).

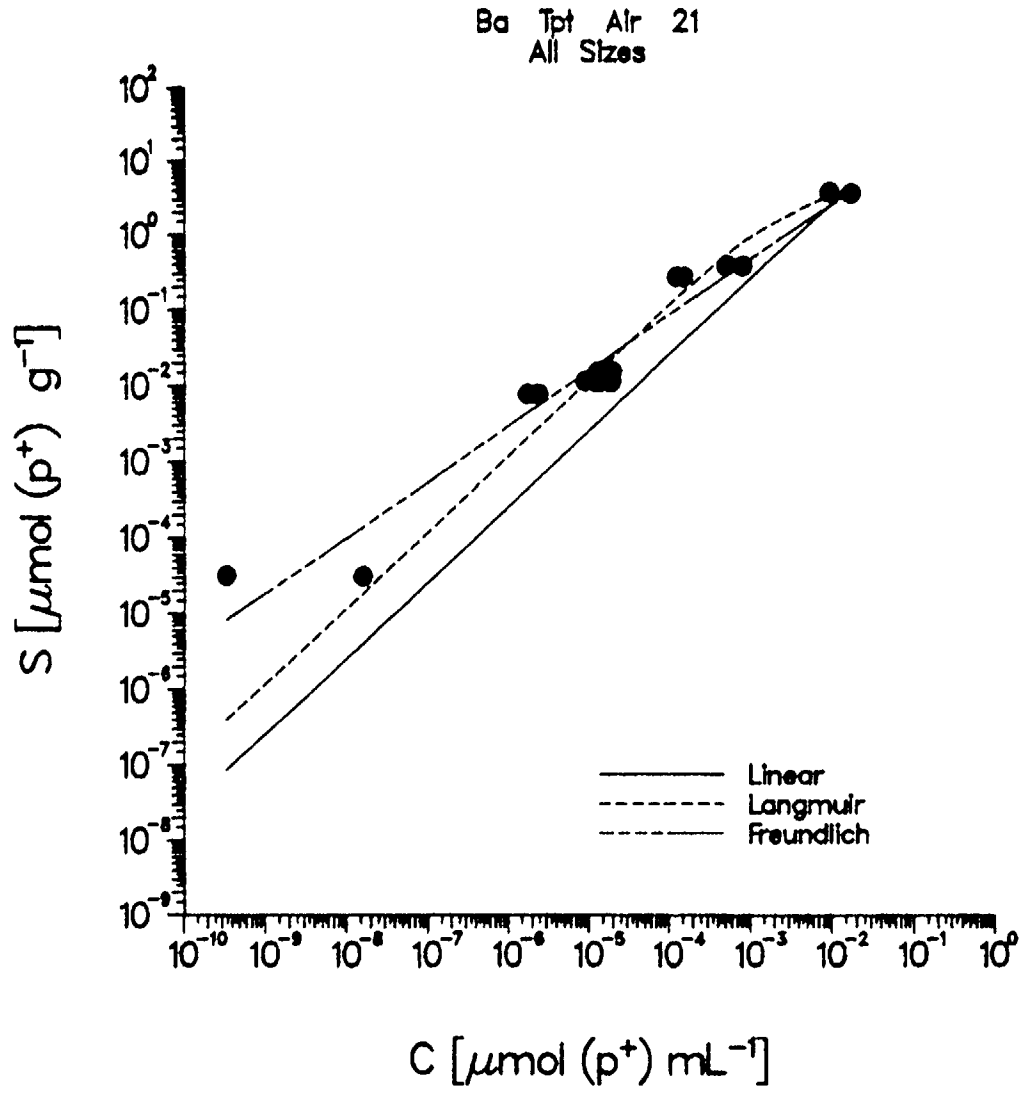
Ba Tpt Air 21
All Sizes
S [μmol (p+) g−1]
C [μmol (p+) mL−1]
Linear
Langmuir
Freundlich

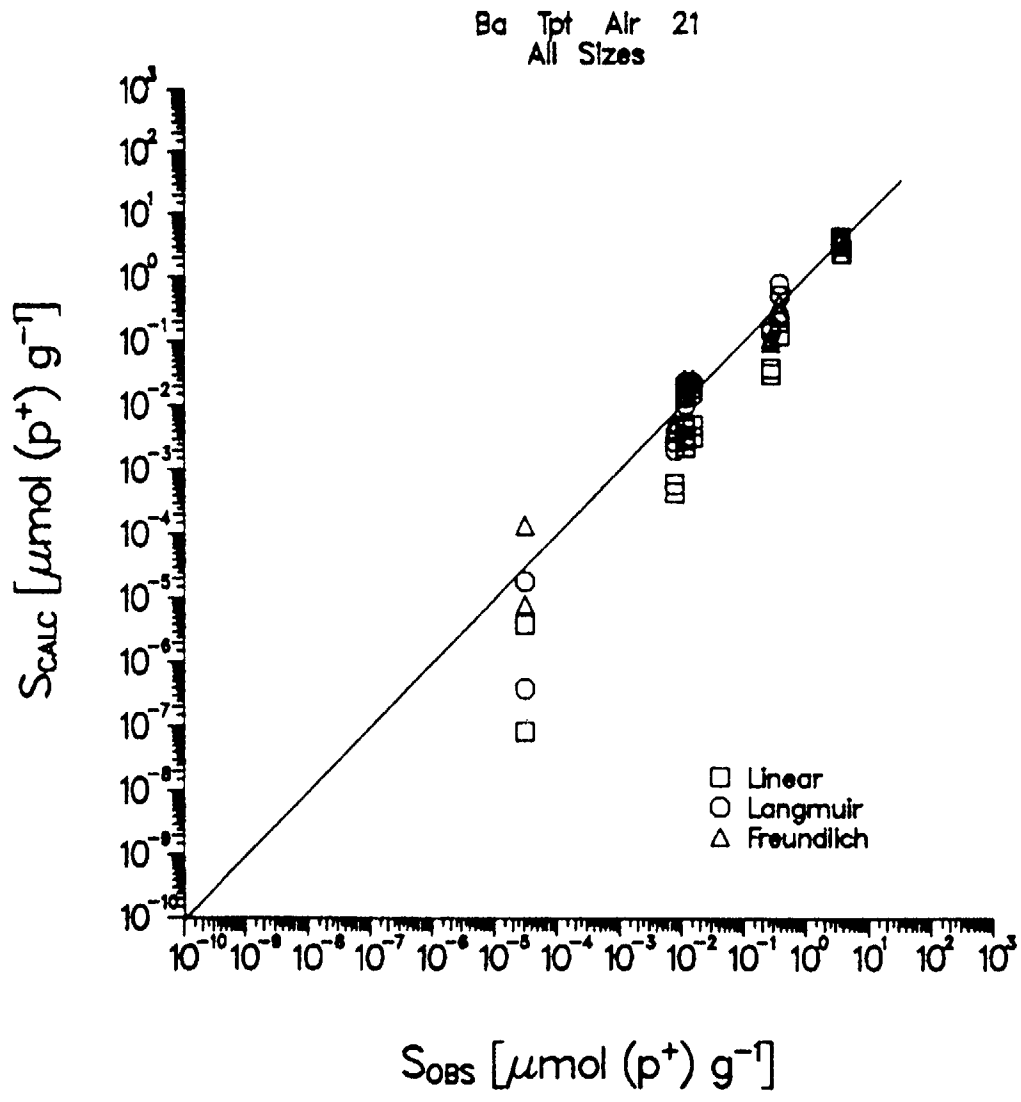
Ba Tpt Air 21
All Sizes
Linear
Langmuir
Freundlich
$S_{CALC}$ [$\mu$mol ($p^+$) $g^{-1}$]
$S_{OBS}$ [$\mu$mol ($p^+$) $g^{-1}$]

ELEMENT = Cs
FORMATION = Tpt
TIME = 21 days
ATMOS = Air
SIZE = All Sizes
SAMPLE = ym-22, gl-1292
ym-30, ja-18

| ISOTHERM | N | ALPHA | BETA | R**2 | SSE |
|---|---|---|---|---|---|
| LINEAR | 18 | 0.0000000 | 10.9385805 | 0.9913 | 0.46852207 |
| Kd = | 10.93858051 | | | | |
| LANGMUIR | 18 | 0.0026129 | 0.0691775 | 0.9893 | 0.00310015 |
| b = | 14.45556831 | | | | |
| k = | 26.47565269 | | | | |
| FREUNDLICH | 18 | 1.1583328 | 0.7405880 | 0.9468 | 0.49543154 |
| K = | 14.39901638 | | | | |
| N = | 0.74058801 | | | | |

N = the number of experimental points
ALPHA and BETA are respectively the intercept and slope from the linear regression analysis
R = correlation coefficient
SSE = standard error
Kd in mL/g
b in micro mol(p+)/g and k in mL/micro mol(p+)
K and N in units corresponding to solute adsorbed S in micro mol(p+)/g and solute in solution C in micro mol(p+).

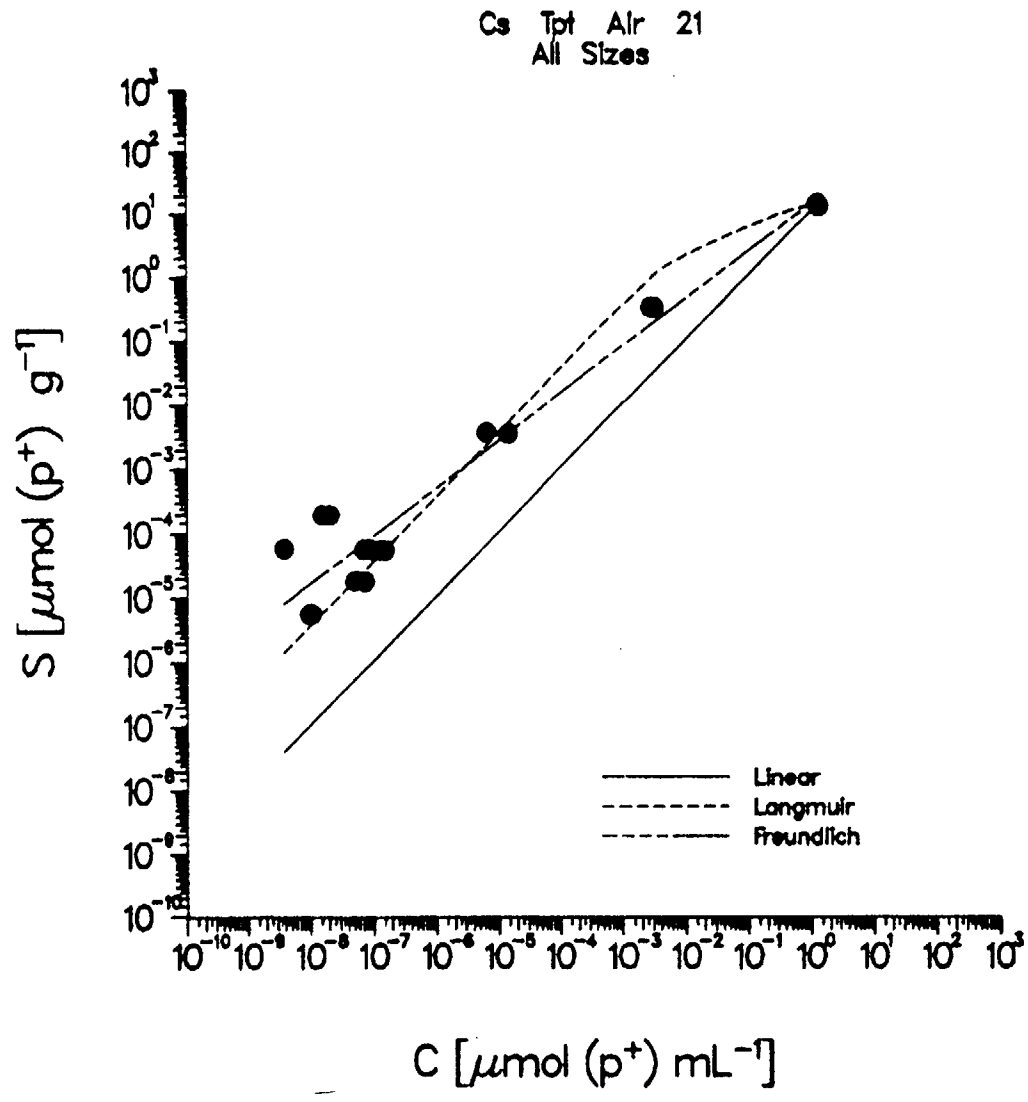
Cs Tpt Air 21
All Sizes
S [μmol (p+) g−1]
C [μmol (p+) mL−1]
Linear
Langmuir
Freundlich

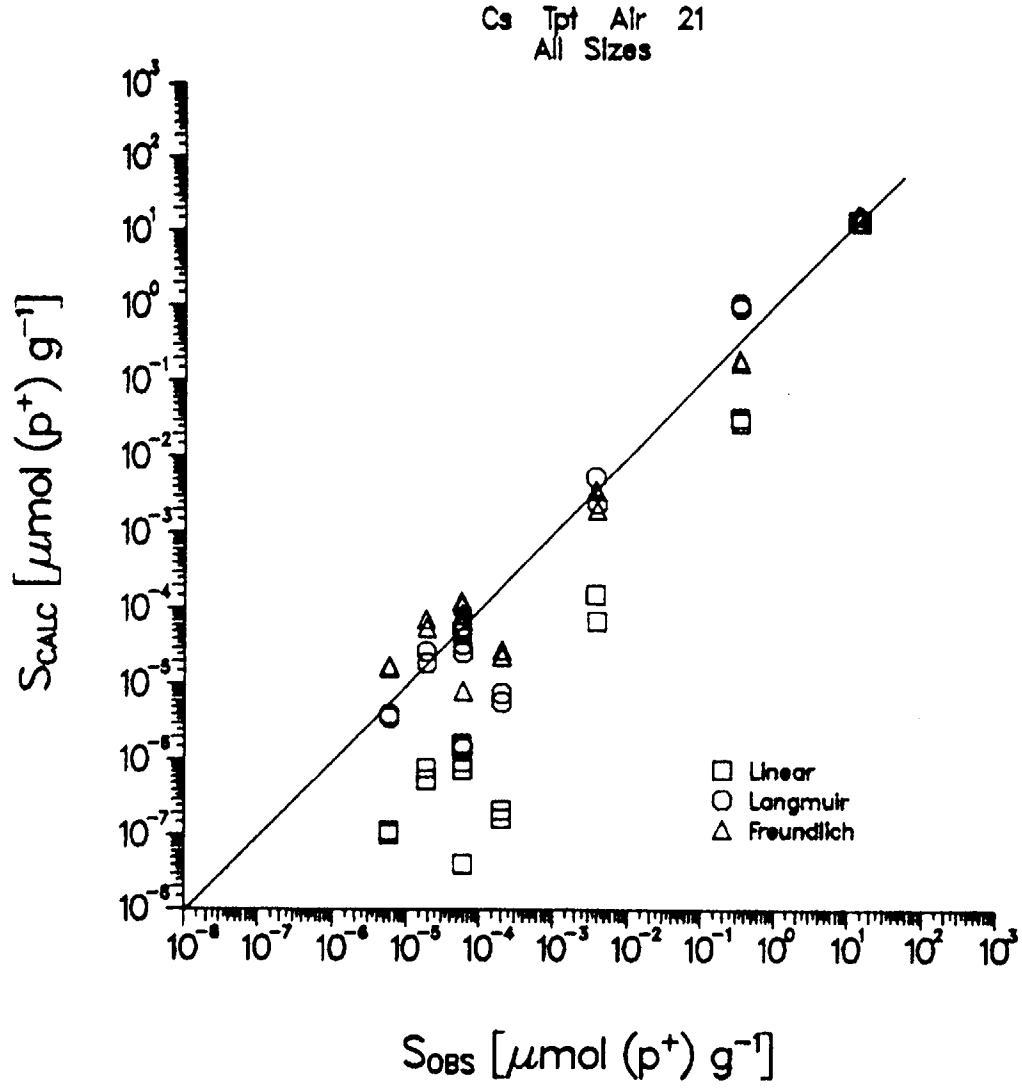
Cs Tpt Air 21
All Sizes
$S_{CALC}$ [$\mu$mol ($p^+$) $g^{-1}$]
$S_{OBS}$ [$\mu$mol ($p^+$) $g^{-1}$]
Linear
Langmuir
Freundlich

ELEMENT = Sr
FORMATION = Tpt
TIME = 21 days
ATMOS = Air
SIZE = All Sizes
SAMPLES = ym-22, gl-1292
ym-30, ja-18

| ISOTHERM | N | ALPHA | BETA | R**2 | SSE |
|---|---|---|---|---|---|
| LINEAR | 18 | 0.0000000 | 13.1282959 | 0.8708 | 6.40218067 |
| Kd = | 13.12829590 | | | | |
| LANGMUIR | 18 | 0.0109052 | 0.0197506 | 0.8638 | 0.00937067 |
| b = | 50.63136292 | | | | |
| k = | 1.81111062 | | | | |
| FREUNDLICH | 18 | 1.1013312 | 0.7166281 | 0.8939 | 0.62069708 |
| K = | 12.62790298 | | | | |
| N = | 0.71662807 | | | | |

N = the number of experimental points
ALPHA and BETA are respectively the intercept and slope from the linear regression analysis
R = correlation coefficient
SSE = standard error
Kd in mL/g
b in micro mol(p+)/g and k in mL/micro mol(p+)
K and N in units corresponding to solute adsorbed S in micro mol(p+)/g and solute in solution C in micro mol(p+).

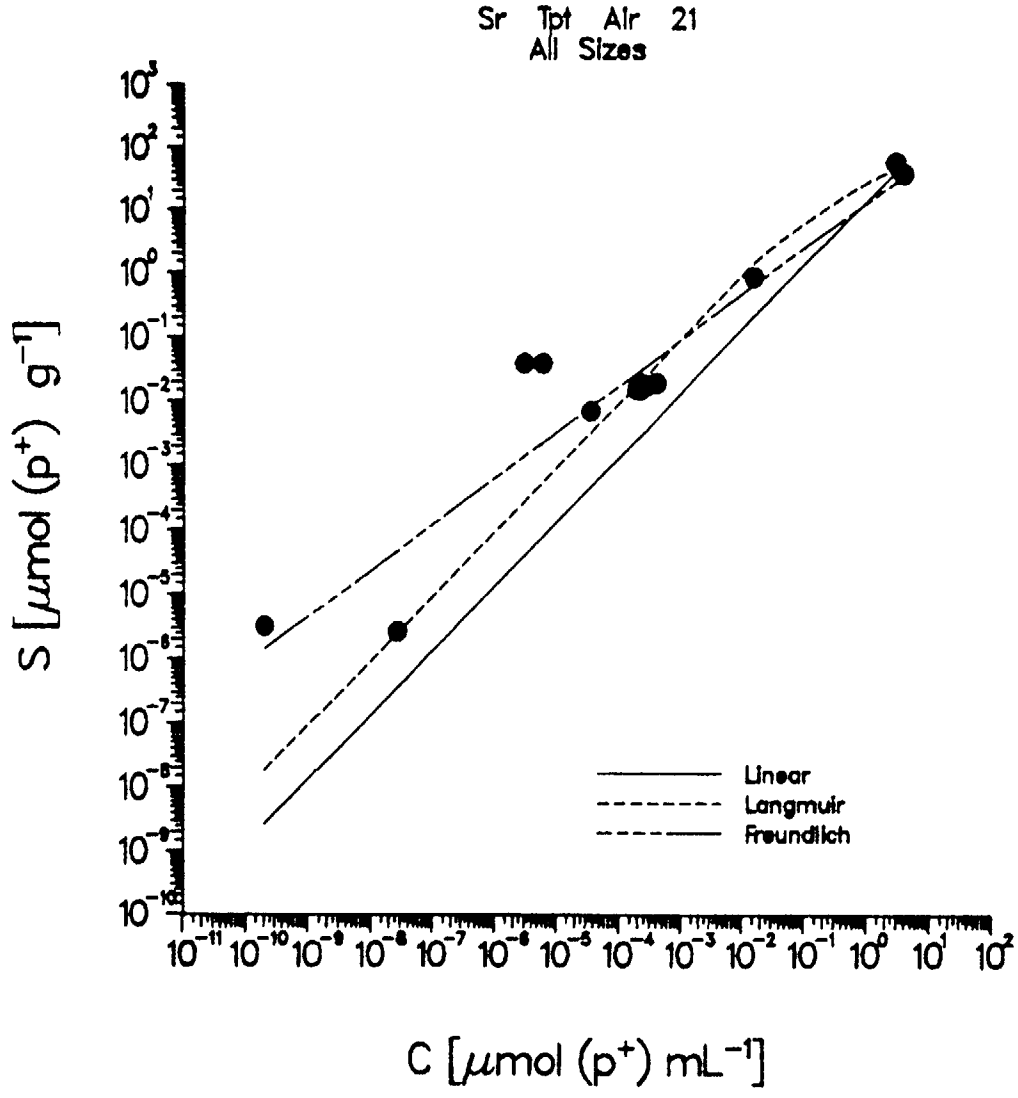
Sr Tpt Air 21
All Sizes
S [μmol (p+) g−1]
C [μmol (p+) mL−1]
Linear
Langmuir
Freundlich

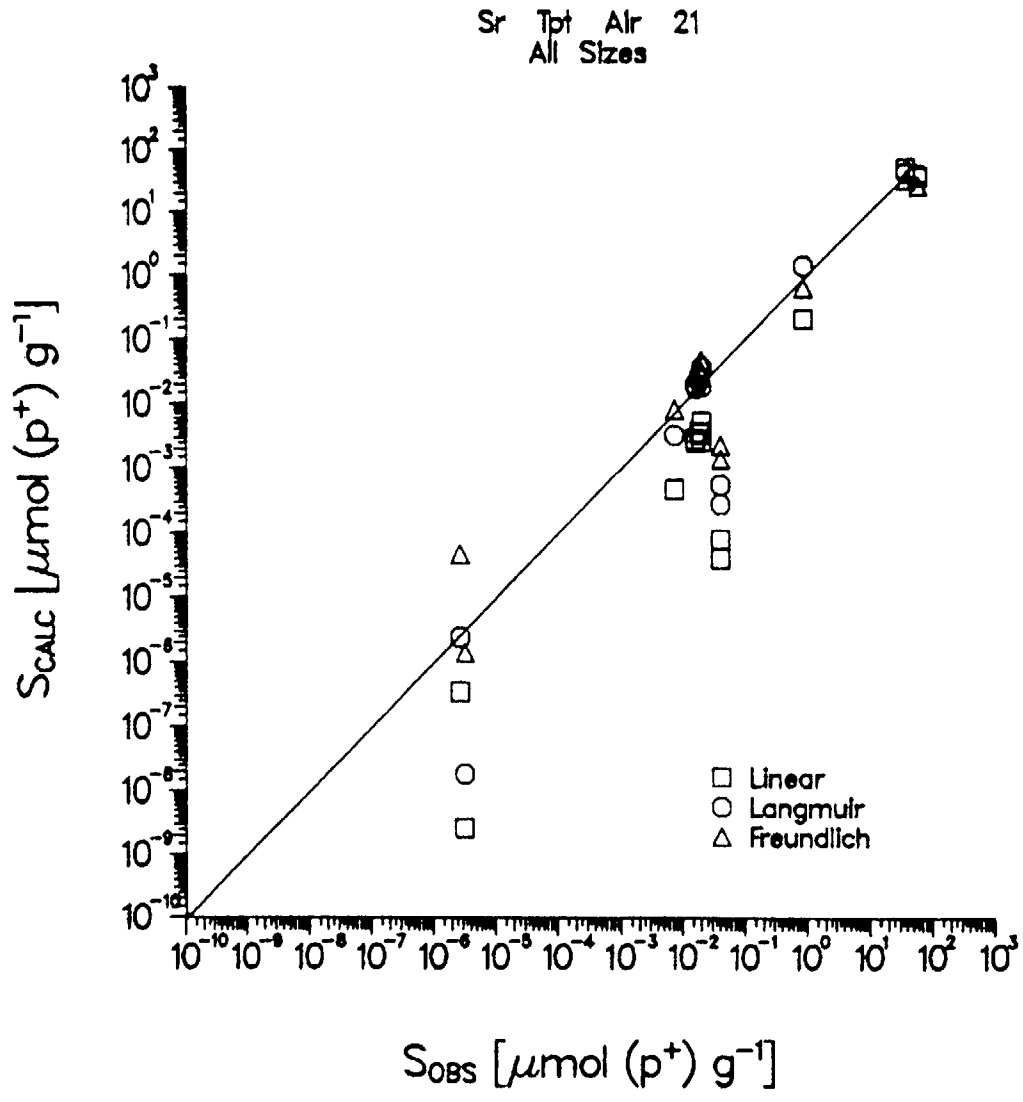
Sr Tpt Air 21
All Sizes
$S_{CALC}$ [$\mu$mol ($p^+$) $g^{-1}$]
$S_{OBS}$ [$\mu$mol ($p^+$) $g^{-1}$]
Linear
Langmuir
Freundlich

ELEMENT = Ce
FORMATION = Tht
TIME = 21 days
ATMOS = Air
SIZE = All Sizes
SAMPLES = gl-1436, ym-38
ym-42

| ISOTHERM | N | ALPHA | BETA | R**2 | SSE |
|---|---|---|---|---|---|
| LINEAR | 4 | 0.0000000 | 900.5843506 | 0.9801 | 0.00591009 |
| Kd = | 900.58435059 | | | | |
| LANGMUIR | 4 | 0.0000195 | 16.7364998 | 0.9999 | 0.00000785 |
| b = | 0.05974965 | | | | |
| k = | 858331.87500000 | | | | |
| FREUNDLICH | 4 | 3.0210185 | 0.8345175 | 0.9345 | 0.86280000 |
| K = | 1049.58715820 | | | | |
| N = | 0.83451748 | | | | |

N = the number of experimental points
ALPHA and BETA are respectively the intercept and slope from the linear regression analysis
R = correlation coefficient
SSE = standard error
Kd in mL/g
b in micromol(p+)/g and k in mL/micromol(p+)
K and N in units corresponding to solute adsorbed S in micromol(p+)/g and solute in solution C in micromol(p+)/mL.

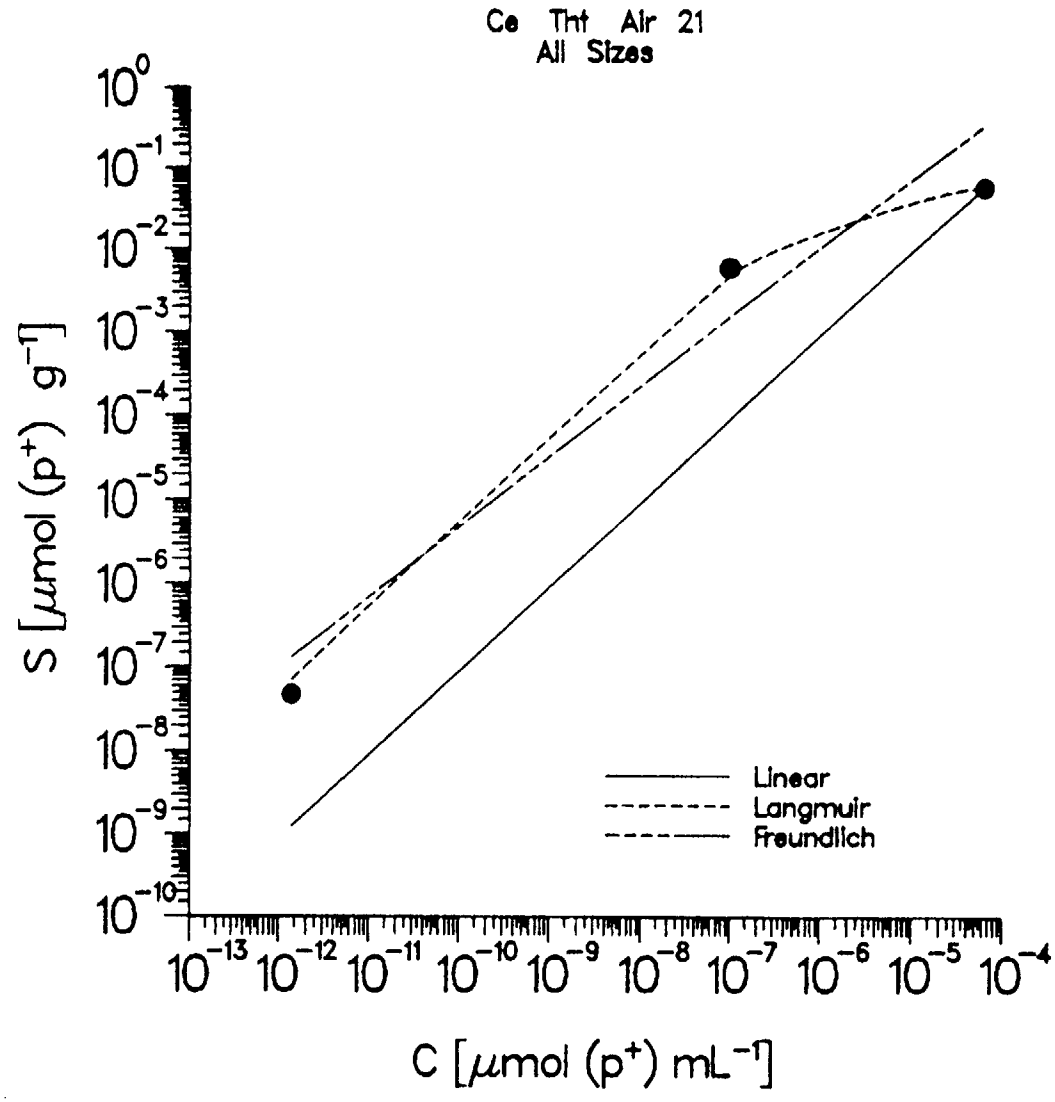
Ce Tht Air 21
All Sizes
S [μmol (p+) g-1]
C [μmol (p+) mL-1]
Linear
Langmuir
Freundlich

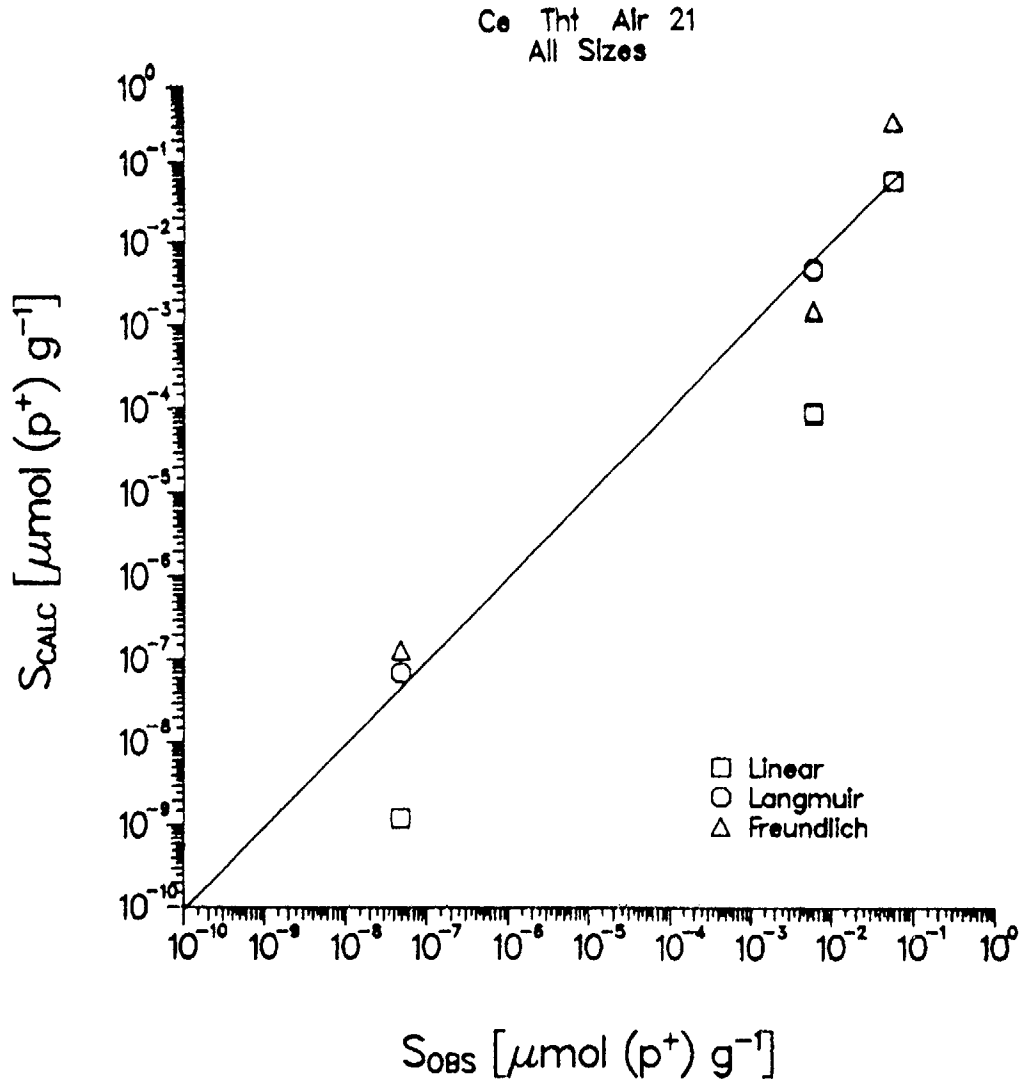
Ce Tht Air 21
All Sizes
$S_{CALC}$ [$\mu$mol ($p^+$) $g^{-1}$]
$S_{OBS}$ [$\mu$mol ($p^+$) $g^{-1}$]
$10^{0}$
$10^{-1}$
$10^{-2}$
$10^{-3}$
$10^{-4}$
$10^{-5}$
$10^{-6}$
$10^{-7}$
$10^{-8}$
$10^{-9}$
$10^{-10}$
Linear
Langmuir
Freundlich

ELEMENT = Eu
FORMATION = Tht
TIME = 21 days
ATMOS = Air
SIZE = All Sizes
SAMPLES = gl-1436, ym-38
ym-42

| ISOTHERM | N | ALPHA | BETA | R**2 | SSE |
|---|---|---|---|---|---|
| LINEAR | 20 | 0.0000000 | 2776.2397461 | 0.7362 | 0.07115218 |
| Kd = | 2776.23974609 | | | | |
| LANGMUIR | 20 | 0.0003724 | 0.3770617 | 0.0033 | 0.00025151 |
| b = | 2.65208578 | | | | |
| k = | 1012.54956055 | | | | |
| FREUNDLICH | 20 | 2.3398213 | 0.7888322 | 0.8888 | 0.38150930 |
| K = | 218.68617249 | | | | |
| N = | 0.78883219 | | | | |

N = the number of experimental points
ALPHA and BETA are respectively the intercept and slope from the linear regression analysis
R = correlation coefficient
SSE = standard error
Kd in mL/g
b in micromol(p+)/g and k in mL/micromol(p+)
K and N in units corresponding to solute adsorbed S in micromol(p+)/g and solute in solution C in micromol(p+)/mL.

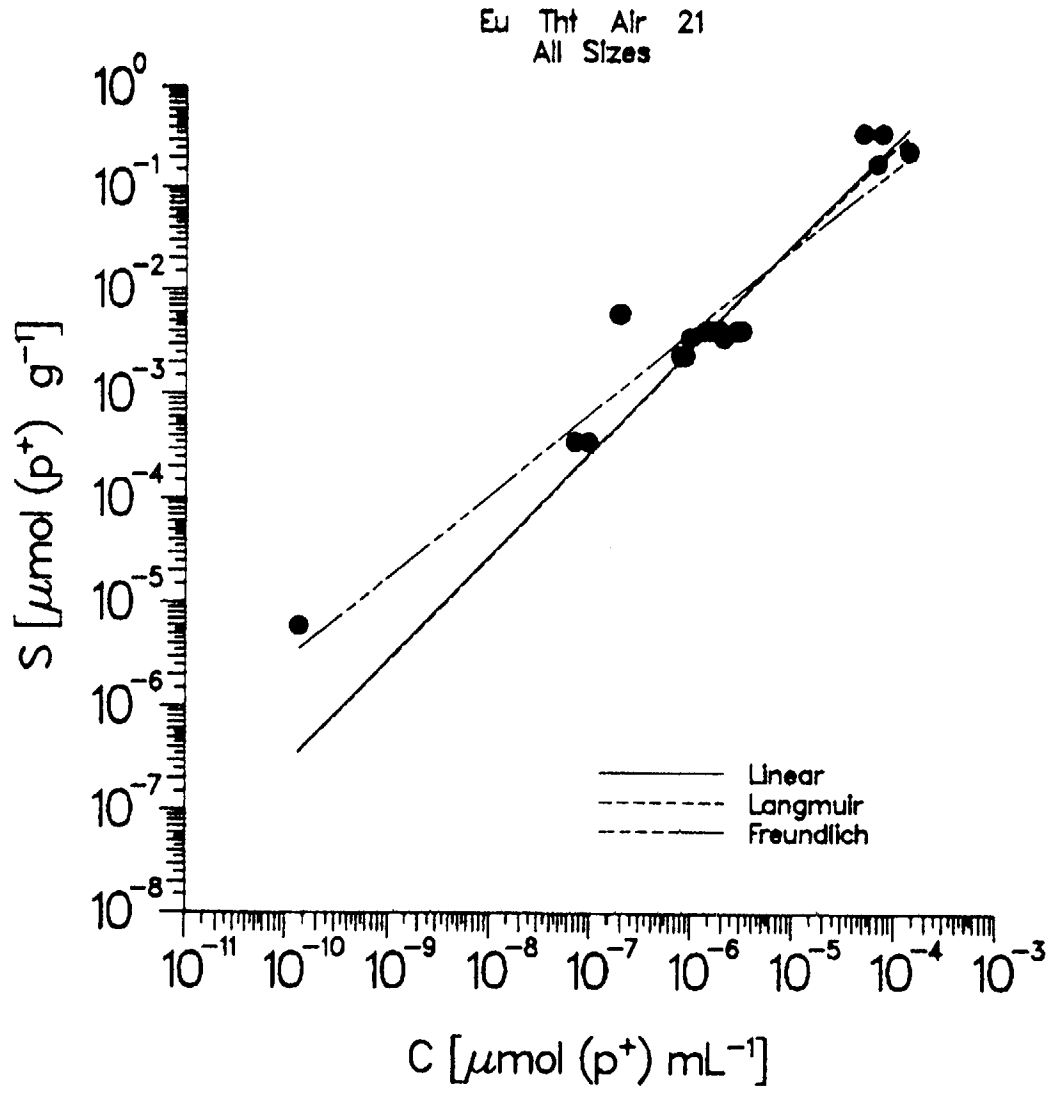
Eu Tht Air 21
All Sizes
S [μmol (p+) g−1]
C [μmol (p+) mL−1]
Linear
Langmuir
Freundlich

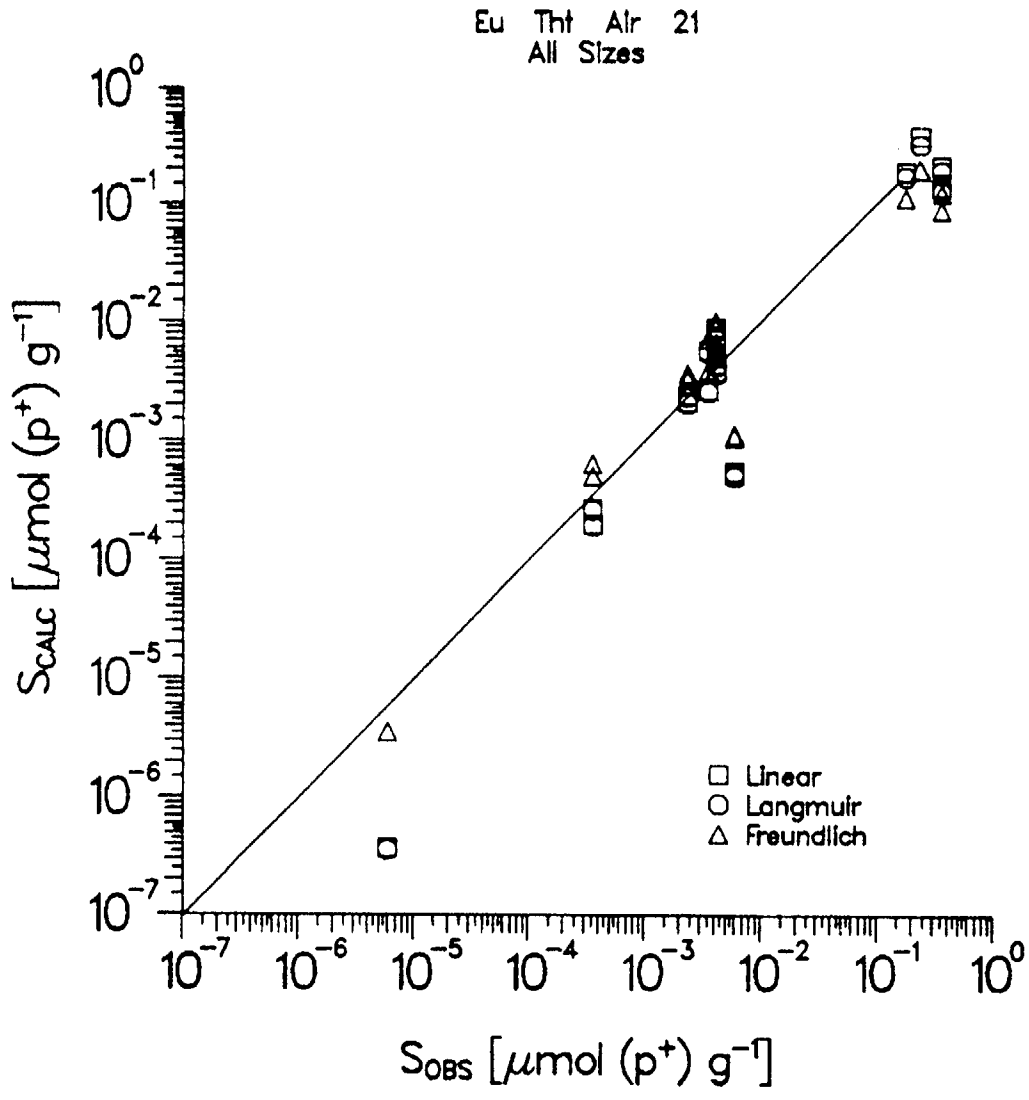
Eu Tht Air 21
All Sizes
$S_{CALC}$ [$\mu$mol ($p^+$) $g^{-1}$]
$S_{OBS}$ [$\mu$mol ($p^+$) $g^{-1}$]
$10^0$
$10^{-1}$
$10^{-2}$
$10^{-3}$
$10^{-4}$
$10^{-5}$
$10^{-6}$
$10^{-7}$
Linear
Langmuir
Freundlich

ELEMENT = Ba
FORMATION = Tht
TIME = 21 days
ATMOS = Air
SIZE = All Sizes
SAMPLES = gl-1436, ym-38
ym-42

| ISOTHERM | n | ALPHA | BETA | R**2 | SSE |
|---|---|---|---|---|---|
| LINEAR | 21 | 0.0000000 | 87120.4453125 | 0.9851 | 0.15961440 |
| Kd = 87120.44531250 | | | | | |
| LANGMUIR | 21 | 0.0000143 | -0.0629072 | 0.0141 | 0.00000728 |
| b = -15.89642715 | | | | | |
| k = -4409.03173828 | | | | | |
| FREUNDLICH | 21 | 4.9258451 | 1.0038248 | 0.9654 | 0.20485014 |
| K = 84303.41406250 | | | | | |
| N = 1.00382483 | | | | | |

n = the number of experimental points
ALPHA and BETA are respectively the intercept and slope from the linear regression analysis
R = correlation coefficient
SSE = standard error
Kd in mL/g
b in micromol(p+)/g and k in mL/micromol(p+)
K and N in units corresponding to solute adsorbed S in micromol(p+)/g and solute in solution C in micromol(p+)/mL.

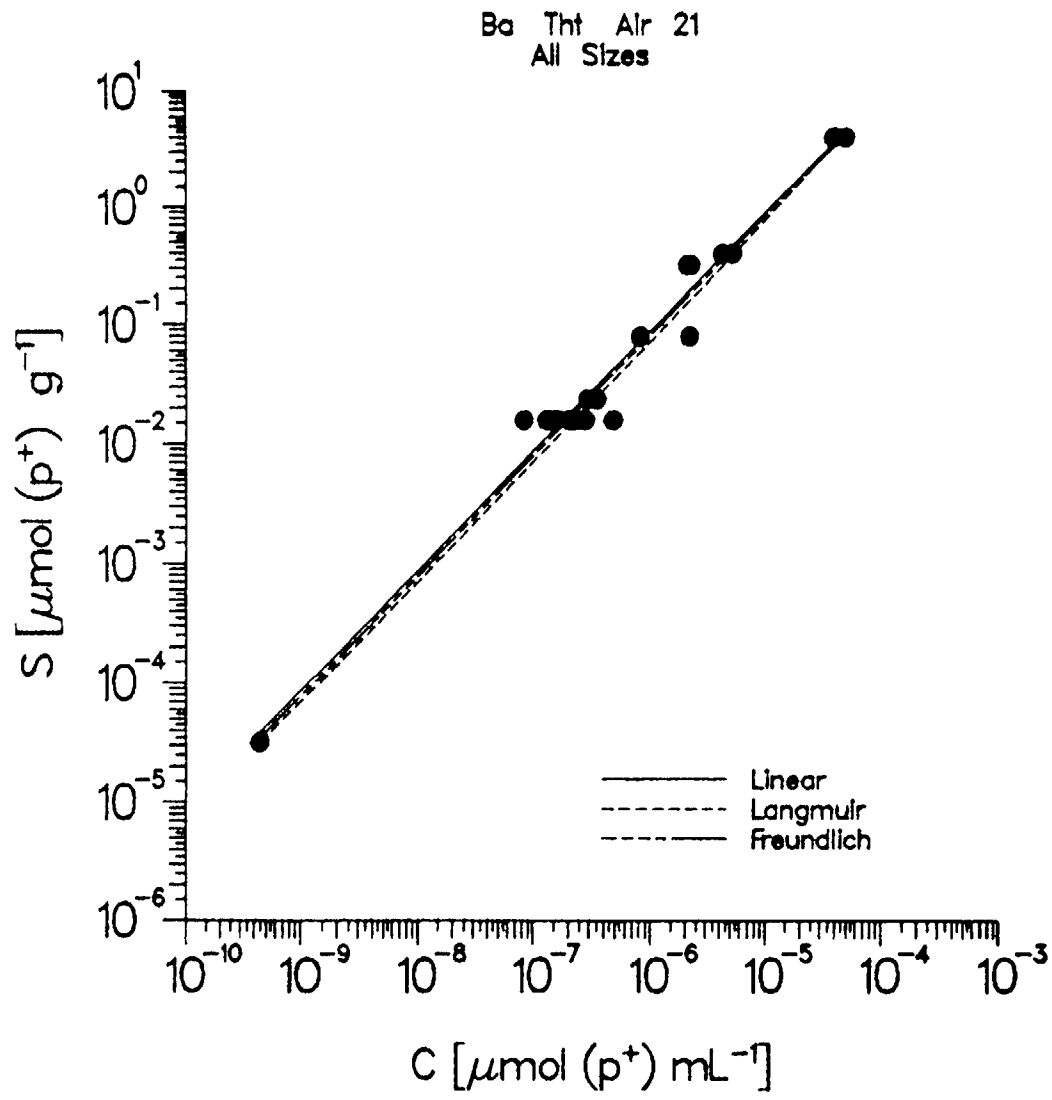
Ba Tht Air 21
All Sizes
S [μmol (p+) g−1]
C [μmol (p+) mL−1]
Linear
Langmuir
Freundlich

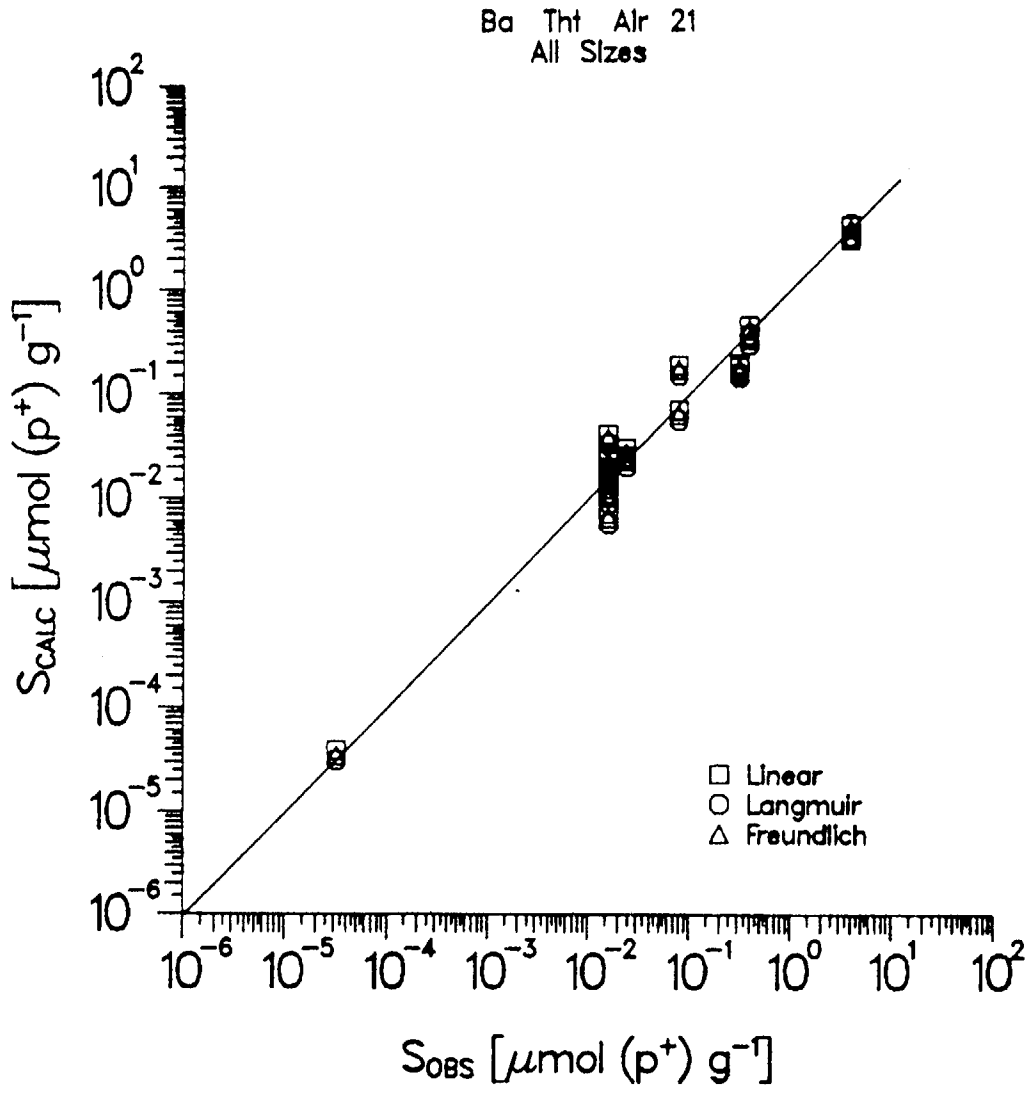
Ba Tht Alr 21
All Sizes
$S_{CALC}$ [$\mu$mol ($p^+$) $g^{-1}$]
$S_{OBS}$ [$\mu$mol ($p^+$) $g^{-1}$]
$10^{2}$
$10^{1}$
$10^{0}$
$10^{-1}$
$10^{-2}$
$10^{-3}$
$10^{-4}$
$10^{-5}$
$10^{-6}$
Linear
Langmuir
Freundlich

ELEMENT = Cs
FORMATION = Tht
TIME = 21 days
ATMOS = Air
SIZE = All Sizes
SAMPLES = gl-1436, ym-38
ym-42

| ISOTHERM | N | ALPHA | BETA | R**2 | SSE |
|---|---|---|---|---|---|
| LINEAR | 20 | 0.0000000 | 3457.2561035 | 0.9998 | 0.31075904 |
| Kd = | 3457.25610352 | | | | |
| LANGMUIR | 20 | 0.0001596 | 0.0075453 | 0.1465 | 0.00009929 |
| b = | 132.53358459 | | | | |
| k = | 47.27558899 | | | | |
| FREUNDLICH | 20 | 3.4211545 | 0.9387101 | 0.9865 | 0.26250869 |
| K = | 2637.26953125 | | | | |
| N = | 0.93871009 | | | | |

N = the number of experimental points
ALPHA and BETA are respectively the intercept and slope from the linear regression analysis
R = correlation coefficient
SSE = standard error
Kd in mL/g
b in micromol(p+)/g and k in mL/micromol(p+)
K and N in units corresponding to solute adsorbed S in micromol(p+)/g and solute in solution C in micromol(p+)/mL.

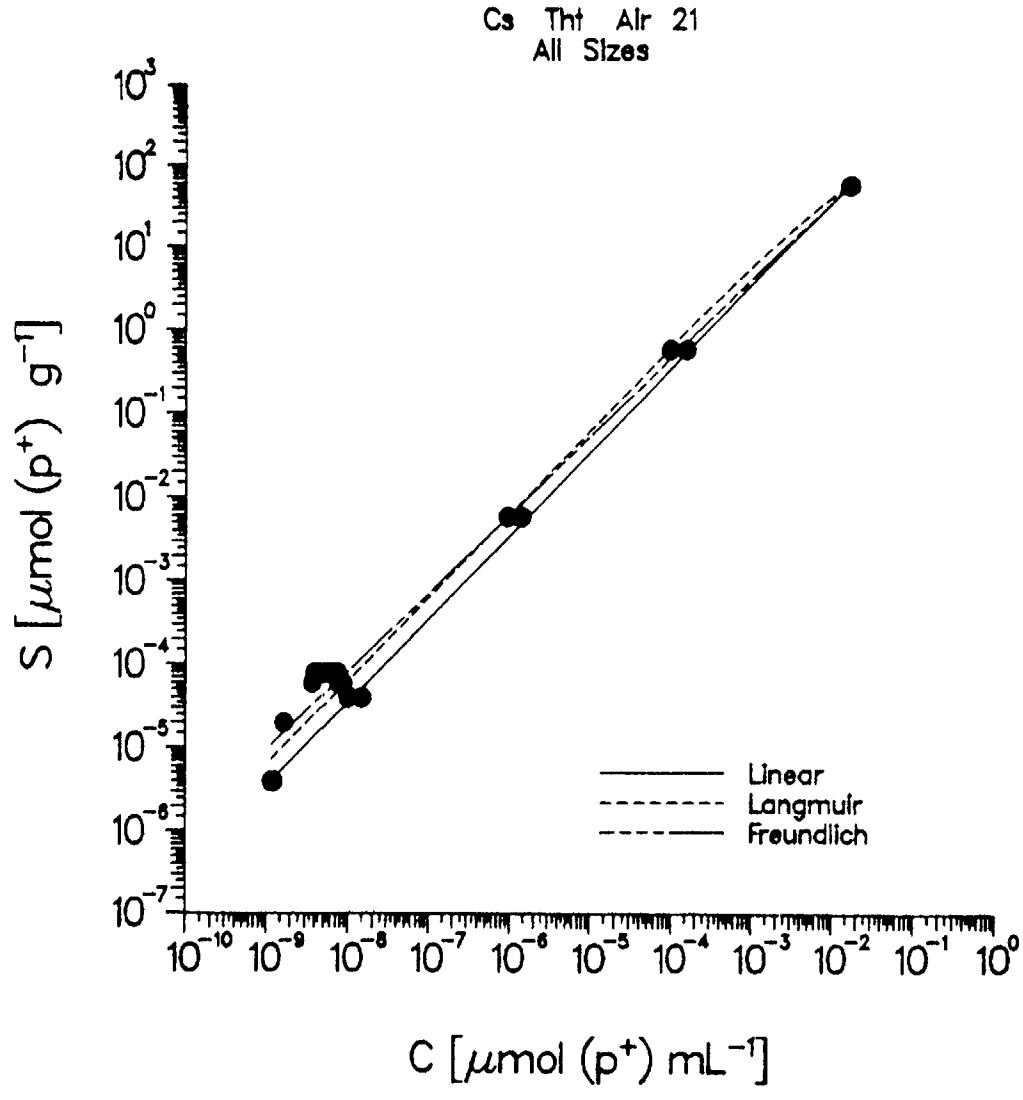
Cs Tht Air 21
All Sizes
S [μmol (p+) g−1]
C [μmol (p+) mL−1]
Linear
Langmuir
Freundlich

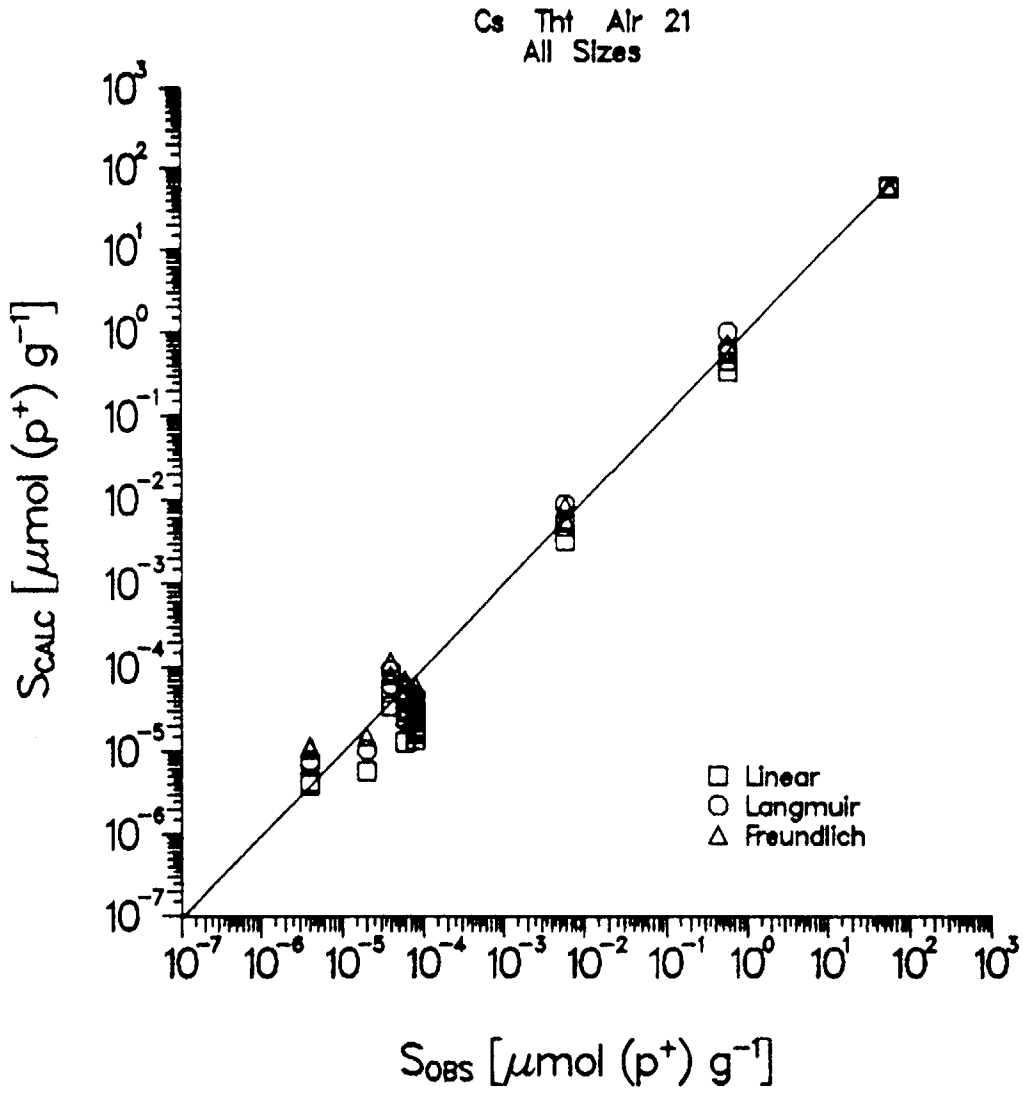
Cs Tht Air 21
All Sizes
$S_{CALC}$ [$\mu$mol ($p^+$) $g^{-1}$]
$S_{OBS}$ [$\mu$mol ($p^+$) $g^{-1}$]
Linear
Langmuir
Freundlich

ELEMENT = Sr
FORMATION = Tht
TIME = 21 days
ATMOS = Air
SIZE = All Sizes
SAMPLES = gl-1436, ym-38
ym-42

| ISOTHERM | N | ALPHA | BETA | R**2 | SSE |
|---|---|---|---|---|---|
| LINEAR | 20 | 0.0000000 | 1317.2322998 | 0.9877 | 2.91322351 |
| Kd = | 1317.23229980 | | | | |
| LANGMUIR | 20 | 0.0001426 | 0.0103094 | 0.6056 | 0.00015649 |
| b = | 96.99874878 | | | | |
| k = | 72.27928162 | | | | |
| FREUNDLICH | 20 | 3.2211151 | 0.8741840 | 0.9430 | 0.40155947 |
| K = | 1663.85363770 | | | | |
| N = | 0.87418395 | | | | |

N = the number of experimental points
ALPHA and BETA are respectively the intercept and slope from the linear regression analysis
R = correlation coefficient
SSE = standard error
Kd in mL/g
b in micromol(p+)/g and k in mL/micromol(p+)
K and N in units corresponding to solute adsorbed S in micromol(p+)/g and solute in solution C in micromol(p+)/mL.

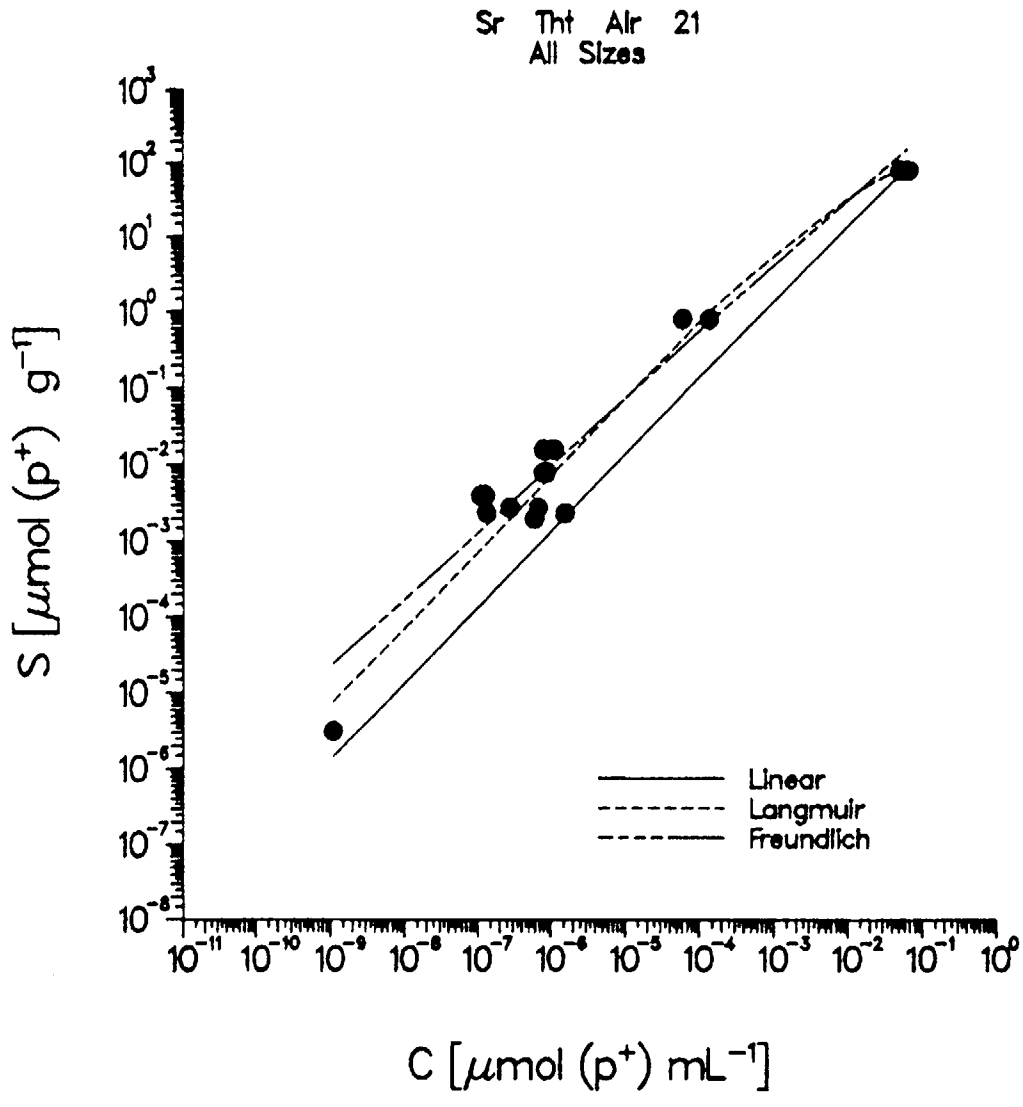
Sr Tht Alr 21
All Sizes
S [μmol (p+) g−1]
C [μmol (p+) mL−1]
Linear
Langmuir
Freundlich

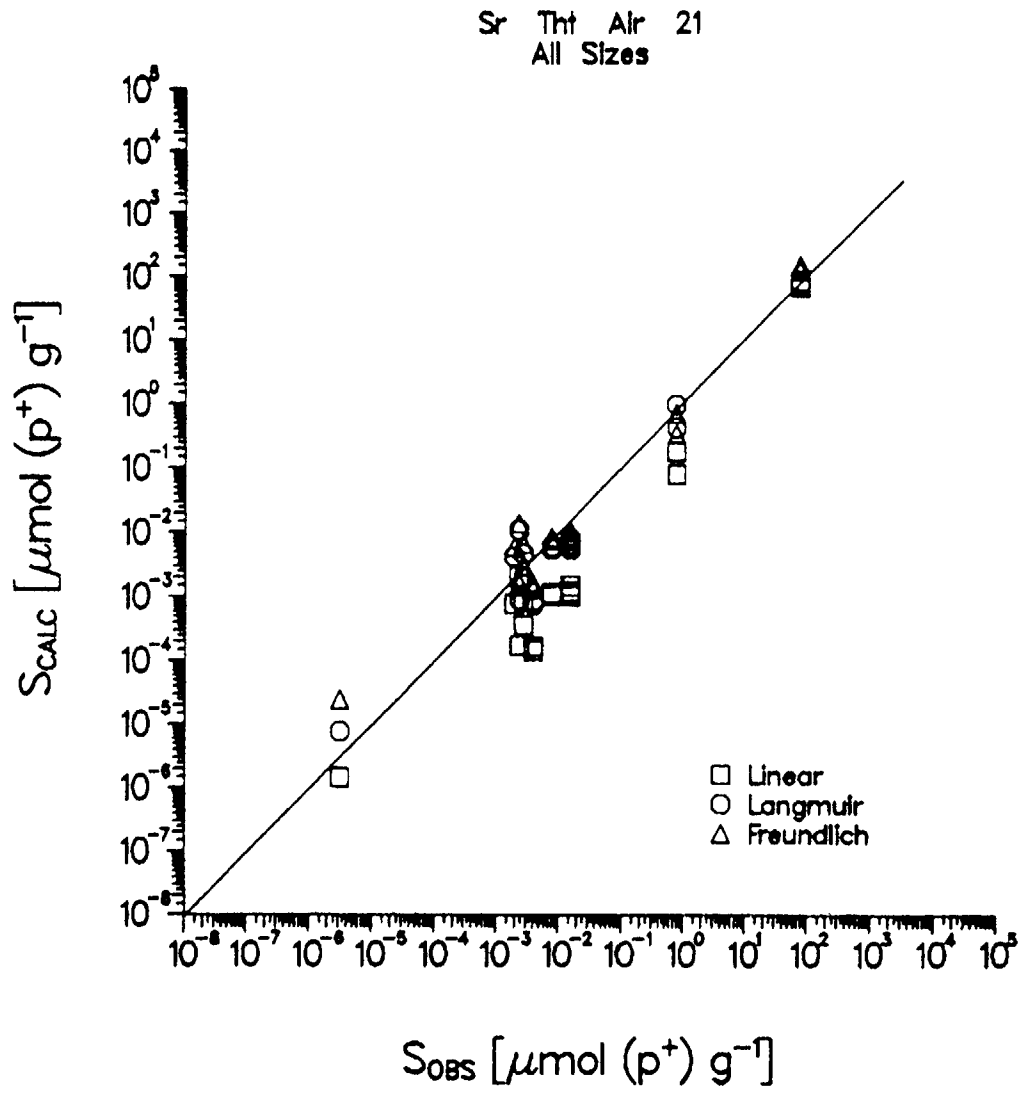
Sr Tht Air 21
All Sizes
Linear
Langmuir
Freundlich
$S_{CALC}$ [$\mu$mol ($p^+$) $g^{-1}$]
$S_{OBS}$ [$\mu$mol ($p^+$) $g^{-1}$]

ELEMENT = Ce
FORMATION = Tcp
TIME = 21 days
ATMOS = Air
SIZE = All Sizes
SAMPLE = gl-1854, gl-1883, gl-1982
ym-45, ym-46, ym-48, ym-49
ja-26

| ISOTHERM | N | ALPHA | BETA | R**2 | SSE |
|---|---|---|---|---|---|
| LINEAR | 9 | 0.0000000 | 652.5839844 | 0.9245 | 0.00938694 |
| Kd = | 652.58398438 | | | | |
| LANGMUIR | 9 | 0.0013542 | 4.8742242 | 0.0405 | 0.00072687 |
| b = | 0.20516086 | | | | |
| k = | 3599.208007 | | | | |
| FREUNDLICH | 9 | 1.5417054 | 0.7233465 | 0.9920 | 0.18194713 |
| K = | 34.81010818 | | | | |
| N = | 0.72334653 | | | | |

N = the number of experimental points
ALPHA and BETA are respectively the intercept and slope from the linear regression analysis
R = correlation coefficient
SSE = standard error
Kd in mL/g
b in micromol(p+)/g and k in mL/micromol(p+)
K and N in units corresponding to solute adsorbed S in micromol(p+)/g and solute in solution C in micro mol(p+)/mL.

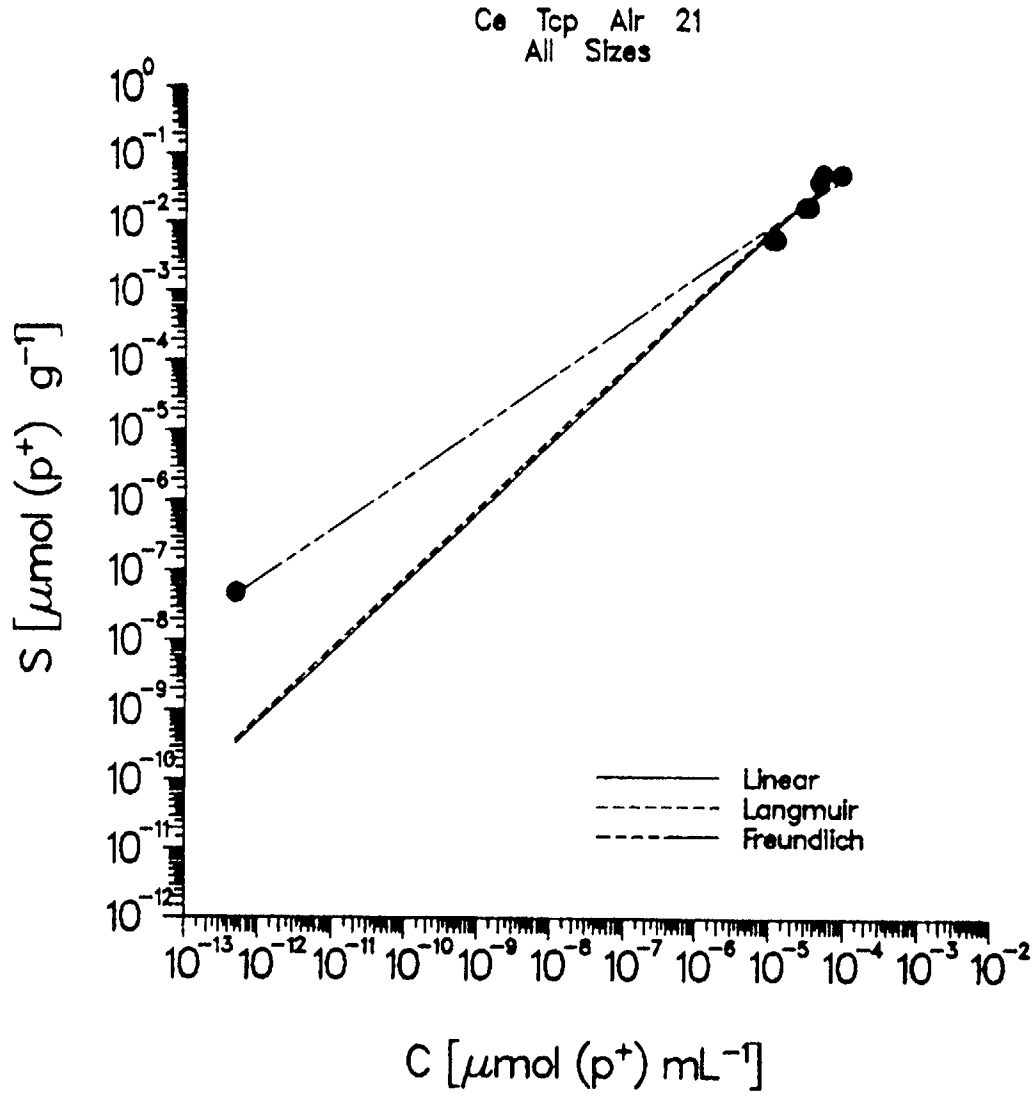
Ce Tcp Air 21
All Sizes
S [μmol (p+) g−1]
C [μmol (p+) mL−1]
Linear
Langmuir
Freundlich

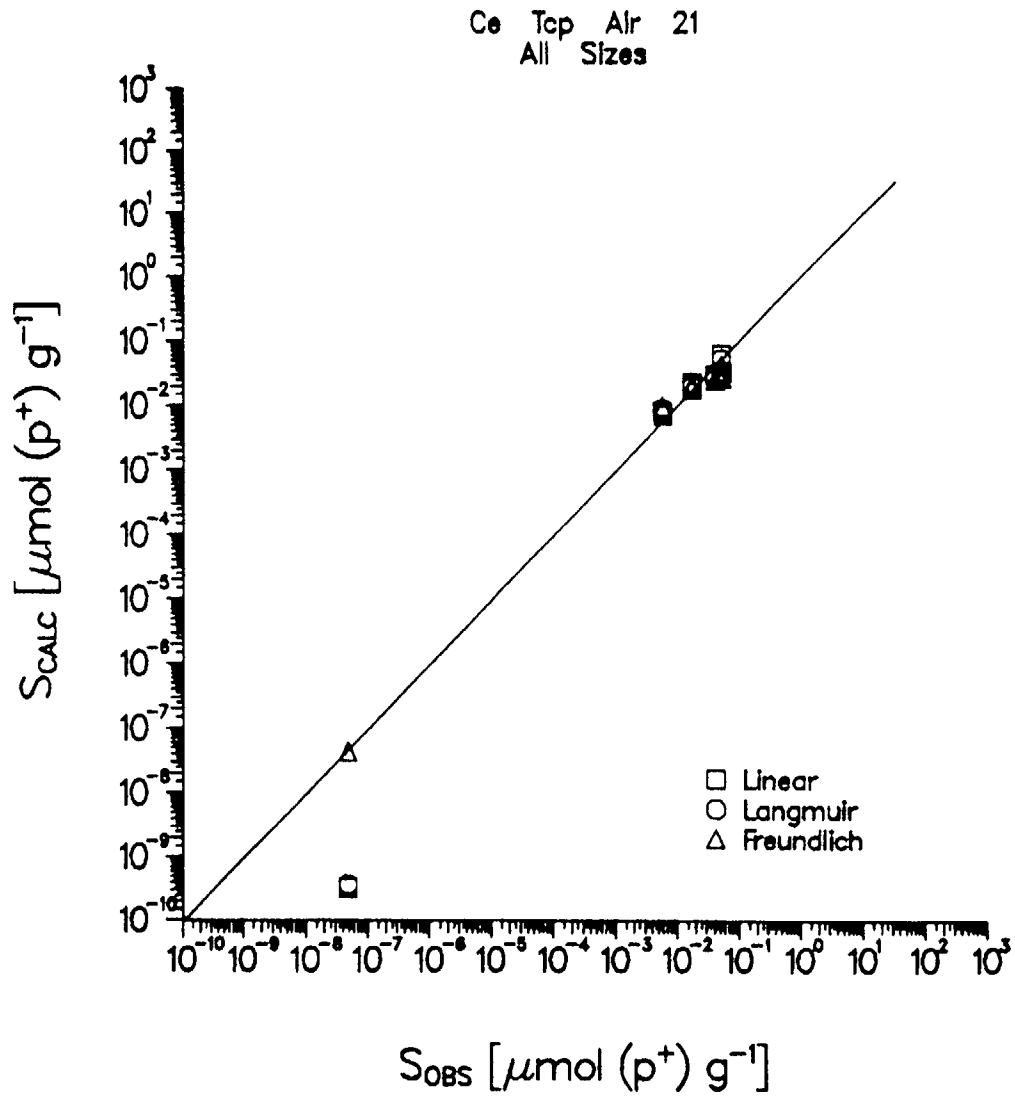
Ce Tcp Air 21
All Sizes
Linear
Langmuir
Freundlich
$S_{CALC}$ [$\mu$mol ($p^+$) $g^{-1}$]
$S_{OBS}$ [$\mu$mol ($p^+$) $g^{-1}$]

ELEMENT = Eu
FORMATION = Tcp
TIME = 21 days
ATMOS = Air
SIZE = All Sizes
SAMPLE = gl-1854, gl-1883, gl-1982
ym-45, ym-46, ym-48, ym-49
ja-26

| ISOTHERM | N | ALPHA | BETA | R**2 | SSE |
|---|---|---|---|---|---|
| LINEAR | 25 | 0.0000000 | 271.0082397 | 0.4108 | 0.00348153 |
| Kd = | 271.00823975 | | | | |
| LANGMUIR | 25 | 0.0022527 | 144.7087097 | 0.0605 | 0.00464259 |
| b = | 0.00691043 | | | | |
| k = | 64239.253906 | | | | |
| FREUNDLICH | 25 | 0.0164816 | 0.4802493 | 0.4959 | 0.63471442 |
| K = | 1.03867972 | | | | |
| N = | 0.48024935 | | | | |

N = the number of experimental points
ALPHA and BETA are respectively the intercept and slope from the linear regression analysis
R = correlation coefficient
SSE = standard error
Kd in mL/g
b in micromol(p+)/g and k in mL/micromol(p+)
K and N in units corresponding to solute adsorbed S in micromol(p+)/g and solute in solution C in micro mol(p+)/mL.

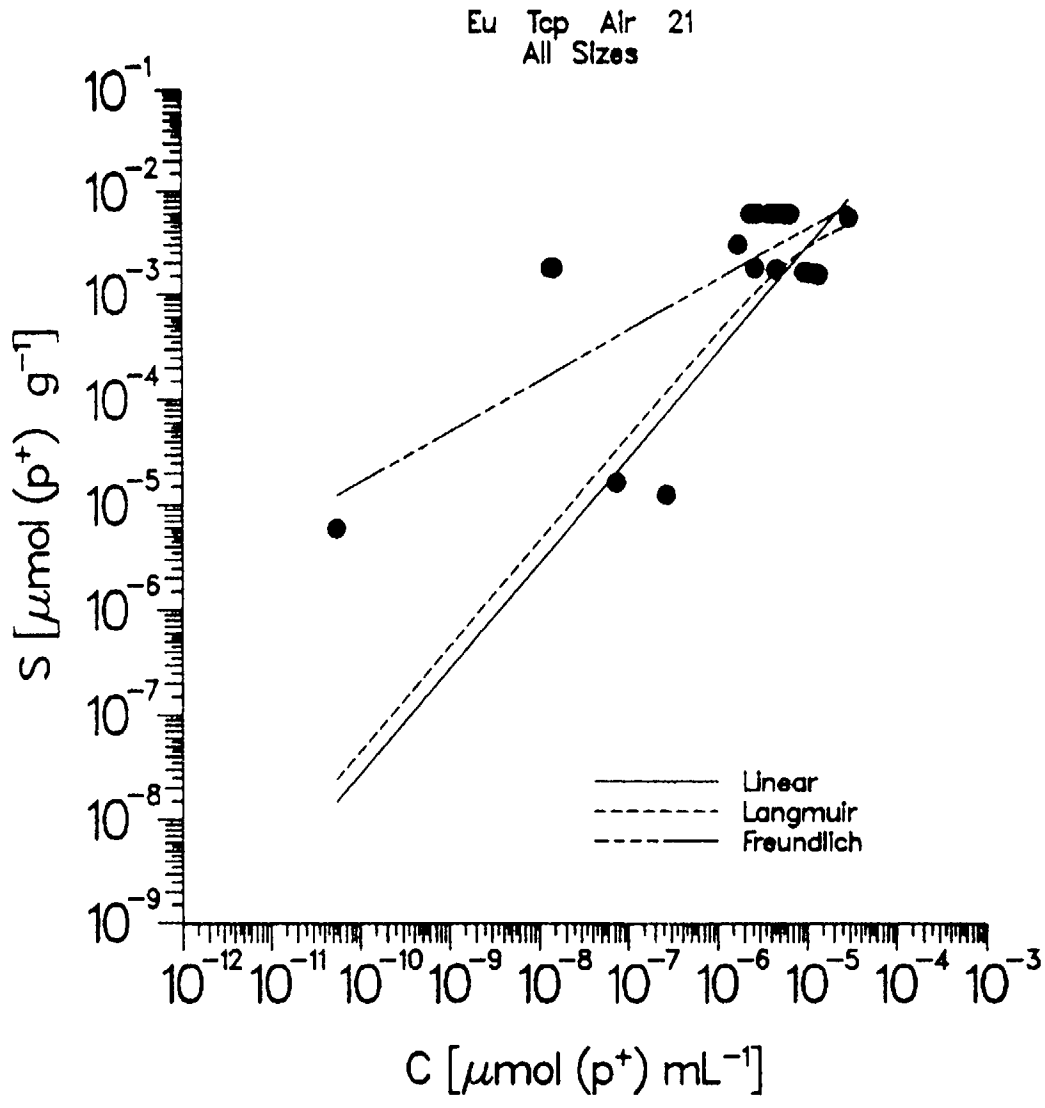
Eu Tcp Air 21
All Sizes
S [μmol (p+) g−1]
C [μmol (p+) mL−1]
Linear
Langmuir
Freundlich

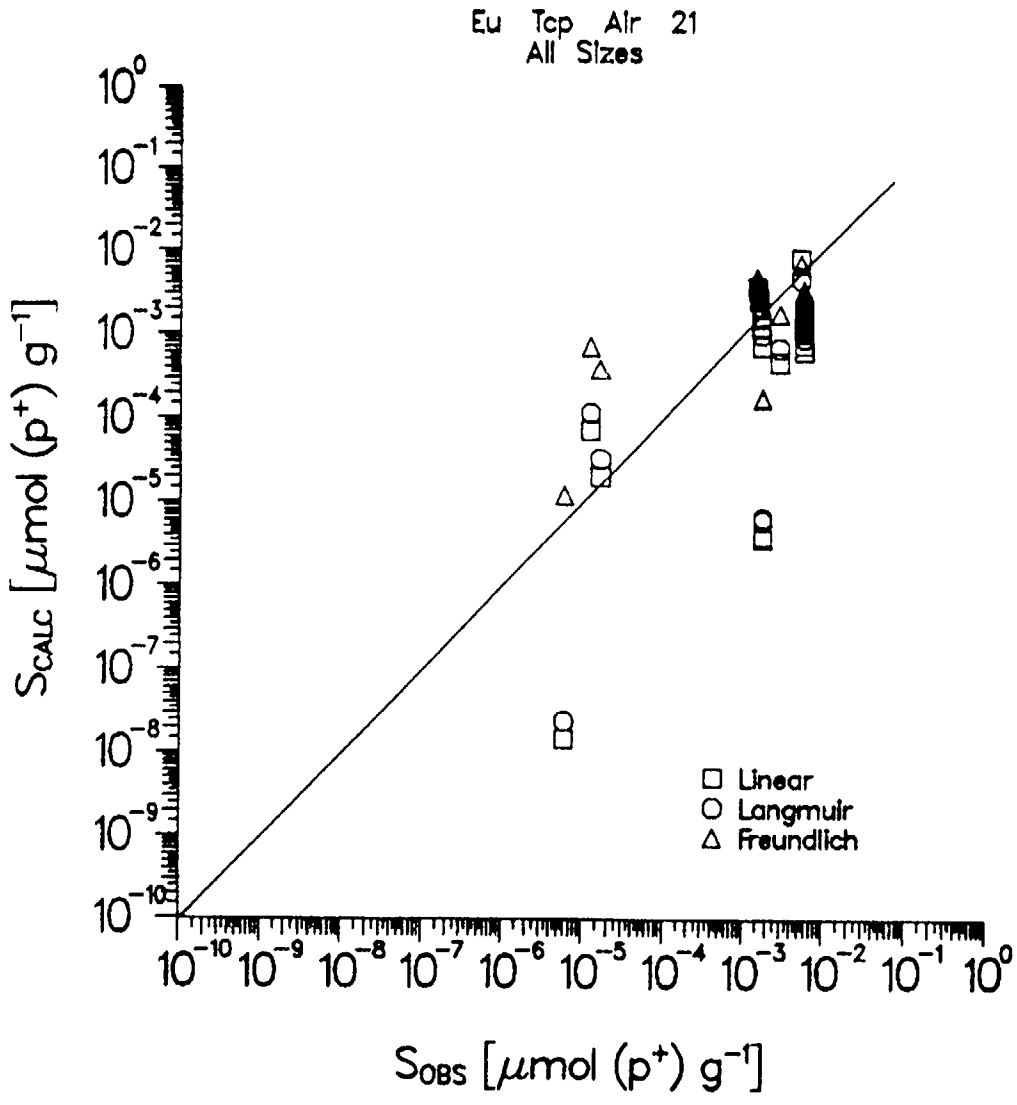
Eu Tcp Air 21
All Sizes
$S_{CALC}$ [$\mu$mol ($p^+$) $g^{-1}$]
$S_{OBS}$ [$\mu$mol ($p^+$) $g^{-1}$]
$10^{0}$
$10^{-1}$
$10^{-2}$
$10^{-3}$
$10^{-4}$
$10^{-5}$
$10^{-6}$
$10^{-7}$
$10^{-8}$
$10^{-9}$
$10^{-10}$
Linear
Langmuir
Freundlich

ELEMENT = Ba
FORMATION = Tcp
TIME = 21 days
ATMOS = Air
SIZE = All Sizes
SAMPLE = gl-1854, gl-1883, gl-1982
ym-45, ym-46, ym-48, ym-49
ja-26

| ISOTHERM | N | ALPHA | BETA | R**2 | SSE |
|---|---|---|---|---|---|
| LINEAR | 25 | 0.0000000 | 210.3516998 | 0.6558 | 0.10491771 |
| Kd = | 210.35169983 | | | | |
| LANGMUIR | 25 | 0.0006894 | 3.3356285 | 0.7305 | 0.00116256 |
| b = | 0.29979357 | | | | |
| k = | 4838.376464 | | | | |
| FREUNDLICH | 25 | 1.6073117 | 0.6591421 | 0.7517 | 0.64302045 |
| K = | 40.48664093 | | | | |
| N = | 0.65914208 | | | | |

N = the number of experimental points
ALPHA and BETA are respectively the intercept and slope from the linear regression analysis
R = correlation coefficient
SSE = standard error
Kd in mL/g
b in micromol(p+)/g and k in mL/micromol(p+)
K and N in units corresponding to solute adsorbed S in micromol(p+)/g and solute in solution C in micro mol(p+)/mL.

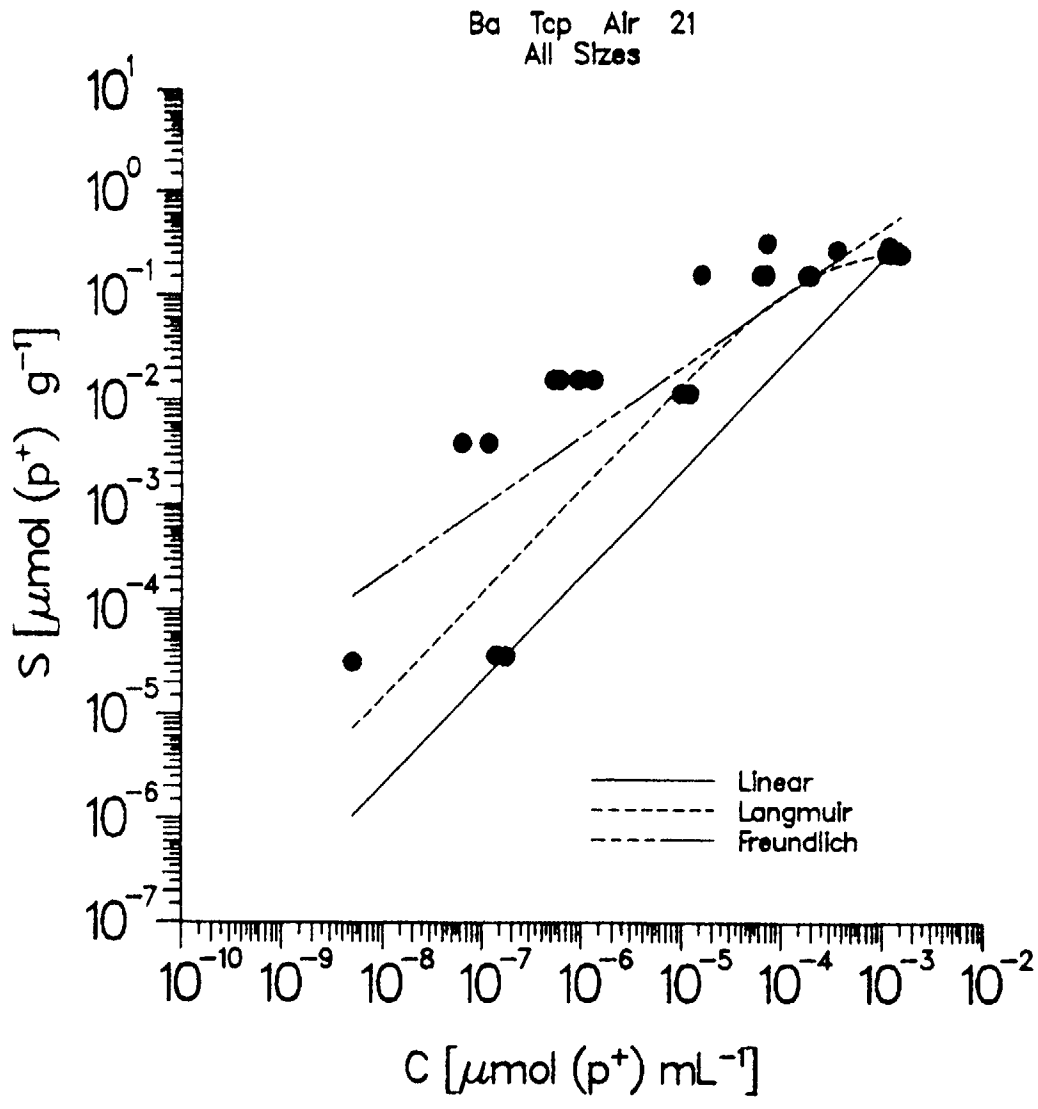
Ba Tcp Air 21
All Sizes
S [μmol (p+) g-1]
C [μmol (p+) mL-1]
Linear
Langmuir
Freundlich

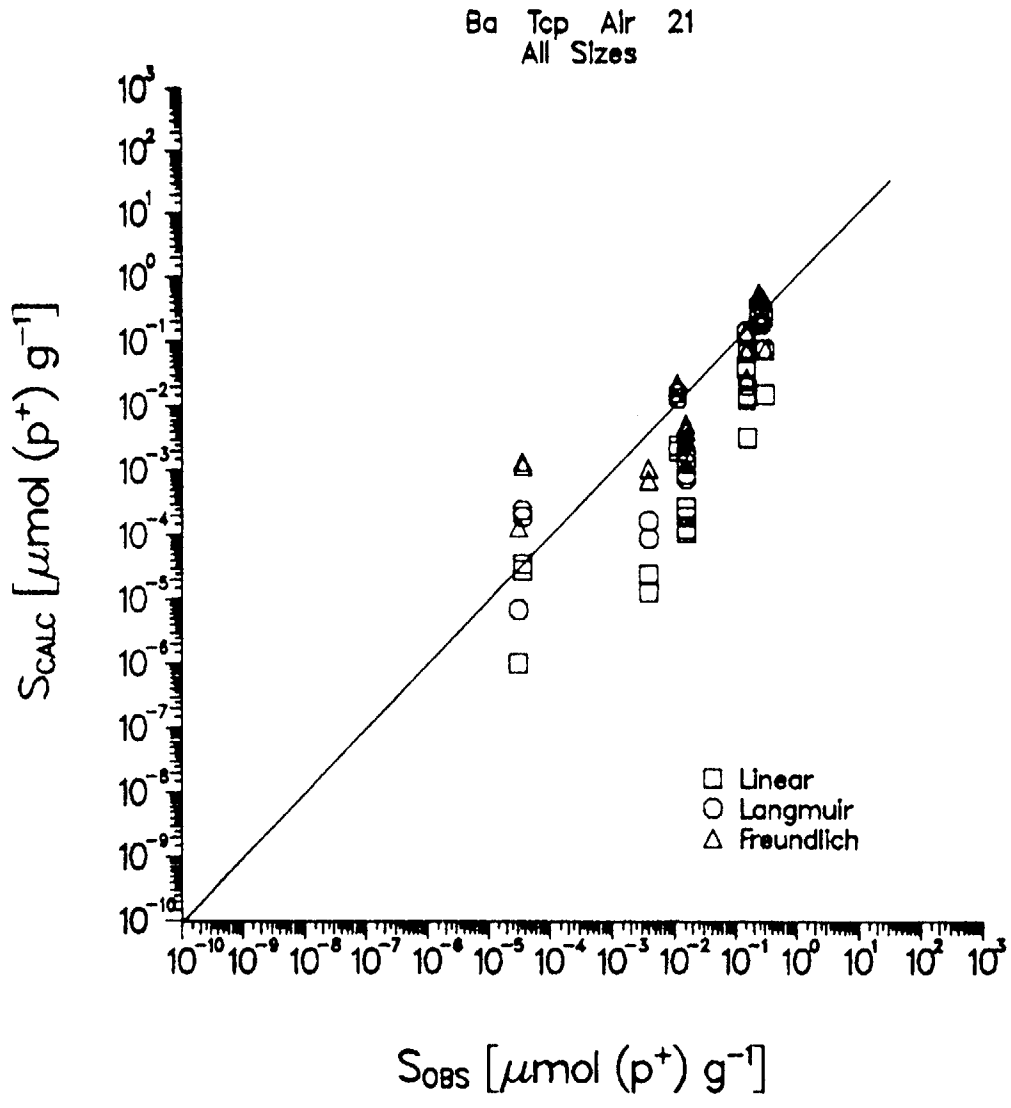
Ba Tcp Air 21
All Sizes
Linear
Langmuir
Freundlich
$S_{CALC}$ [$\mu$mol ($p^+$) $g^{-1}$]
$S_{OBS}$ [$\mu$mol ($p^+$) $g^{-1}$]

ELEMENT = Cs
FORMATION = Tcp
TIME = 21 days
ATMOS = Air
SIZE = All Sizes
SAMPLE = gl-1854, gl-1883, gl-1982
ym-45, ym-46, ym-48, ym-49
ja-26

| ISOTHERM | N | ALPHA | BETA | R**2 | SSE |
|---|---|---|---|---|---|
| LINEAR | 25 | 0.0000000 | 272.5692139 | 0.5948 | 0.00004310 |
| Kd = | 272.56921387 | | | | |
| LANGMUIR | 25 | 0.0002369 | 12718.3984375 | 0.9237 | 0.00051828 |
| b = | 0.00007863 | | | | |
| k = | 53690008.000 | | | | |
| FREUNDLICH | 25 | -2.8141172 | 0.1987261 | 0.5067 | 0.18125145 |
| K = | 0.00153420 | | | | |
| N = | 0.19872607 | | | | |

N = the number of experimental points
ALPHA and BETA are respectively the intercept and slope from the linear regression analysis
R = correlation coefficient
SSE = standard error
Kd in mL/g
b in micromol(p+)/g and k in mL/micromol(p+)
K and N in units corresponding to solute adsorbed S in micromol(p+)/g and solute in solution C in micro mol(p+)/mL.

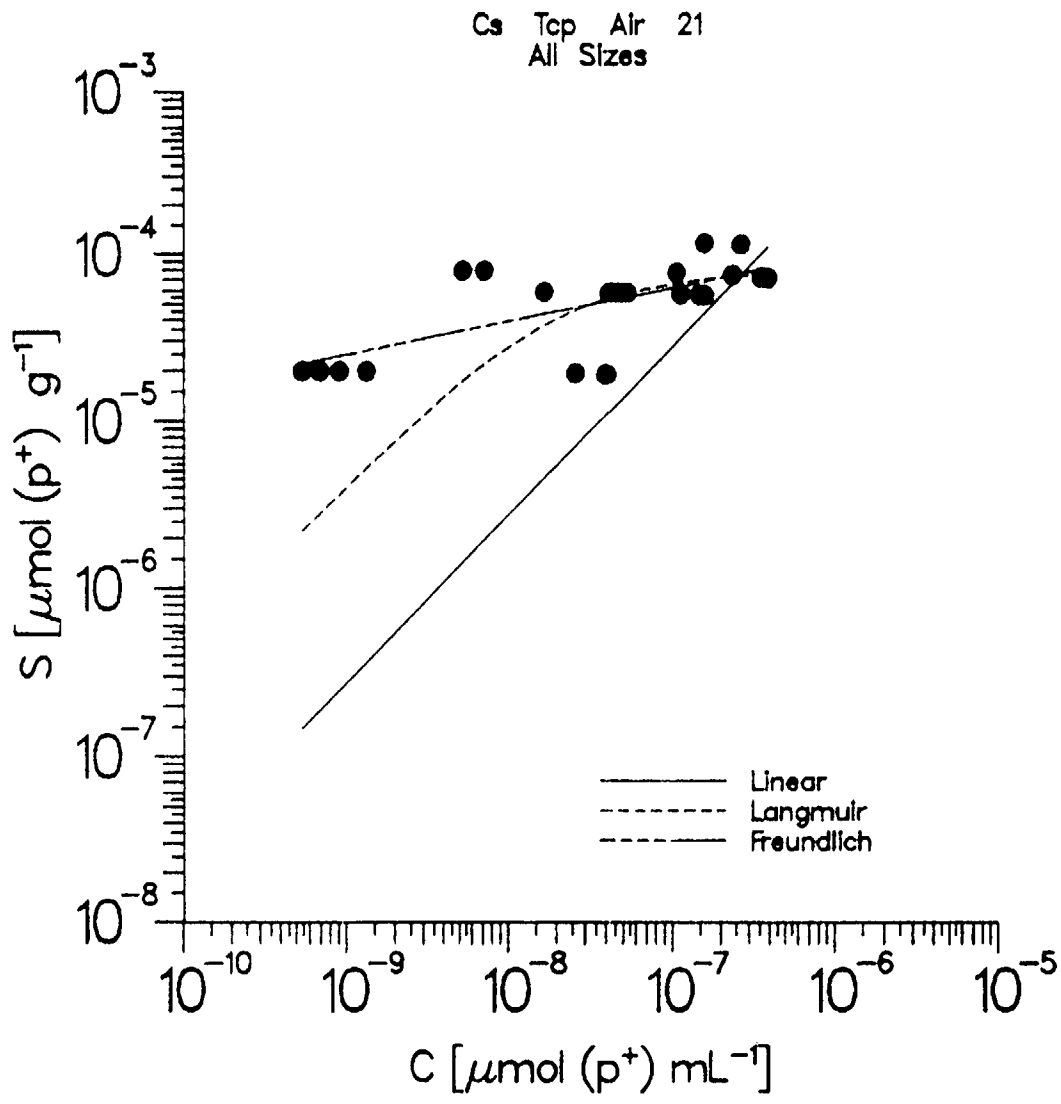
Cs Tcp Air 21
All Sizes
S [μmol (p+) g-1]
C [μmol (p+) mL-1]
Linear
Langmuir
Freundlich

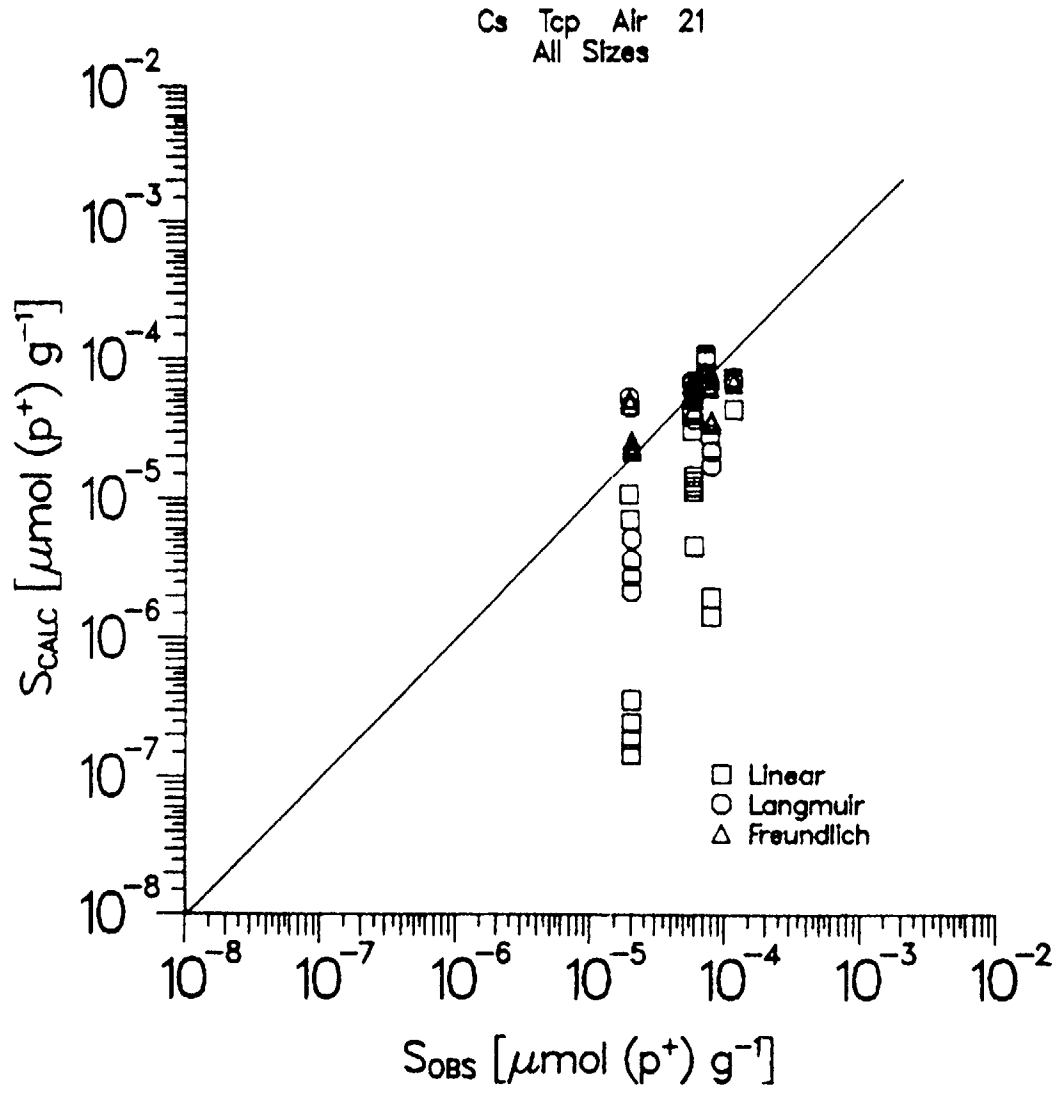
Cs Tcp Air 21
All Sizes
$S_{CALC}$ [$\mu$mol ($p^+$) $g^{-1}$]
$S_{OBS}$ [$\mu$mol ($p^+$) $g^{-1}$]
$10^{-2}$
$10^{-3}$
$10^{-4}$
$10^{-5}$
$10^{-6}$
$10^{-7}$
$10^{-8}$
Linear
Langmuir
Freundlich

ELEMENT = Sr
FORMATION = Tcp
TIME = 21 days
ATMOS = Air
SIZE = All Sizes
SAMPLE = gl-1854, gl-1883, gl-1982
ym-45, ym-46, ym-48, ym-49
ja-26

| ISOTHERM | N | ALPHA | BETA | R**2 | SSE |
|---|---|---|---|---|---|
| LINEAR | 25 | 0.0000000 | 37.7320862 | 0.4251 | 0.00638130 |
| Kd = | 37.73208618 | | | | |
| LANGMUIR | 25 | 0.0036624 | 133.2613831 | 0.7441 | 0.00855169 |
| b = | 0.00750405 | | | | |
| k = | 36385.96484 | | | | |
| FREUNDLICH | 25 | 0.4087899 | 0.6156070 | 0.5758 | 0.86051714 |
| K = | 2.56324363 | | | | |
| N = | 0.61560702 | | | | |

N = the number of experimental points
ALPHA and BETA are respectively the intercept and slope from the linear regression analysis
R = correlation coefficient
SSE = standard error
Kd in mL/g
b in micromol(p+)/g and k in mL/micromol(p+)
K and N in units corresponding to solute adsorbed S in micromol(p+)/g and solute in solution C in micromol(p+)/mL.

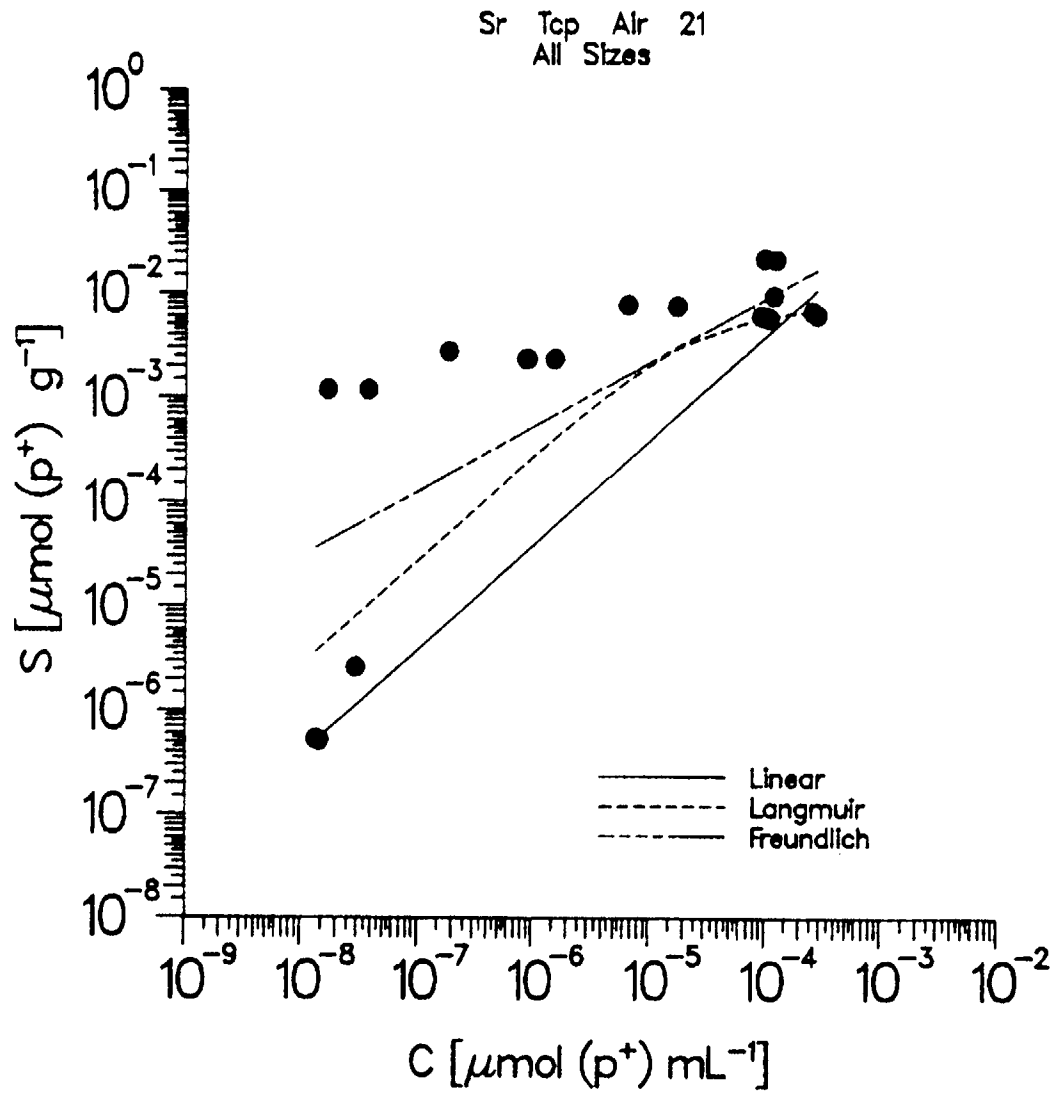
Sr Tcp Air 21
All Sizes
S [μmol (p+) g−1]
C [μmol (p+) mL−1]
Linear
Langmuir
Freundlich

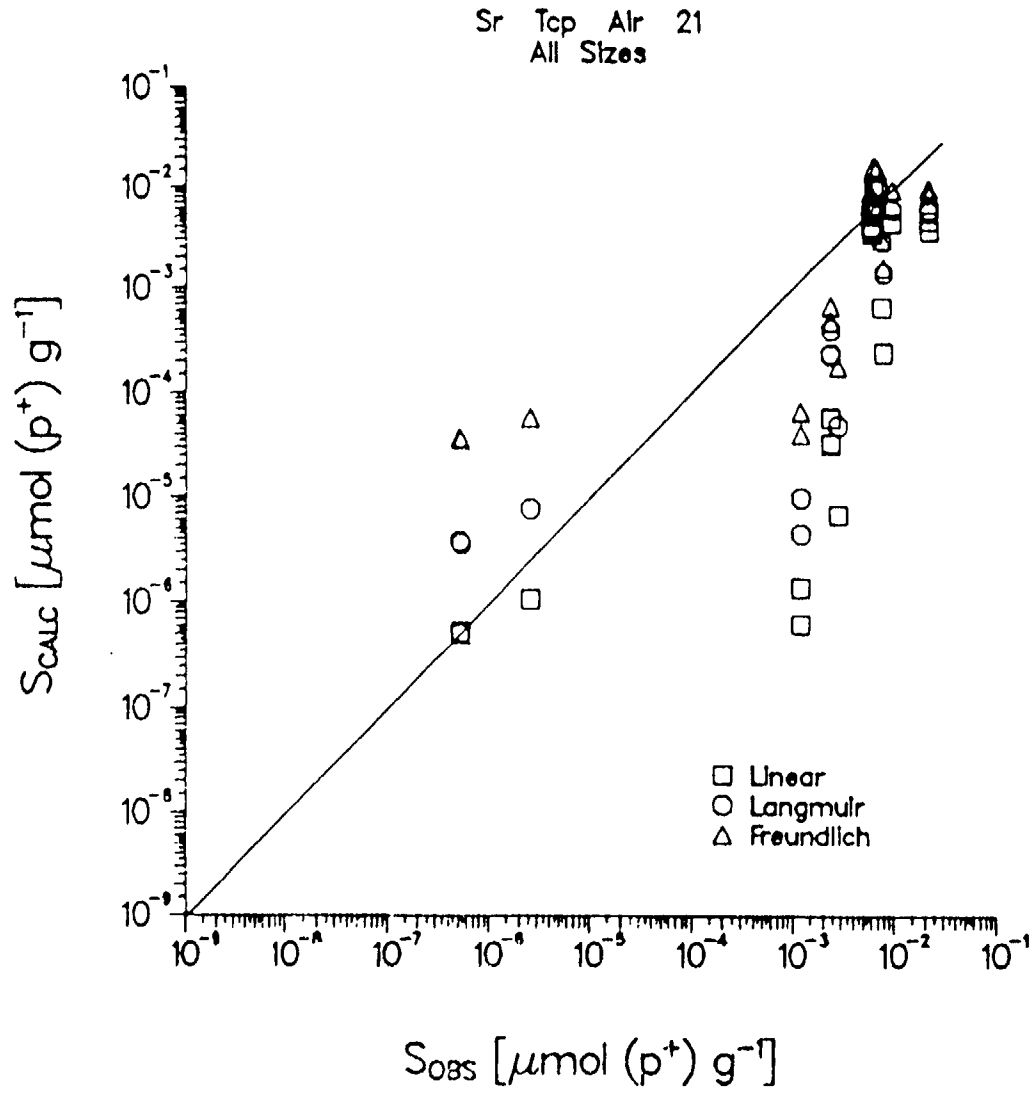
Sr Tcp Air 21
All Sizes
$S_{CALC}$ [$\mu$mol ($p^+$) $g^{-1}$]
$S_{OBS}$ [$\mu$mol ($p^+$) $g^{-1}$]
Linear
Langmuir
Freundlich

ELEMENT - Eu
FORMATION - Tcb
TIME - 21 days
ATMOS - Air
SIZE - All Sizes
SAMPLE - ja-28, ja-32, ym-54
gl-2233, gl-2289, gl-2333
gl-2410, gl-2476, gl-2363

| ISOTHERM | N | ALPHA | BETA | R**2 | SSE |
|---|---|---|---|---|---|
| LINEAR | 34 | 0.0000000 | 79.2906418 | 0.8619 | 0.00289860 |
| Kd = | 79.29064178 | | | | |
| LANGMUIR | 34 | 0.0011785 | 32.0329170 | 0.9244 | 0.00080389 |
| b = | 0.03121789 | | | | |
| k = | 27180.6895 | | | | |
| FREUNDLICH | 34 | 1.2175593 | 0.6958010 | 0.8143 | 0.31675020 |
| K = | 16.50286484 | | | | |
| N = | 0.69580102 | | | | |

N = the number of experimental points
ALPHA and BETA are respectively the intercept and slope from the linear regression analysis
R = correlation coefficient
SSE = standard error
Kd in mL/g
b in micromol(p+)/g and k in mL/micromol(p+)
K and N in units corresponding to solute adsorbed S in micromol(p+)/g and solute in solution C in micromol(p+)/mL.

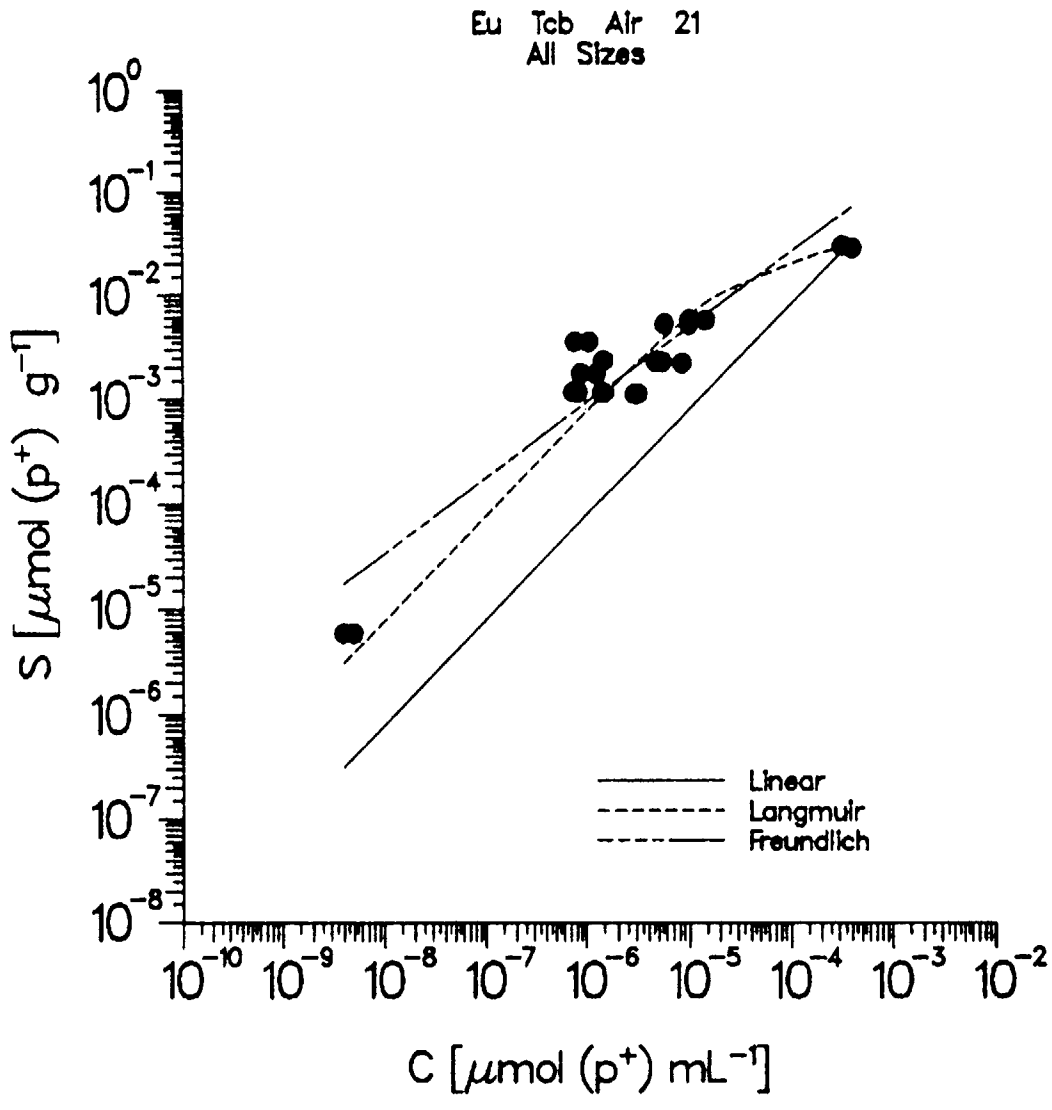
Eu Tcb Air 21
All Sizes
S [μmol (p+) g−1]
C [μmol (p+) mL−1]
Linear
Langmuir
Freundlich

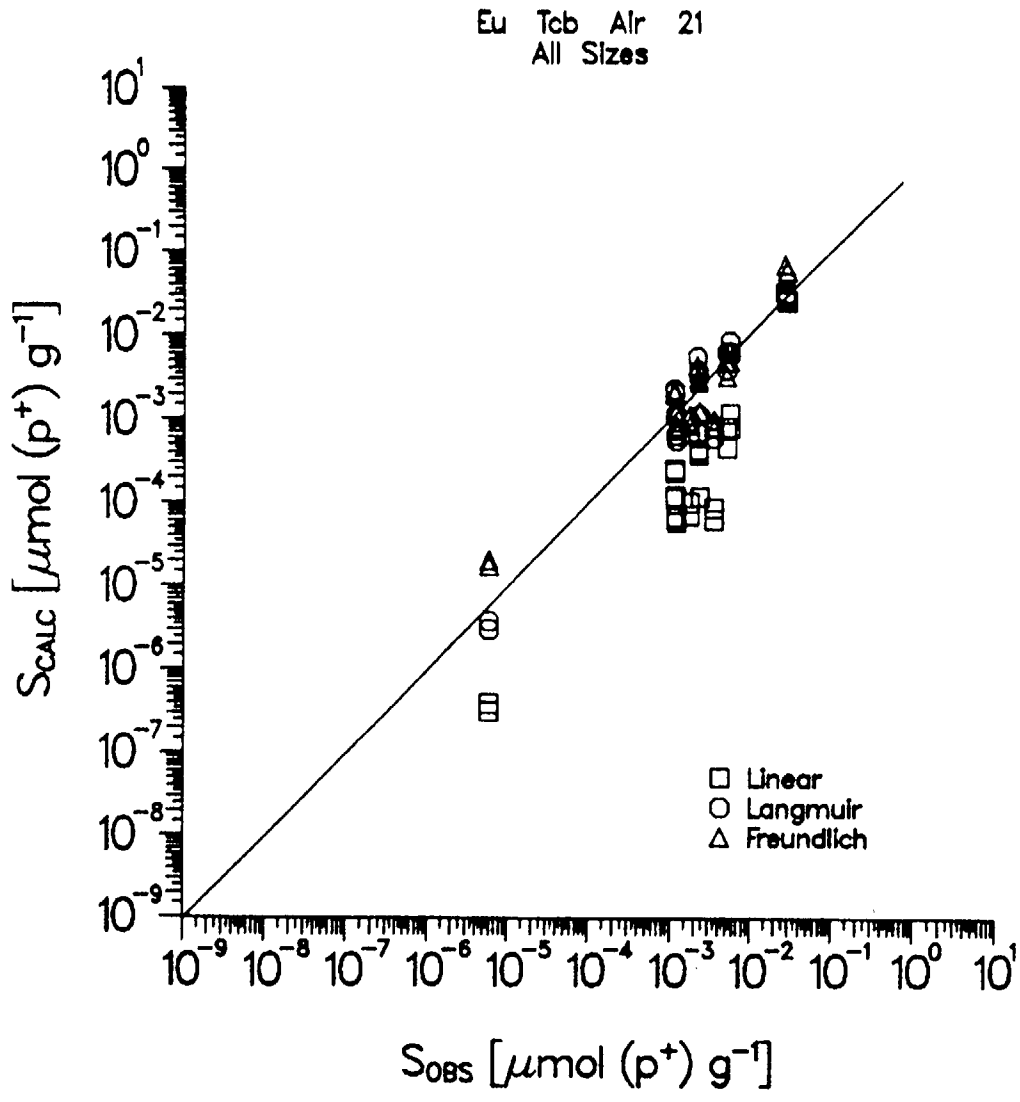
Eu Tcb Air 21
All Sizes
$S_{CALC}$ [$\mu$mol ($p^+$) $g^{-1}$]
$S_{OBS}$ [$\mu$mol ($p^+$) $g^{-1}$]
$10^{1}$
$10^{0}$
$10^{-1}$
$10^{-2}$
$10^{-3}$
$10^{-4}$
$10^{-5}$
$10^{-6}$
$10^{-7}$
$10^{-8}$
$10^{-9}$
Linear
Langmuir
Freundlich

ELEMENT = Ba
FORMATION = Tcb
TIME = 21 days
ATMOS = Air
SIZE = All Sizes
SAMPLE = ja-28, ja-32, ym-54
gl-2233, gl-2289, gl-2333
gl-2410, gl-2476, gl-2363

| ISOTHERM | N | ALPHA | BETA | R**2 | SSE |
|---|---|---|---|---|---|
| LINEAR | 32 | 0.0000000 | 782.2355957 | 0.5988 | 0.06489543 |
| Kd = | 782.23559570 | | | | |
| LANGMUIR | 32 | 0.0017517 | 2.6716630 | 0.0149 | 0.00199796 |
| b = | 0.37429869 | | | | |
| k = | 1525.15906 | | | | |
| FREUNDLICH | 32 | -0.0398977 | 0.3813742 | 0.3175 | 0.71818525 |
| K = | 0.91222572 | | | | |
| N = | 0.38137421 | | | | |

N = the number of experimental points
ALPHA and BETA are respectively the intercept and slope from the linear regression analysis
R = correlation coefficient
SSE = standard error
Kd in mL/g
b in micromol(p+)/g and k in mL/micromol(p+)
K and N in units corresponding to solute adsorbed S in micromol(p+)/g and solute in solution C in micromol(p+)/mL.

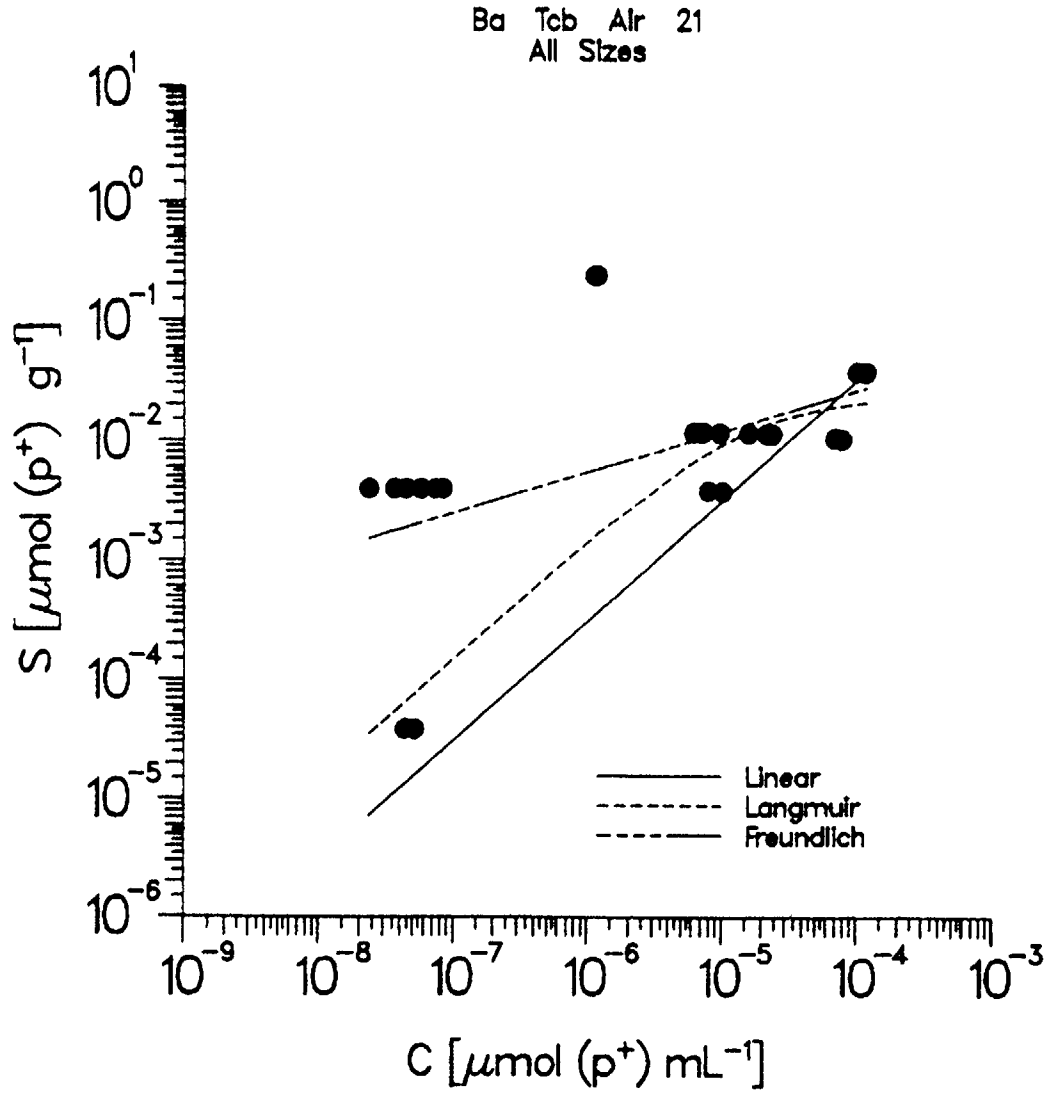
Ba Tcb Air 21
All Sizes
S [μmol (p+) g-1]
C [μmol (p+) mL-1]
Linear
Langmuir
Freundlich

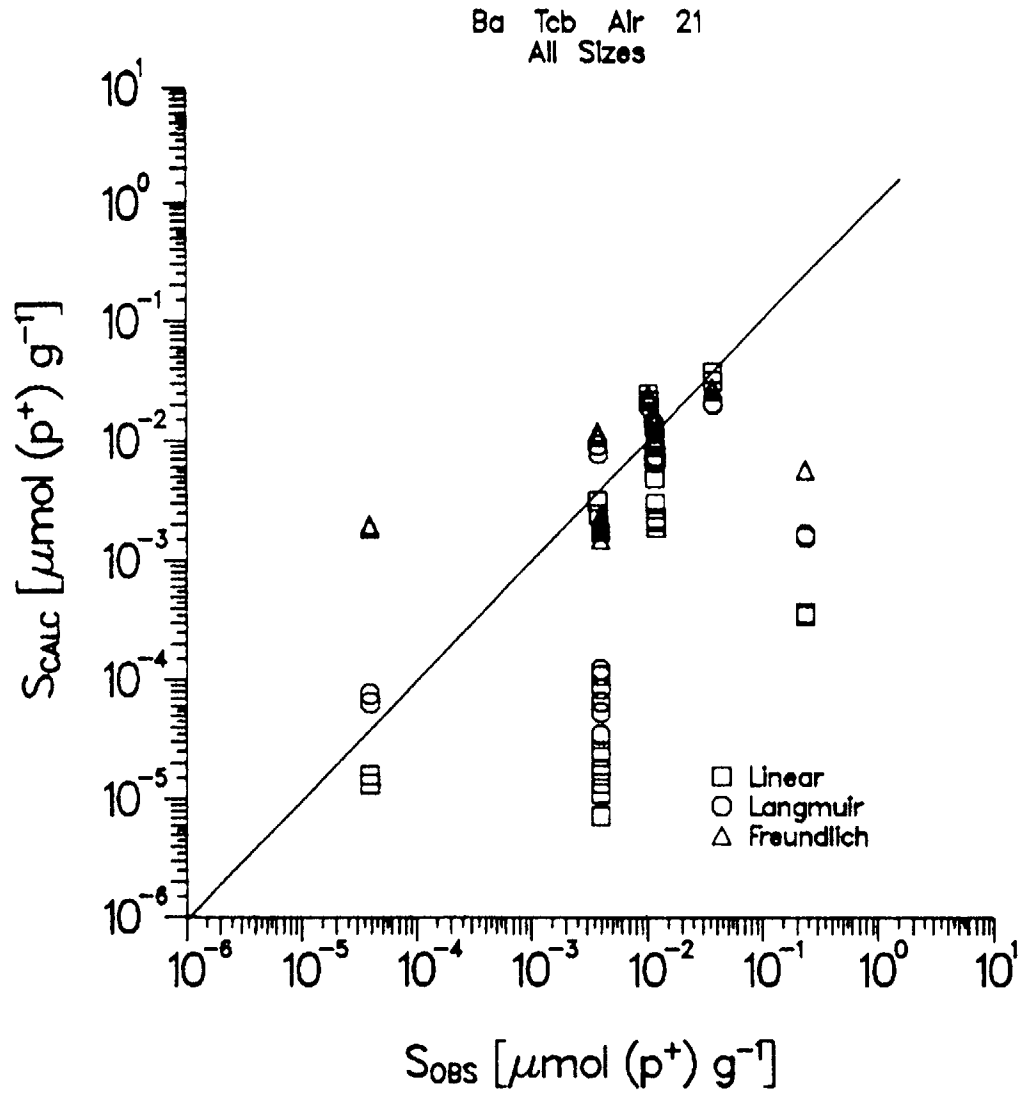
Ba Tcb Air 21
All Sizes
$S_{CALC}$ [$\mu$mol ($p^+$) $g^{-1}$]
$S_{OBS}$ [$\mu$mol ($p^+$) $g^{-1}$]
Linear
Langmuir
Freundlich

ELEMENT = Cs
FORMATION = Tcb
TIME = 21 days
ATMOS = Air
SIZE = All Sizes
SAMPLE = ja-28, ja-32, ym-54
gl-2233, gl-2289, gl-2333
gl-2410, gl-2476, gl-2363

| ISOTHERM | N | ALPHA | BETA | R**2 | SSE |
|---|---|---|---|---|---|
| LINEAR | 35 | 0.0000000 | 299.7982178 | 0.2682 | 0.00007815 |
| Kd = | 299.79821777 | | | | |
| LANGMUIR | 35 | -0.0000685 | 19912.7050781 | 0.6877 | 0.00153105 |
| b = | 0.00005022 | | | | |
| k = | -290627520.0 | | | | |
| FREUNDLICH | 35 | -4.6855955 | -0.0727179 | 0.0606 | 0.21968605 |
| K = | 0.00002063 | | | | |
| N = | -0.07271790 | | | | |

N = the number of experimental points
ALPHA and BETA are respectively the intercept and slope from the linear regression analysis
R = correlation coefficient
SSE = standard error
Kd in mL/g
b in micromol(p+)/g and k in mL/micromol(p+)
K and N in units corresponding to solute adsorbed S in micromol(p+)/g and solute in solution C in micromol(p+)/mL.

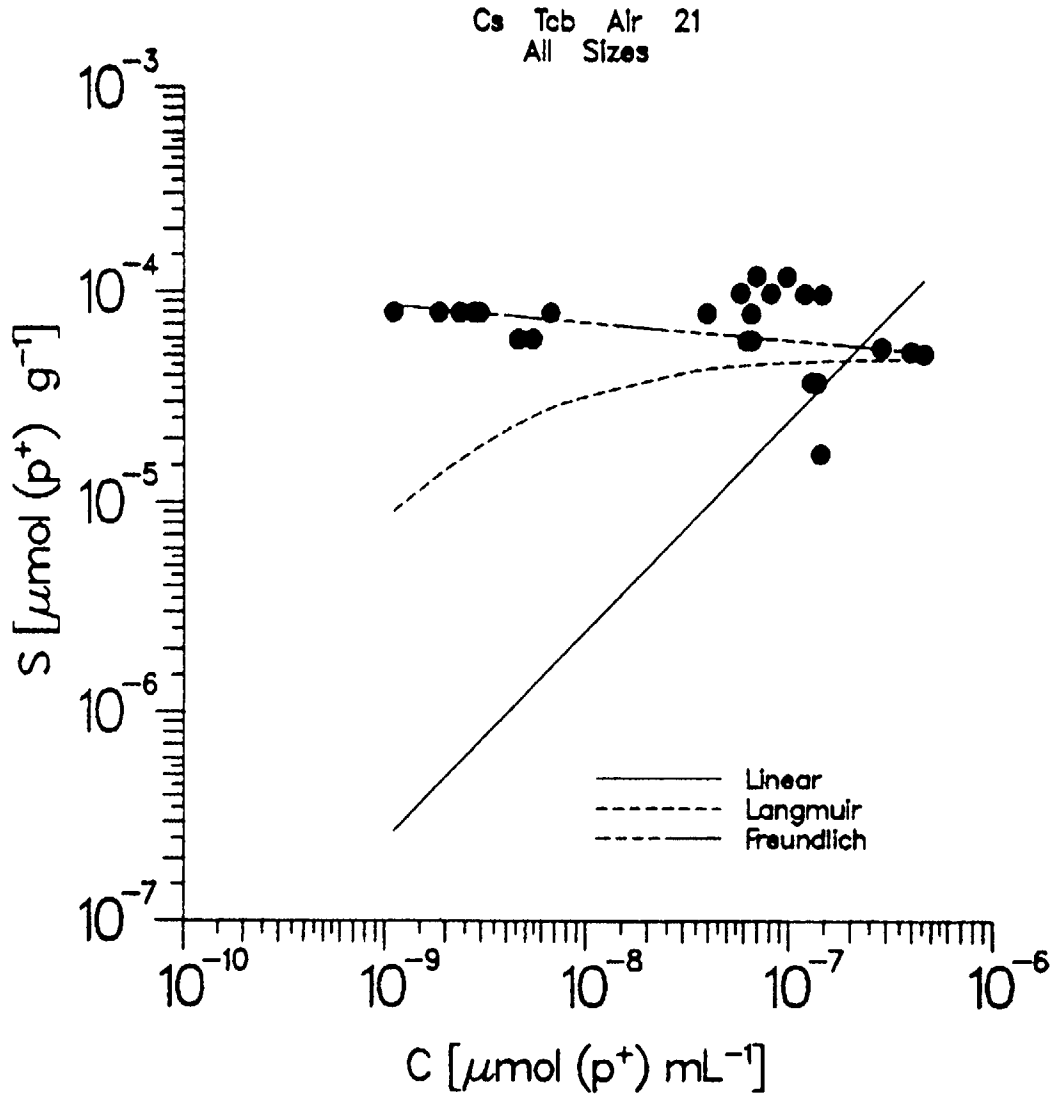
Cs Tcb Air 21
All Sizes
S [μmol (p+) g-1]
C [μmol (p+) mL-1]
Linear
Langmuir
Freundlich

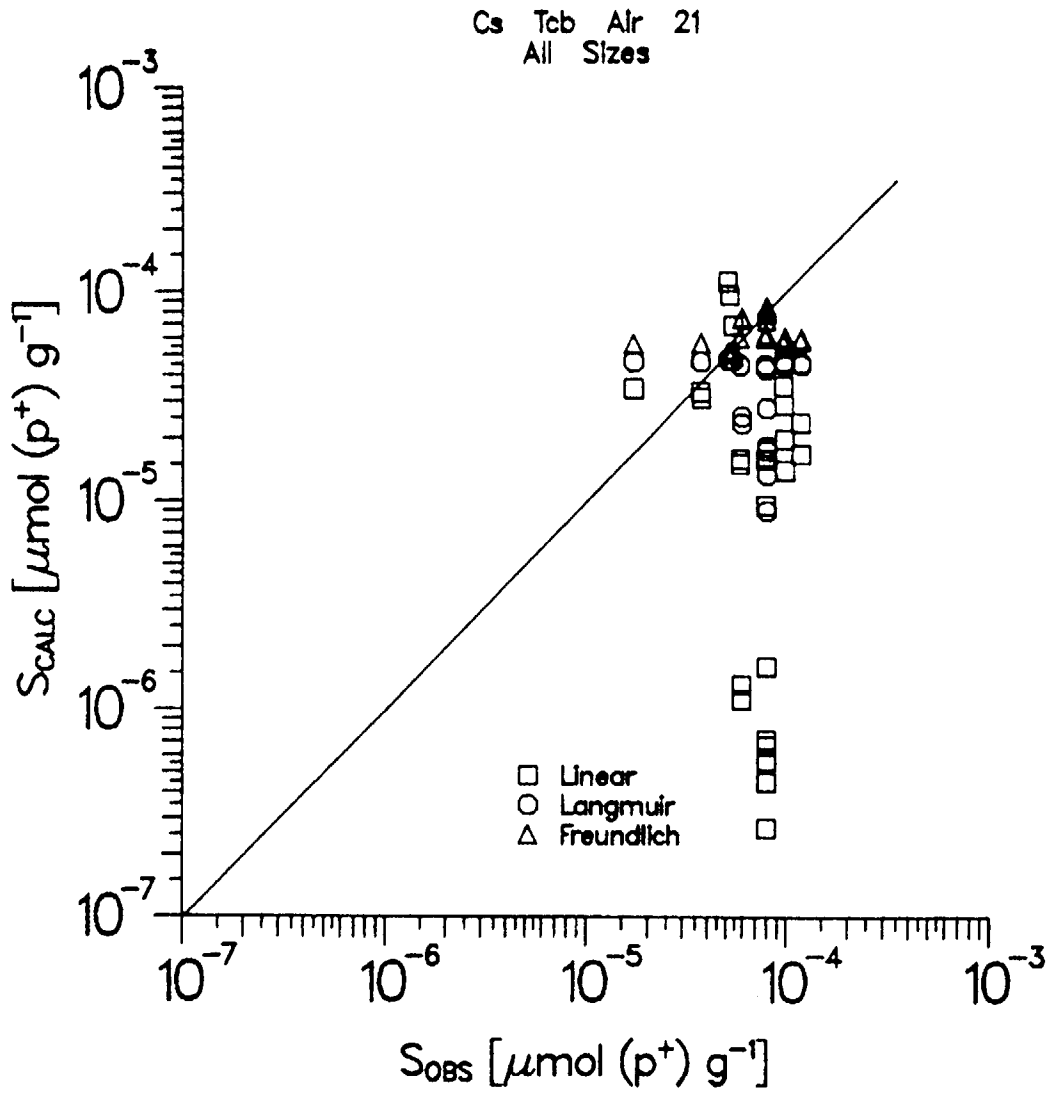
Cs Tcb Air 21
All Sizes
$10^{-3}$
$10^{-4}$
$10^{-5}$
$10^{-6}$
$10^{-7}$
$S_{CALC}$ [$\mu$mol ($p^+$) $g^{-1}$]
Linear
Langmuir
Freundlich
$10^{-7}$
$10^{-6}$
$10^{-5}$
$10^{-4}$
$10^{-3}$
$S_{OBS}$ [$\mu$mol ($p^+$) $g^{-1}$]

ELEMENT = Sr
FORMATION = Tcb
TIME = 21 days
ATMOS = Air
SIZE = All Sizes
SAMPLE = ja-28, ja-32, ym-54
gl-2233, gl-2289, gl-2333
gl-2410, gl-2476, gl-2363

| ISOTHERM | N | ALPHA | BETA | R**2 | SSE |
|---|---|---|---|---|---|
| LINEAR | 34 | 0.0000000 | 55.5507927 | 0.8090 | 0.00970933 |
| Kd = | 55.55079269 | | | | |
| LANGMUIR | 34 | 0.0047607 | 22.1895924 | 0.5599 | 0.00559750 |
| b = | 0.04506617 | | | | |
| k = | 4661.030761 | | | | |
| FREUNDLICH | 34 | 0.4074574 | 0.5562370 | 0.6956 | 0.62923747 |
| K = | 2.55539083 | | | | |
| N = | 0.55623704 | | | | |

N = the number of experimental points
ALPHA and BETA are respectively the intercept and slope from the linear regression analysis
R = correlation coefficient
SSE = standard error
Kd in mL/g
b in micromol(p+)/g and k in mL/micromol(p+)
K and N in units corresponding to solute adsorbed S in micromol(p+)/g and solute in solution C in micromol(p+)/mL.

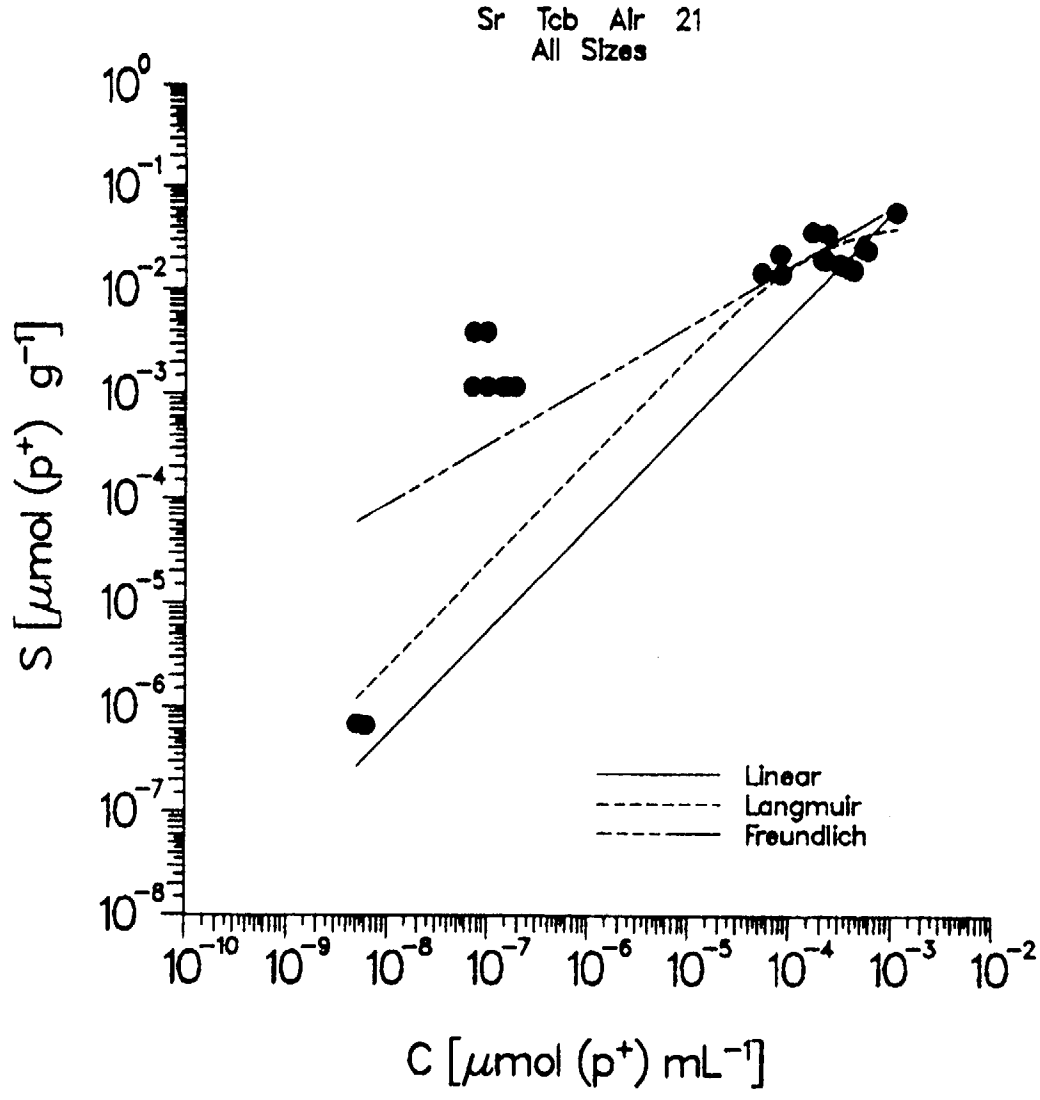
Sr Tcb Air 21
All Sizes
S [μmol (p+) g-1]
C [μmol (p+) mL-1]
Linear
Langmuir
Freundlich

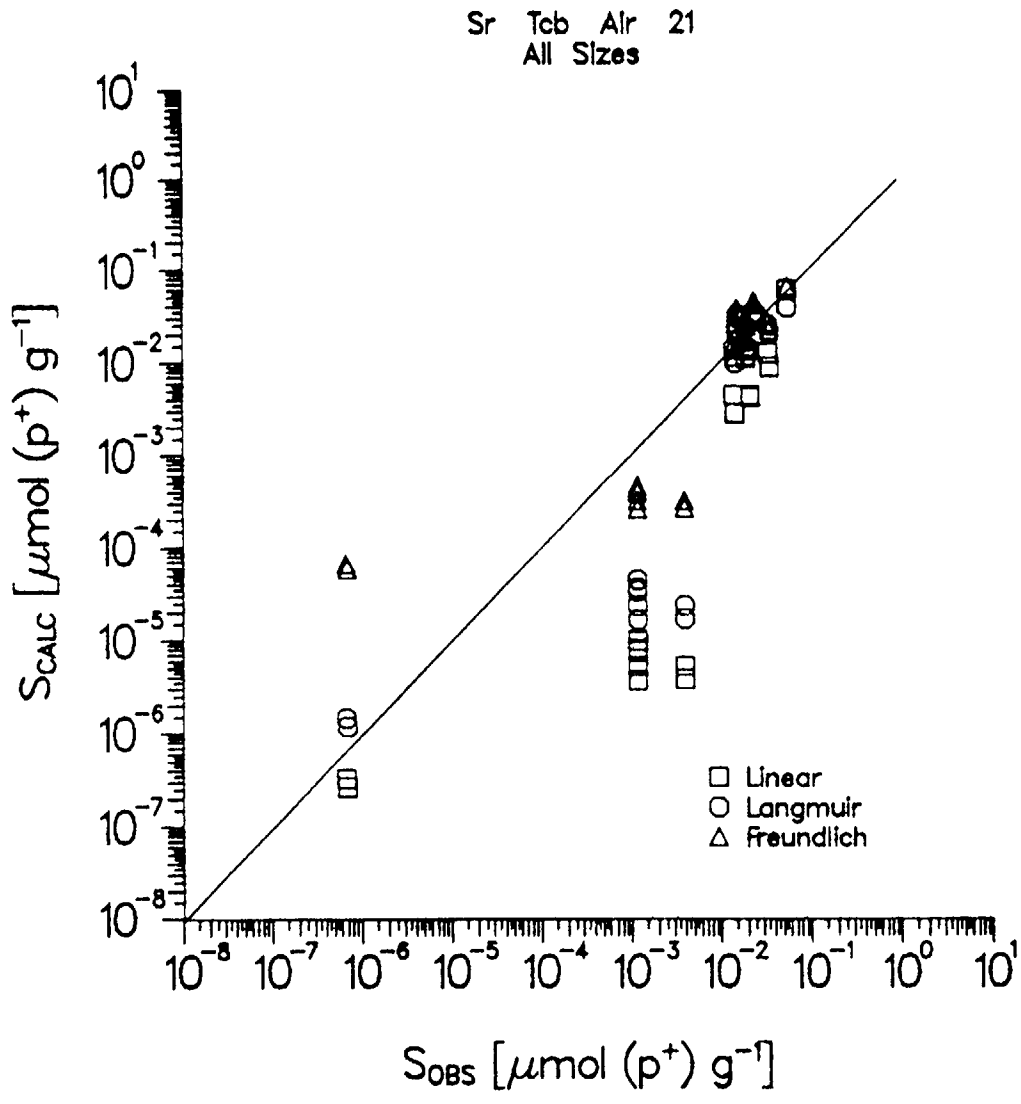
Sr Tcb Air 21
All Sizes
$S_{CALC}$ [$\mu$mol ($p^+$) $g^{-1}$]
$S_{OBS}$ [$\mu$mol ($p^+$) $g^{-1}$]
$10^{1}$
$10^{0}$
$10^{-1}$
$10^{-2}$
$10^{-3}$
$10^{-4}$
$10^{-5}$
$10^{-6}$
$10^{-7}$
$10^{-8}$
Linear
Langmuir
Freundlich

ELEMENT = Ce
FORMATION = Tcb
TIME = 21 days
ATMOS = Air
SIZE = All Sizes
SAMPLE = ja-28, ja-32, ym-54
gl-2233, gl-2289, gl-2333
gl-2410, gl-2476, gl-2363

| ISOTHERM | N | ALPHA | BETA | R**2 | SSE |
|---|---|---|---|---|---|
| LINEAR | 8 | 0.0000000 | 83.1219482 | 0.8280 | 0.01441253 |
| Kd = | 83.12194824 | | | | |
| LANGMUIR | 8 | 0.0016217 | 22.6662579 | 0.9149 | 0.00192191 |
| b = | 0.04411844 | | | | |
| k = | 13977.04395 | | | | |
| FREUNDLICH | 8 | 0.6069187 | 0.5955552 | 0.8906 | 0.23566556 |
| K = | 4.04500151 | | | | |
| N = | 0.59555519 | | | | |

N = the number of experimental points
ALPHA and BETA are respectively the intercept and slope from the linear regression analysis
R = correlation coefficient
SSE = standard error
Kd in mL/g
b in micromol(p+)/g and k in mL/micromol(p+)
K and N in units corresponding to solute adsorbed S in micromol(p+)/g and solute in solution C in micromol(p+)/mL.

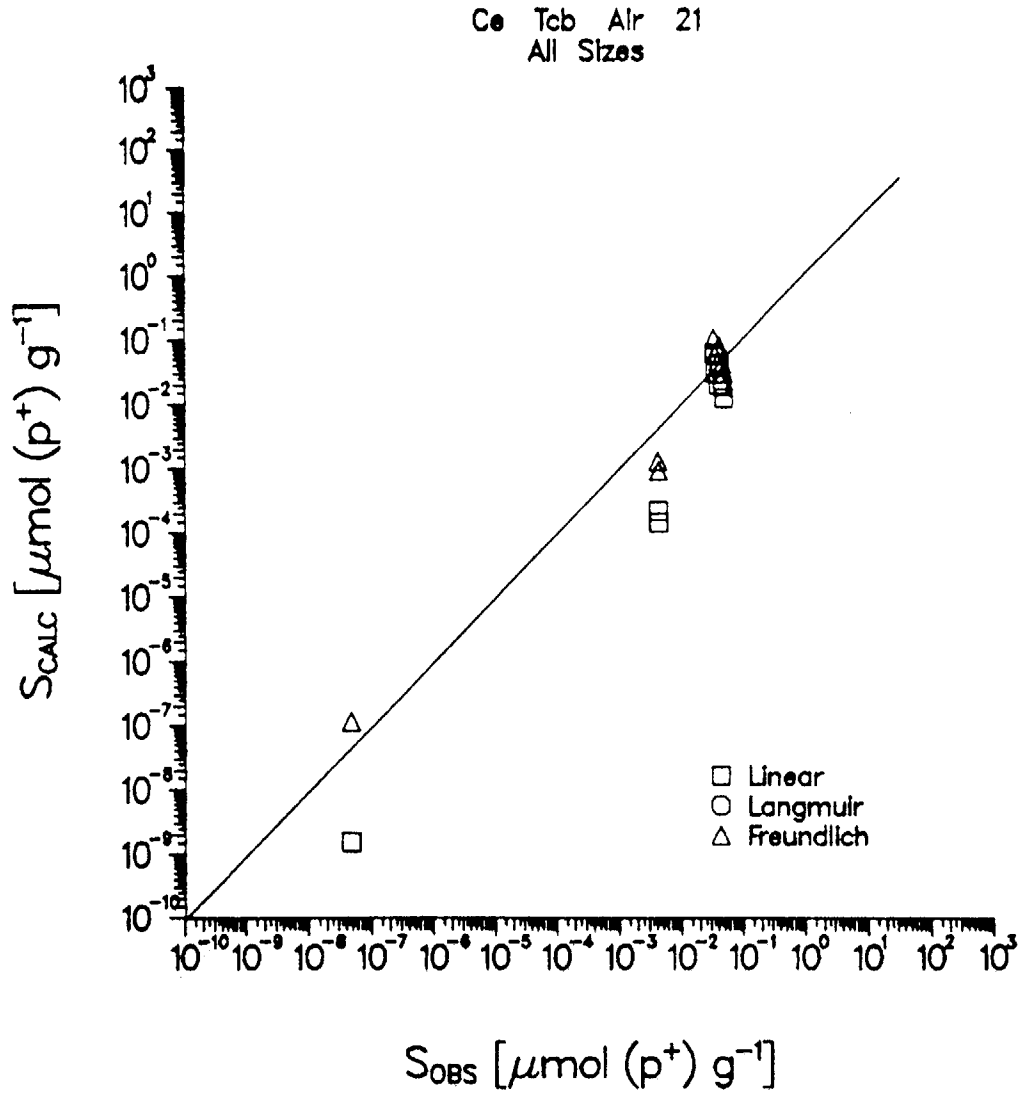
Ce Tcb Air 21
All Sizes
$S_{CALC}$ [$\mu$mol ($p^+$) $g^{-1}$]
$S_{OBS}$ [$\mu$mol ($p^+$) $g^{-1}$]
Linear
Langmuir
Freundlich

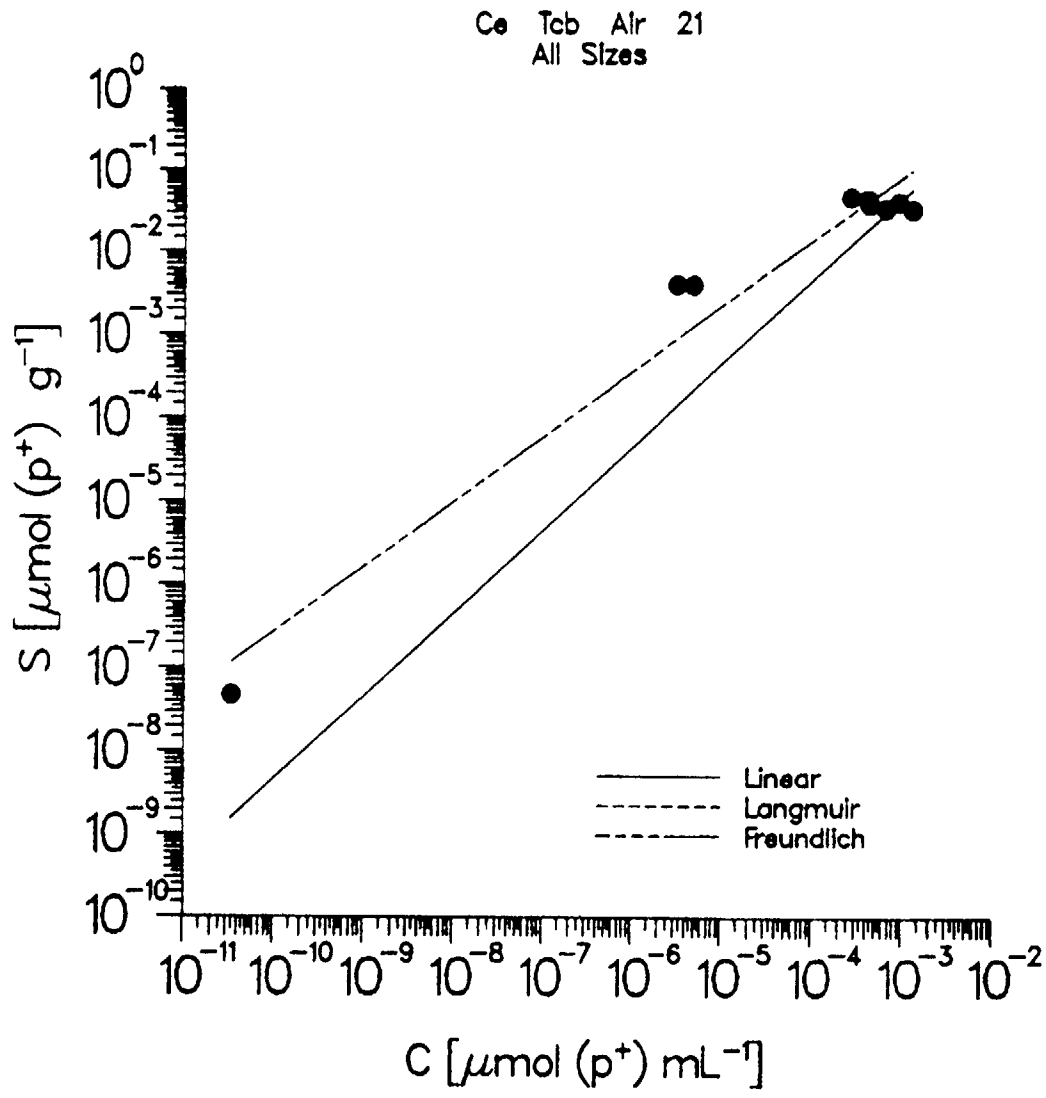
Ce Tcb Air 21
All Sizes
S [μmol (p+) g−1]
C [μmol (p+) mL−1]
Linear
Langmuir
Freundlich

ELEMENT = Ce
FORMATION = Tct
TIME = 21 days
ATMOS = Air
SIZE = All Sizes
SAMPLE = gl-2698, gl-2840, gl-2854
gl-2901, gl-3116, ja-37

| ISOTHERM | N | ALPHA | BETA | R**2 | SSE |
|---|---|---|---|---|---|
| LINEAR | 6 | 0.0000000 | 104.8313370 | 0.8494 | 0.00200447 |
| Kd = | 104.83133698 | | | | |
| LANGMUIR | 6 | -0.0001960 | 206.1669464 | 0.9960 | 0.00037699 |
| b = | 0.00485044 | | | | |
| k = | -1051694.25 | | | | |
| FREUNDLICH | 6 | -1.0574173 | 0.2810357 | 0.9844 | 0.07052707 |
| K = | 0.08761586 | | | | |
| N = | 0.28103569 | | | | |

N = the number of experimental points
ALPHA and BETA are respectively the intercept and slope from the linear regression analysis
R = correlation coefficient
SSE = standard error
Kd in mL/g
b in micromol(p+)/g and k in mL/micromol(p+)
K and N in units corresponding to solute adsorbed S in micromol(p+)/g and solute in solution C in micromol(p+)/mL.

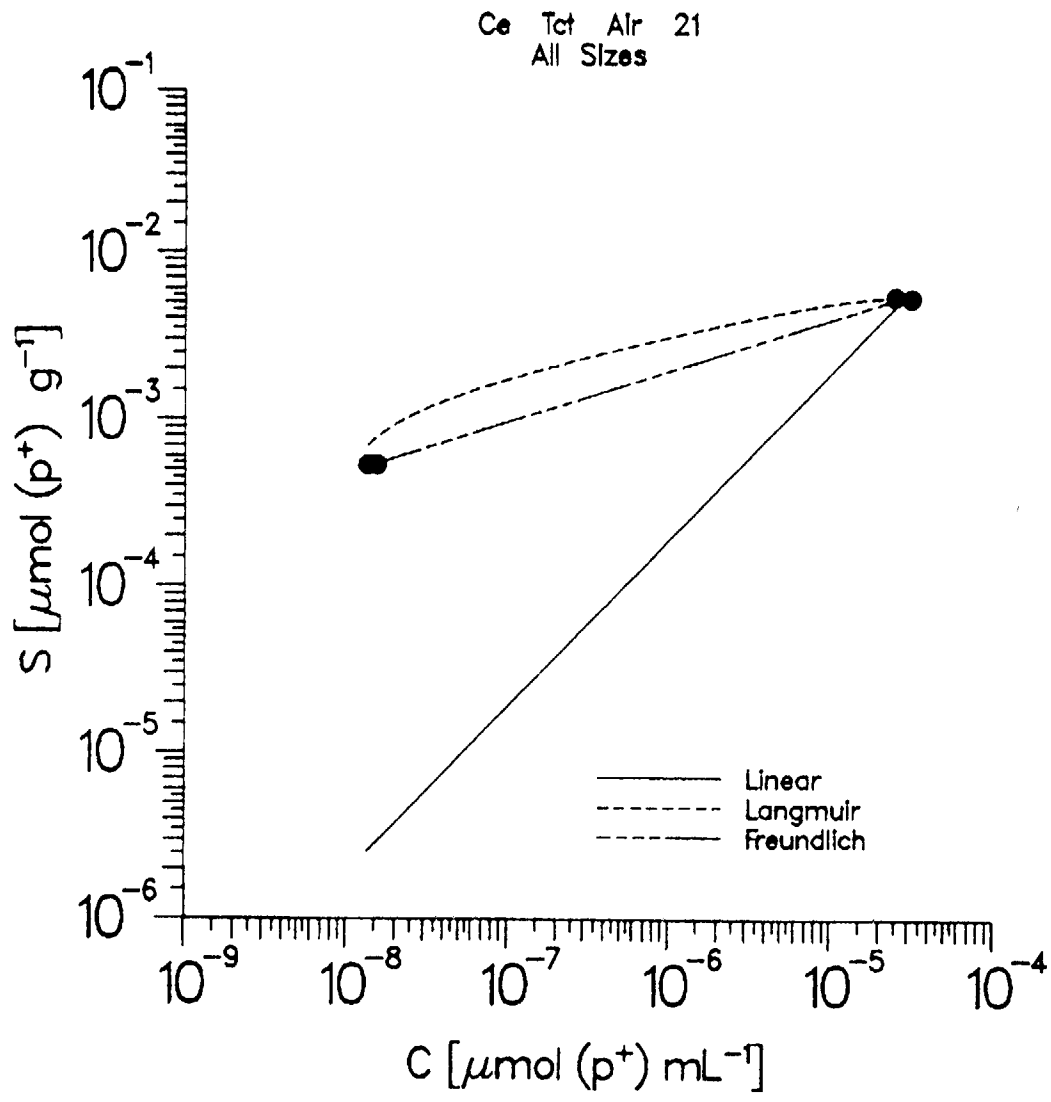
Ce Tct Air 21
All Sizes
S [μmol (p+) g-1]
C [μmol (p+) mL-1]
10-1
10-2
10-3
10-4
10-5
10-6
10-9
10-8
10-7
10-6
10-5
10-4
Linear
Langmuir
Freundlich

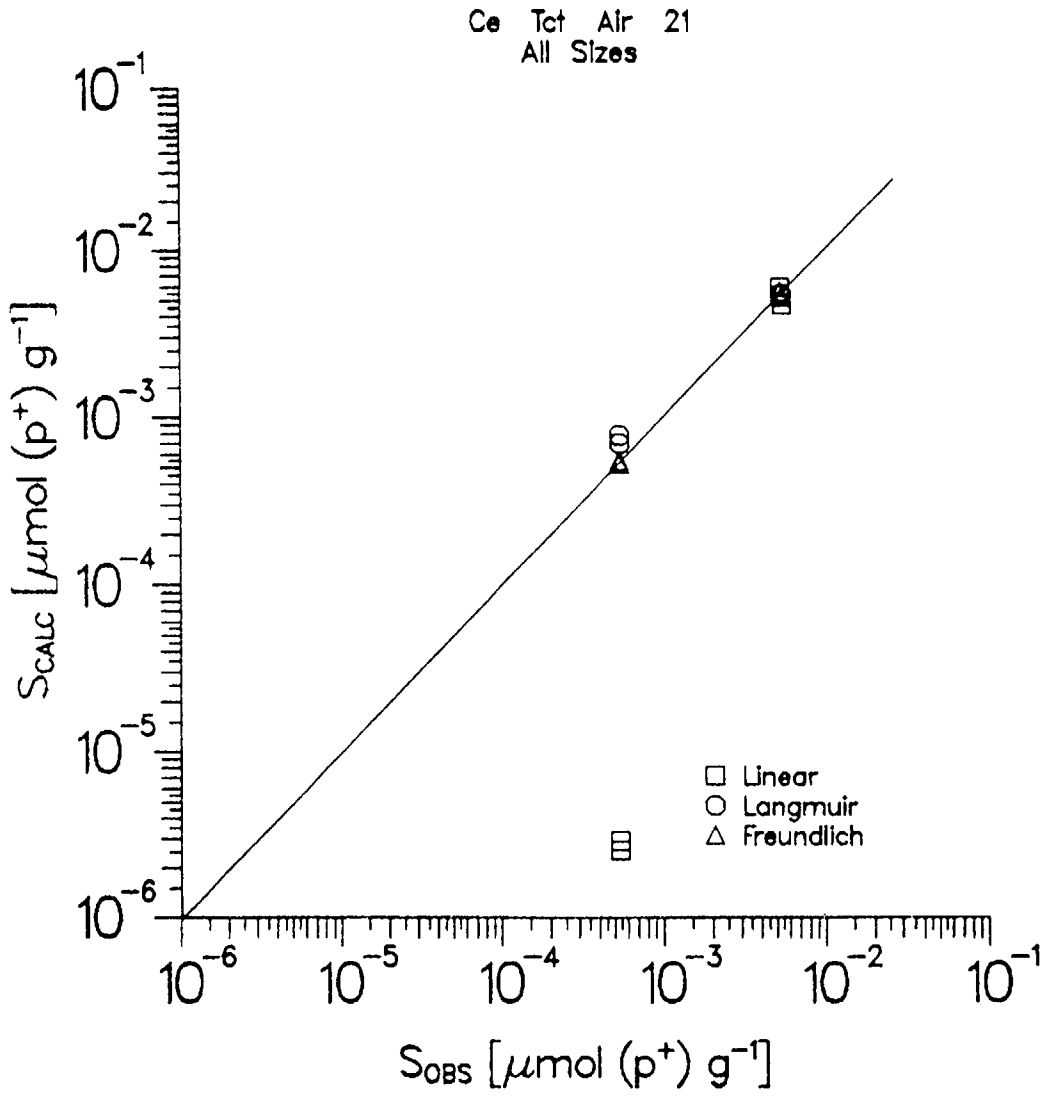
Ce Tct Air 21
All Sizes
$10^{-1}$
$10^{-2}$
$10^{-3}$
$10^{-4}$
$10^{-5}$
$10^{-6}$
$S_{CALC}$ [$\mu$mol ($p^+$) $g^{-1}$]
$10^{-6}$
$10^{-5}$
$10^{-4}$
$10^{-3}$
$10^{-2}$
$10^{-1}$
$S_{OBS}$ [$\mu$mol ($p^+$) $g^{-1}$]
Linear
Langmuir
Freundlich

ELEMENT = Eu
FORMATION = Tct
TIME = 21 days
ATMOS = Air
SIZE = All Sizes
SAMPLE = gl-2698, gl-2840, gl-2854
gl-2901, gl-3116, ja-37

| ISOTHERM | N | ALPHA | BETA | R**2 | SSE |
|---|---|---|---|---|---|
| LINEAR | 12 | 0.0000000 | 158.7687836 | 0.5579 | 0.00900878 |
| Kd = | 158.76878357 | | | | |
| LANGMUIR | 12 | 0.0003466 | 45.2917557 | 0.9803 | 0.00036257 |
| b = | 0.02207907 | | | | |
| k = | 130693.0546875 | | | | |
| FREUNDLICH | 12 | -0.6449764 | 0.2838752 | 0.5267 | 0.38011524 |
| K = | 0.22647674 | | | | |
| N = | 0.28387523 | | | | |

N = the number of experimental points
ALPHA and BETA are respectively the intercept and slope from the linear regression analysis
R = correlation coefficient
SSE = standard error
Kd in mL/g
b in micromol(p+)/g and k in mL/micromol(p+)
K and N in units corresponding to solute adsorbed S in micromol(p+)/g and solute in solution C in micromol(p+)/mL.

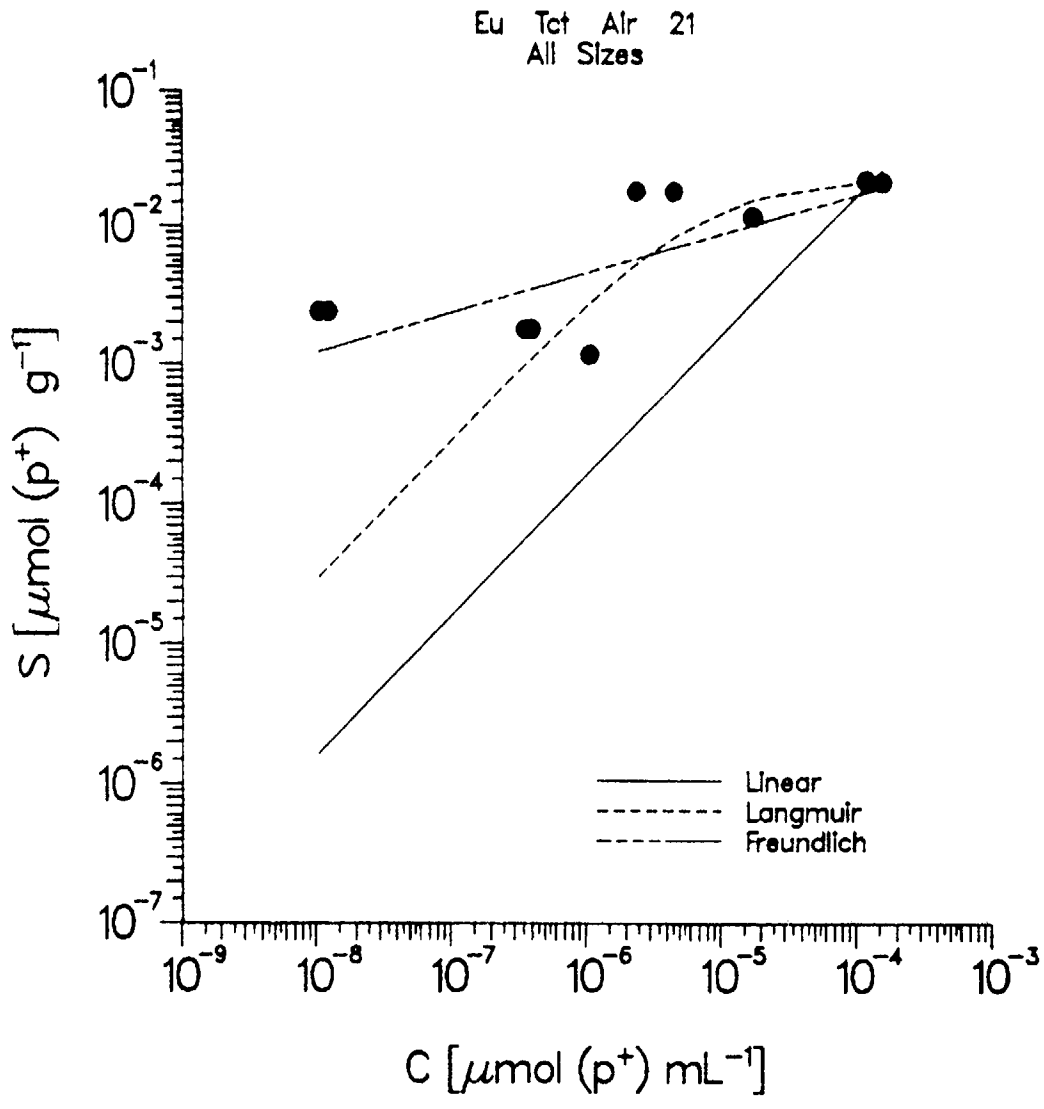
Eu Tot Air 21
All Sizes
S [μmol (p+) g-1]
C [μmol (p+) mL-1]
Linear
Langmuir
Freundlich

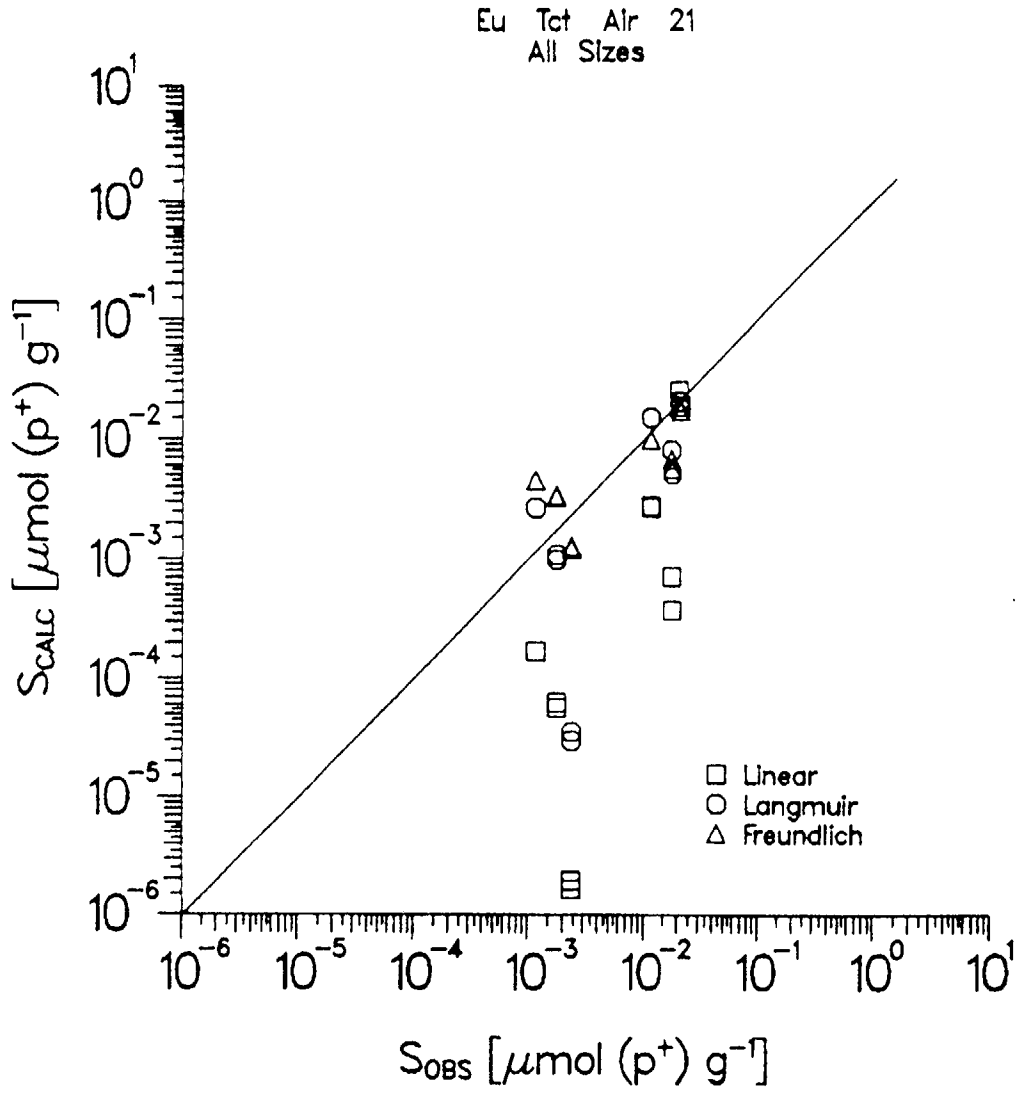
Eu Tct Air 21
All Sizes
$S_{CALC}$ [$\mu$mol ($p^+$) $g^{-1}$]
$S_{OBS}$ [$\mu$mol ($p^+$) $g^{-1}$]
$10^{1}$
$10^{0}$
$10^{-1}$
$10^{-2}$
$10^{-3}$
$10^{-4}$
$10^{-5}$
$10^{-6}$
Linear
Langmuir
Freundlich

ELEMENT = Ba
FORMATION = Tct
TIME = 21 days
ATMOS = Air
SIZE = All Sizes
SAMPLE = gl-2698, gl-2840, gl-2854
gl-2901, gl-3116, ja-37

| ISOTHERM | N | ALPHA | BETA | R**2 | SSE |
|---|---|---|---|---|---|
| LINEAR | 12 | 0.0000000 | 949.2368164 | 0.0496 | 0.21344635 |
| Kd = | 949.23681641 | | | | |
| LANGMUIR | 12 | 0.0003109 | 10.2722054 | 0.6396 | 0.00033218 |
| b = | 0.09735008 | | | | |
| k = | 33042.16796875 | | | | |
| FREUNDLICH | 12 | -0.4262900 | 0.1784030 | 0.0200 | 0.80267102 |
| K = | 0.37472266 | | | | |
| N = | 0.17840299 | | | | |

N = the number of experimental points
ALPHA and BETA are respectively the intercept and slope from the linear regression analysis
R = correlation coefficient
SSE = standard error
Kd in mL/g
b in micromol(p+)/g and k in mL/micromol(p+)
K and N in units corresponding to solute adsorbed S in micromol(p+)/g and solute in solution C in micromol(p+)/mL.

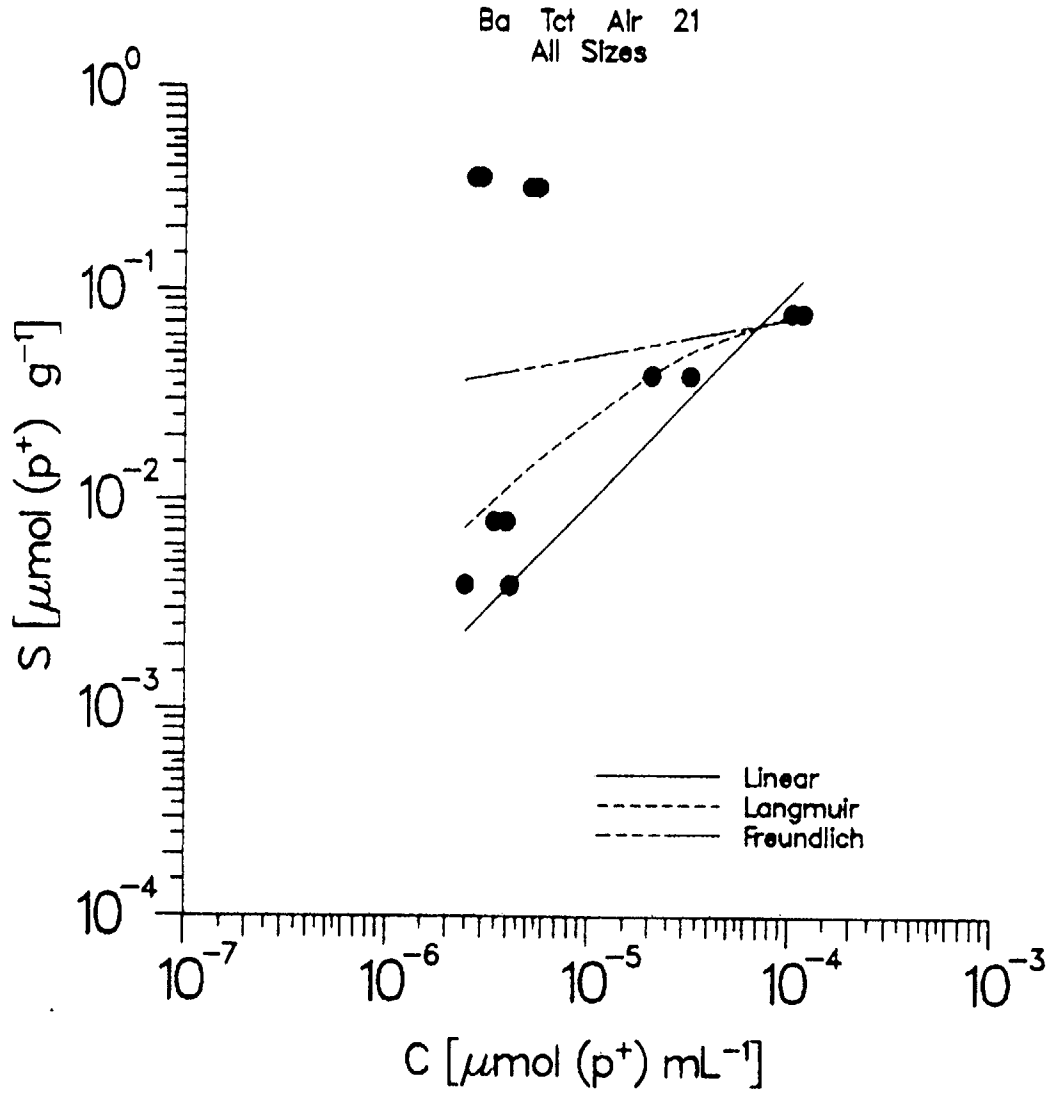
Ba Tct Air 21
All Sizes
S [μmol (p+) g−1]
C [μmol (p+) mL−1]
10^0
10^−1
10^−2
10^−3
10^−4
10^−7
10^−6
10^−5
10^−4
10^−3
Linear
Langmuir
Freundlich

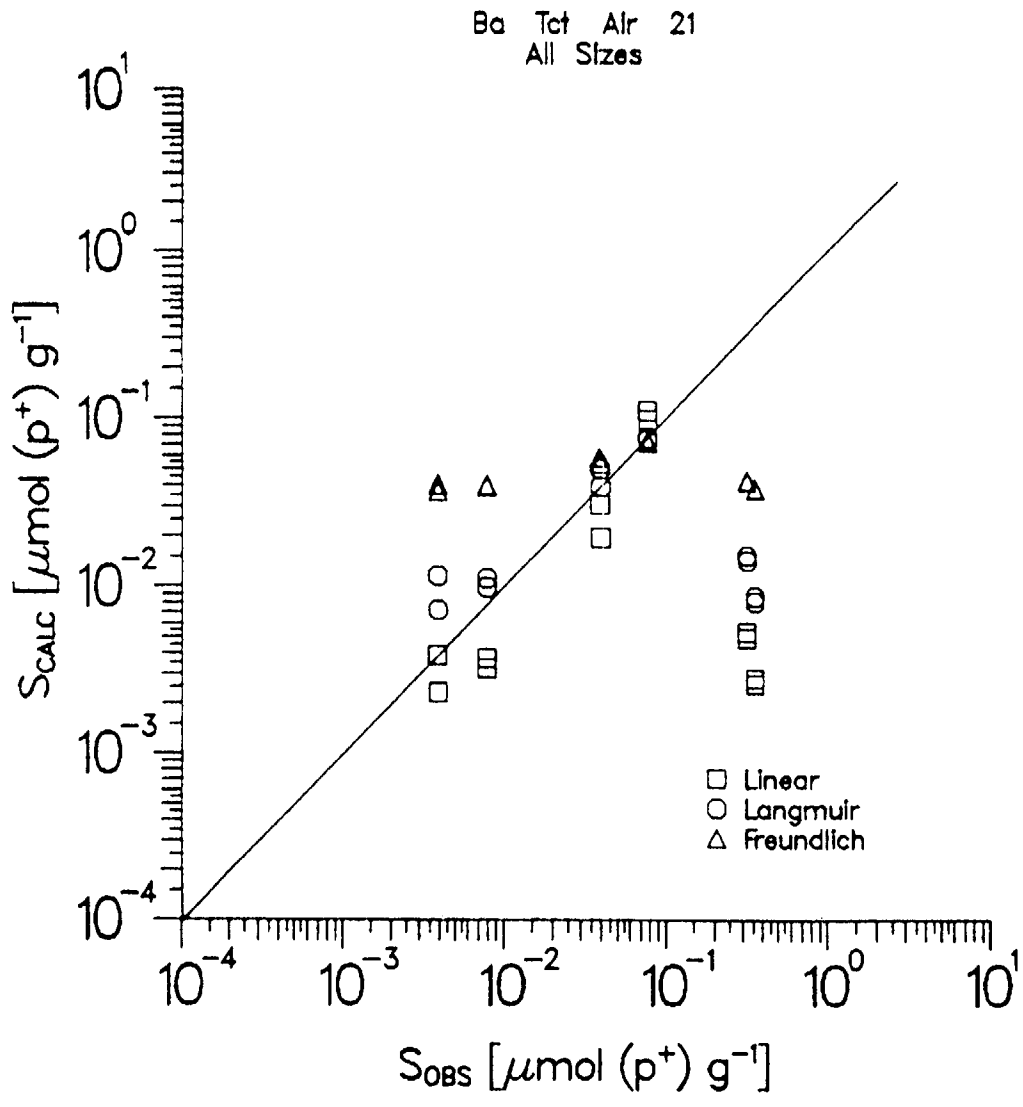
Ba Tct Air 21
All Sizes
$S_{CALC}$ [$\mu$mol ($p^+$) $g^{-1}$]
$S_{OBS}$ [$\mu$mol ($p^+$) $g^{-1}$]
$10^{1}$
$10^{0}$
$10^{-1}$
$10^{-2}$
$10^{-3}$
$10^{-4}$
Linear
Langmuir
Freundlich

ELEMENT = Cs
FORMATION = Tct
TIME = 21 days
ATMOS = Air
SIZE = All Sizes
SAMPLE = gl-2698, gl-2840, gl-2854
gl-2901, gl-3116, ja-37

| ISOTHERM | N | ALPHA | BETA | R**2 | SSE |
|---|---|---|---|---|---|
| LINEAR | 36 | 0.0000000 | 20.7846336 | 0.9886 | 0.38613573 |
| Kd = | 20.78463364 | | | | |
| LANGMUIR | 36 | 0.0058916 | 0.0799923 | 0.6989 | 0.00854316 |
| b = | 12.50120544 | | | | |
| k = | 13.57728863 | | | | |
| FREUNDLICH | 36 | 1.1475337 | 0.6967567 | 0.9914 | 0.17415506 |
| K = | 14.04538536 | | | | |
| N = | 0.69675672 | | | | |

N = the number of experimental points
ALPHA and BETA are respectively the intercept and slope from the linear regression analysis
R = correlation coefficient
SSE = standard error
Kd in mL/g
b in micromol(p+)/g and k in mL/micromol(p+)
K and N in units corresponding to solute adsorbed S in micromol(p+)/g and solute in solution C in micromol(p+).

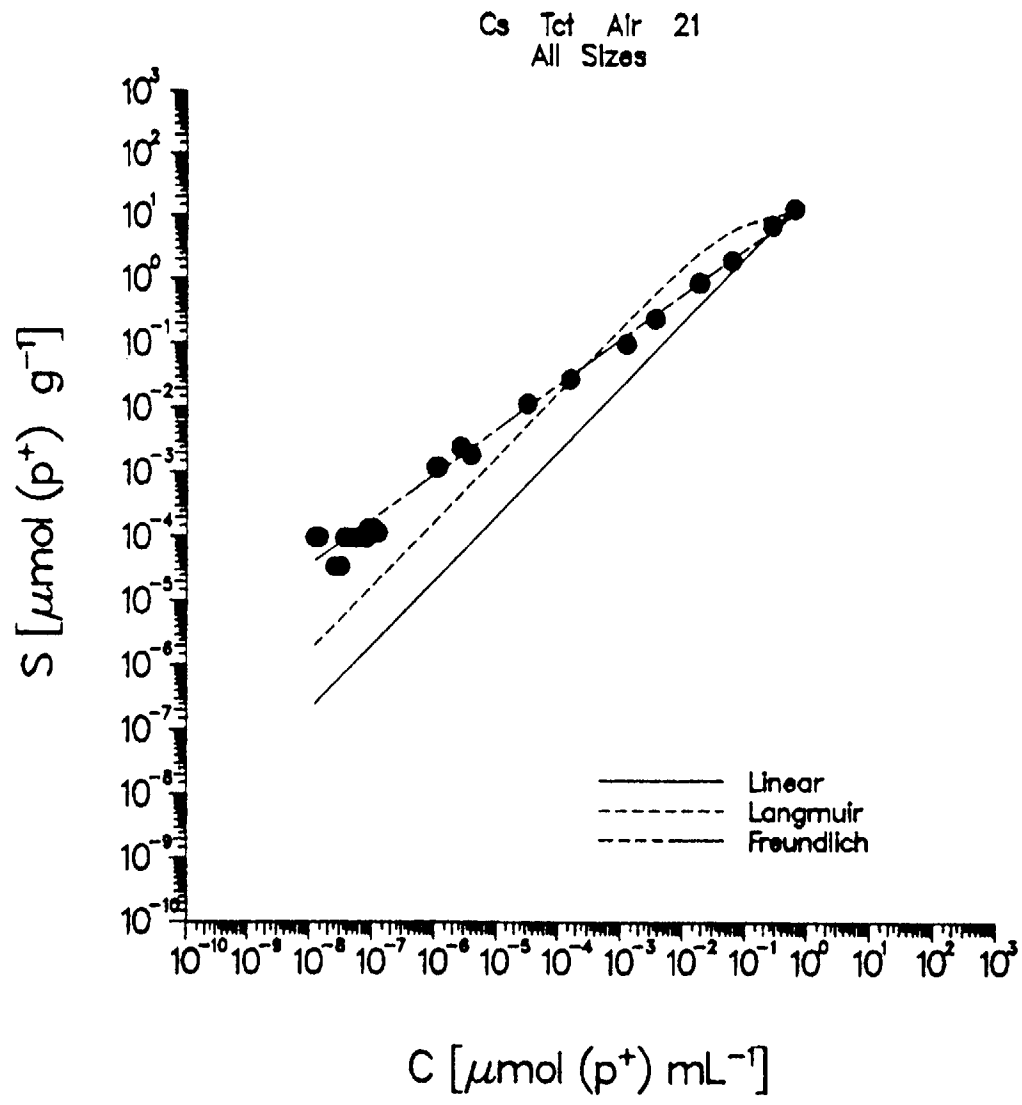
Cs Tct Air 21
All Sizes
S [μmol (p+) g−1]
C [μmol (p+) mL−1]
Linear
Langmuir
Freundlich

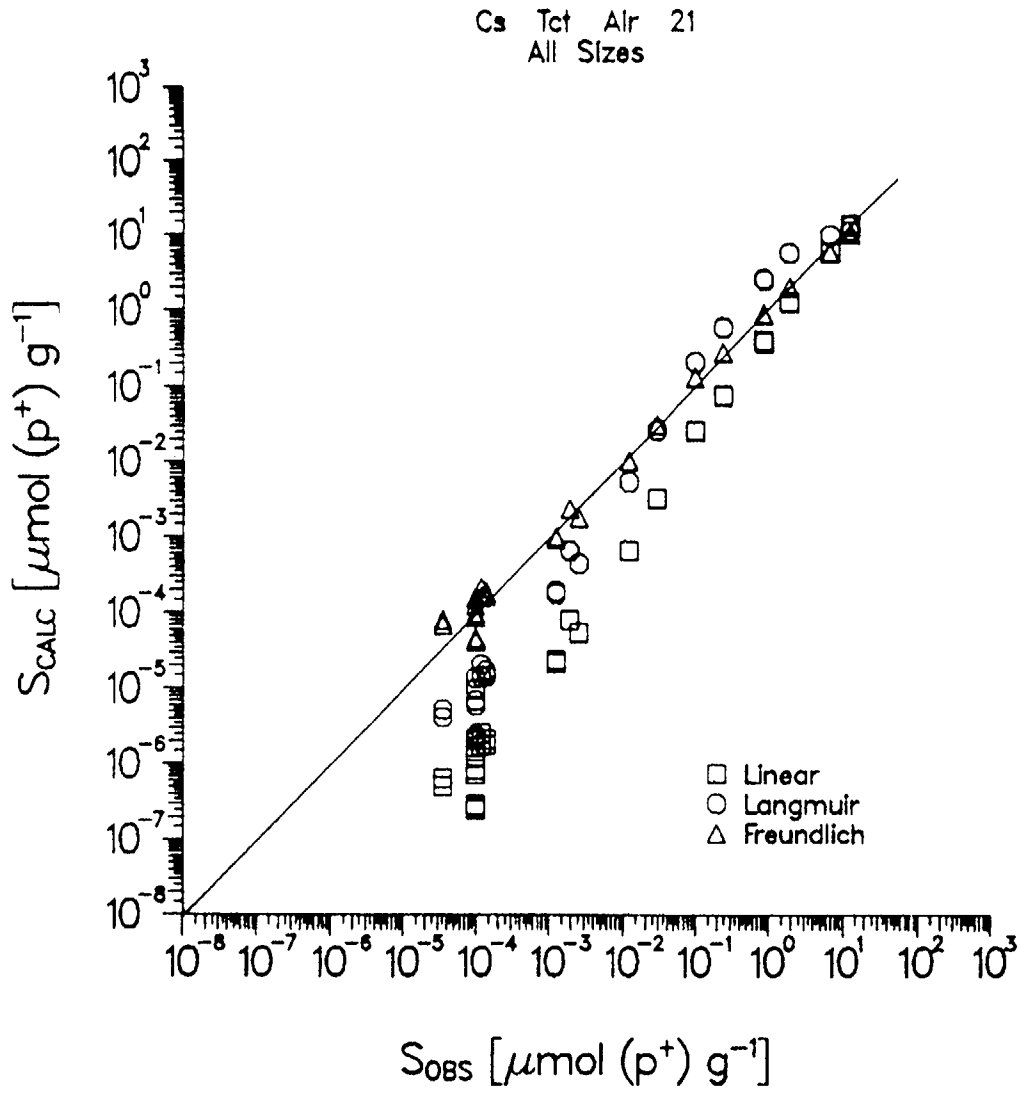
Cs Tct Air 21
All Sizes
$S_{CALC}$ [$\mu$mol ($p^+$) $g^{-1}$]
$S_{OBS}$ [$\mu$mol ($p^+$) $g^{-1}$]
$10^{3}$
$10^{2}$
$10^{1}$
$10^{0}$
$10^{-1}$
$10^{-2}$
$10^{-3}$
$10^{-4}$
$10^{-5}$
$10^{-6}$
$10^{-7}$
$10^{-8}$
Linear
Langmuir
Freundlich

ELEMENT = Sr
FORMATION = Tct
TIME = 21 days
ATMOS = Air
SIZE = All Sizes
SAMPLE = gl-2698, gl-2840, gl-2854
gl-2901, gl-3116, ja-37

| ISOTHERM | N | ALPHA | BETA | R**2 | SSE |
|---|---|---|---|---|---|
| LINEAR | 36 | 0.0000000 | 11.7582045 | 0.8664 | 2.50288343 |
| Kd = | 11.75820446 | | | | |
| LANGMUIR | 36 | 0.0130842 | 0.0512120 | 0.9356 | 0.00660968 |
| b = | 19.52666473 | | | | |
| k = | 3.9140484333 | | | | |
| FREUNDLICH | 36 | 0.9864843 | 0.6011319 | 0.8997 | 0.38164452 |
| K = | 9.69358349 | | | | |
| N = | 0.60113192 | | | | |

N = the number of experimental points
ALPHA and BETA are respectively the intercept and slope from the linear regression analysis
R = correlation coefficient
SSE = standard error
Kd in mL/g
b in micromol(p+)/g and k in mL/micromol(p+)
K and N in units corresponding to solute adsorbed S in micromol(p+)/g and solute in solution C in micromol(p+)/mL.

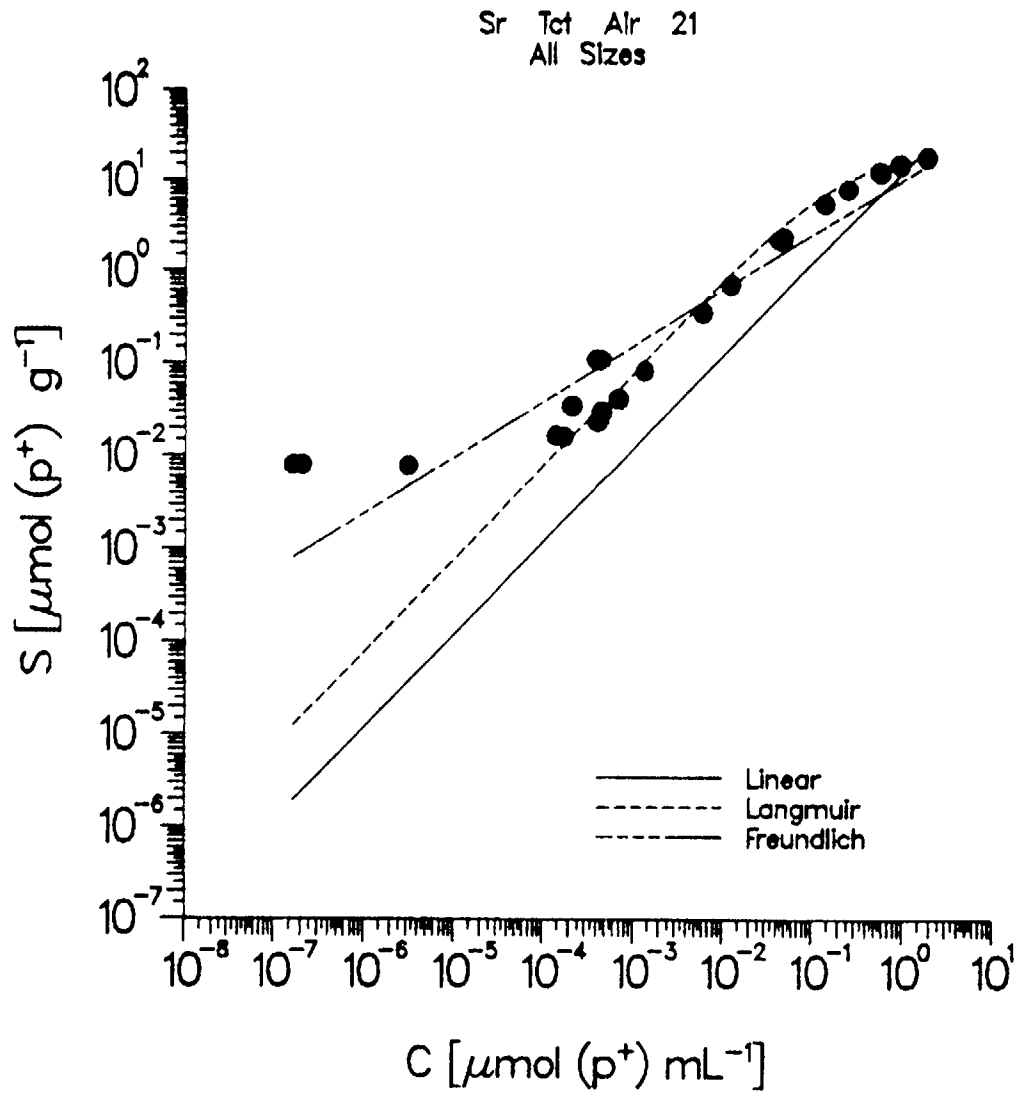
Sr Tct Air 21
All Sizes
S [μmol (p+) g−1]
C [μmol (p+) mL−1]
Linear
Langmuir
Freundlich

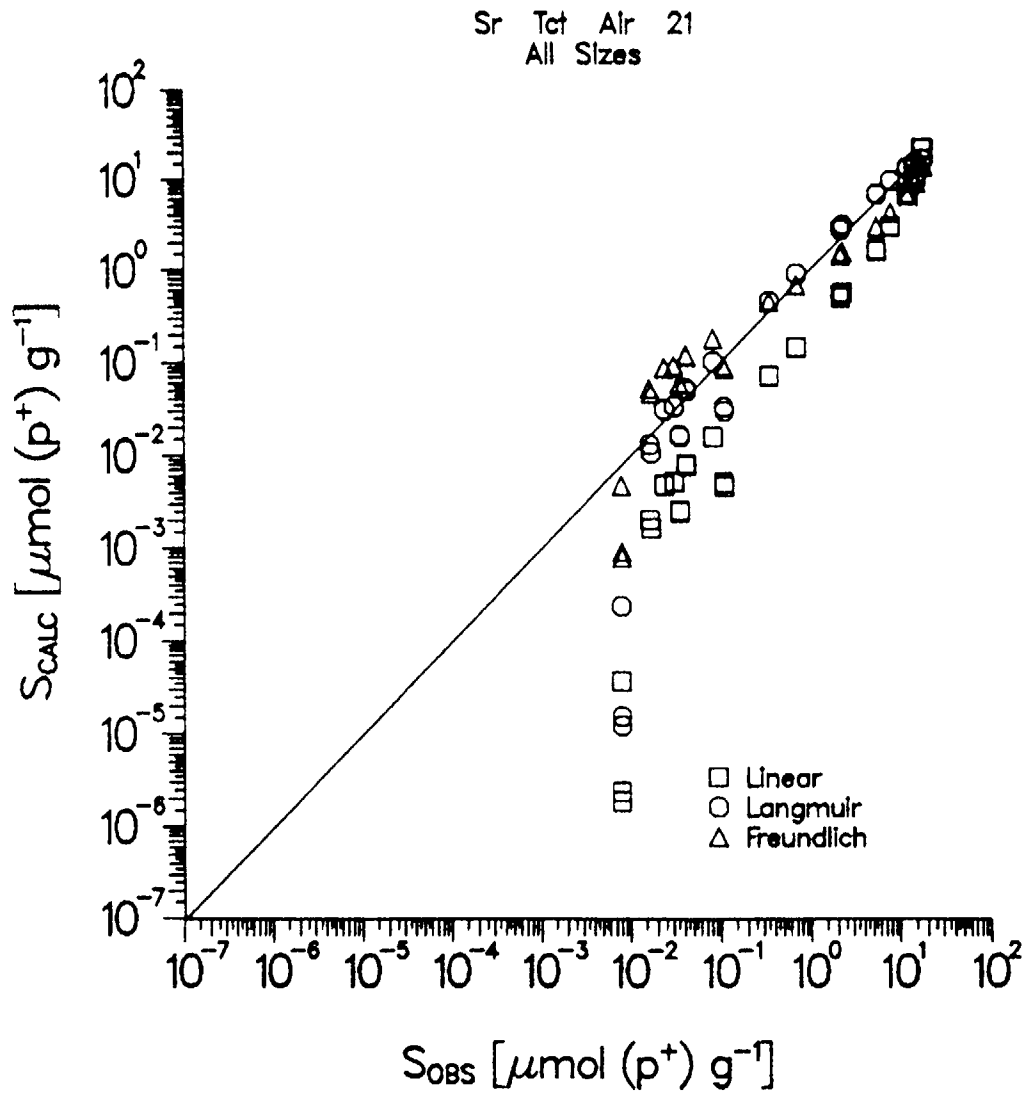
Sr Tct Air 21
All Sizes
$S_{CALC}$ [$\mu$mol ($p^+$) $g^{-1}$]
$S_{OBS}$ [$\mu$mol ($p^+$) $g^{-1}$]
$10^{2}$
$10^{1}$
$10^{0}$
$10^{-1}$
$10^{-2}$
$10^{-3}$
$10^{-4}$
$10^{-5}$
$10^{-6}$
$10^{-7}$
Linear
Langmuir
Freundlich

☆U.S. GOVERNMENT PRINTING OFFICE: 1987—773-103/60033

Printed in the United States of America
Available from
National Technical Information Service
US Department of Commerce
5285 Port Royal Road
Springfield, VA 22161

Microfiche (A01)

| Page Range | NTIS Price Code | Page Range | NTIS Price Code | Page Range | NTIS Price Code | Page Range | NTIS Price Code |
|---|---|---|---|---|---|---|---|
| 001-025 | A02 | 151-175 | A08 | 301-325 | A14 | 451-475 | A20 |
| 026-050 | A03 | 176-200 | A09 | 326-350 | A15 | 476-500 | A21 |
| 051-075 | A04 | 201-225 | A10 | 351-375 | A16 | 501-525 | A22 |
| 076-100 | A05 | 226-250 | A11 | 376-400 | A17 | 526-550 | A23 |
| 101-125 | A06 | 251-275 | A12 | 401-425 | A18 | 551-575 | A24 |
| 126-150 | A07 | 276-300 | A13 | 426-450 | A19 | 576-600 | A25 |
| | | | | | | 601-up* | A99 |

*Contact NTIS for a price quote.

Published in Journal of Physical Chemistry, July 13, 1989, 5617–5623, by the American Chemical Society

# Deconvolution of Multivalent Cation-Exchange Isotherms

**Inés R. Triay and Robert S. Rundberg***

*Los Alamos National Laboratory, Los Alamos, New Mexico 87545* *(Received: April 25, 1988; In Final Form: September 28, 1988)*

A method of deconvolution has been developed to determine the site-specific selectivity coefficients for divalent and trivalent exchange in relatively rigid exchangers. The technique involves the measurement of ion-exchange isotherms and the application of the numerical approach of regularization to effect deconvolution. The method has been designed and extensively tested with computer-generated isotherms. The results of these numerical studies indicate that this approach can successfully recover selectivity coefficient distributions from divalent and trivalent isotherms. If a careful accounting of the exchanging cations is maintained, this method can be applied to systems undergoing ion exchange by different mechanisms.

## Introduction

The method of deconvolution of monovalent ion-exchange isotherms[1] has been applied to isotherms obtained from the literature describing the behavior of exchanging univalent cations in the zeolites Na–X and Na–Y. The number of cations exchanging with a particular selectivity coefficient obtained from deconvolution[2] has been correlated with the cation-site populations in the exchanger obtained crystallographically. The results indicate that the selectivity coefficients obtained from deconvolution are site specific and can be used to study the effects of the exchanger's structure on cation-exchange properties.

The objective of this work was to design a method to deconvolve ion-exchange isotherms resulting from divalent and trivalent cations that are undergoing exchange. The method involves maintaining a careful accounting of the exchanging cations in order to determine the different species involved in the observed exchange. An ion-exchange isotherm (defined as the equilibrium solid-phase concentration of a given ion as a function of the aqueous-phase concentration when the temperature is held constant) needs to be determined for each of the different exchange processes. For instance, multivalent cation exchange can exhibit "over exchange". This phenomenon has been experimentally observed by McCusker and Seff[3] for the $Cd^{2+}$ exchange in zeolite A. These authors reported the extensive participation of $CdCl^+$ and $CdOH^+$ in the ion exchange process. In this case, an isotherm must be measured for each of the Cd species in the solid phase.

The thermodynamics for ion exchange have been reviewed by Cremers.[4] The theoretical basis for ion exchange involving several groups of homogeneous sites in the exchanger has been examined by Barrer and Klinowski.[5] Among the authors who have successfully analyzed ion exchange in terms of different types of sites, Barrer and Munday[6] interpreted exchange isotherms in the zeolite K–F by assuming two types of sites; Brouwer et al.[7] described the exchange of cesium and rubidium ions in illite clay in terms of three kinds of sites. Consequently, the ion-exchange process is assumed to be a set of simultaneous equilibria as in eq 1, where

$$z_2M_1^{z_1+}(s^1) + z_1M_2^{z_2+}(aq) = z_2M_1^{z_1+}(aq) + z_1M_2^{z_2+}(s^1) \quad (1a)$$

$$z_2M_1^{z_1+}(s^j) + z_1M_2^{z_2+}(aq) = z_2M_1^{z_1+}(aq) + z_1M_2^{z_2+}(s^j) \quad (1b)$$

$s^1, \ldots, s^j$ represent different sites in the exchanger. The selectivity coefficient for the exchange in site $i$, $K^i$, is given in eq 2, where

$$K^i = \frac{(q_2^i/Q^i)^{z_1}(a_1)^{z_2}}{(q_1^i/Q^i)^{z_2}(a_2)^{z_1}} \quad (2)$$

$a_1$ and $a_2$ are the activities in the aqueous phase of the cation to be exchanged and the ingoing cation, respectively; $q_1^i$ and $q_2^i$ are the concentrations of these cations in site $i$ of the exchanger (expressed as equivalents per gram of exchanger); and $Q^i$ is the total equivalents of exchangeable cations in site $i$ of the exchanger per gram of exchanger.

The equivalent fraction of $M_2^{z_2+}$ in site $i$ at a given concentration of $M_2^{z_2+}$ in the aqueous phase follows immediately from eq 2 as

(1) Triay, I. R.; Rundberg, R. S. *J. Phys. Chem.* **1987**, *91*, 5269.
(2) Triay, I. R.; Rundberg, R. S. Application of Deconvolution to the Analysis of Univalent Ion-Exchange Isotherms in Zeolites X and Y. Submitted for publication in *Zeolites*.
(3) McCusker, L. B.; Seff, K. *J. Am. Chem. Soc.* **1978**, *100*, 5052.
(4) Cremers, A. In *Molecular Sieves—II*; Katzer, J. R., Ed.; ACS Symposium Series 40; American Chemical Society: Washington, DC, 1977; p 179.
(5) Barrer, R. M.; Klinowski, J. *J. Chem. Soc., Faraday Trans. I* **1972**, *68*, 73.
(6) Barrer, R. M.; Munday, B. M. *J. Chem. Soc. A* **1971**, 2914.
(7) Brouwer, E.; Baeyens, B.; Maes, A.; Cremers, A. *J. Phys. Chem.* **1983**, *87*, 1213.

a result of mass balance considerations. For instance, the equivalent fraction in site $i$ of the solid phase for an ingoing divalent cation exchanging with a monovalent cation ($z_1 = 1$, $z_2 = 2$) is given in eq 3, where $C_0$ is the total concentration of cations

Divalent Case

$$\frac{q_2^i}{Q^i} = \theta_2(C_2, K^i) = \tfrac{1}{2}[2 + d - (4d + d^2)^{1/2}] \qquad (3)$$

$$d = \frac{(C_0^2/C_2 - 2C_0 + C_2)\gamma_1^2}{K^i\gamma_2}$$

in the aqueous phase (in terms of normality), $C_2$ is the aqueous-phase concentration of the ingoing cation, and $\gamma_1$ and $\gamma_2$ are the activity coefficients in the aqueous phase of the cation to be exchanged and the ingoing cation, respectively. Similarly, the equivalent fraction in site $i$ of the solid phase for an ingoing trivalent cation exchanging with a monovalent cation ($z_1 = 1$, $z_2 = 3$) is given in eq 4.

Trivalent Case

$$\theta_2(C_2, K^i) = X + Y + 1 \qquad (4)$$

$$X = (-y/2 + (y^2/4 + x^3/27)^{1/2})^{1/3}$$

$$Y = (-y/2 - (y^2/4 + x^3/27)^{1/2})^{1/3}$$

$$x = \tfrac{1}{3}(3w - p^2) \qquad y = \tfrac{1}{27}(2p^3 - 9pw + 27r)$$

$$p = -3 \qquad w = 3 + \frac{(C_0^3/C_2 - 3C_0^2 + 3C_2C_0 - C_2^2)\gamma_1^3}{K^i\gamma_2}$$

$$r = -1$$

In the general case, the total equivalent fraction of $M_2^{z_2+}$ in the solid phase is given by eq 5, where $q_2$ is the total equivalents of $M_2^{z_2+}$ in the solid phase per gram of exchanger and $Q$ is the

$$\frac{q_2(C_2)}{Q} = \sum_{i=1}^{j} \frac{Q^i}{Q}\theta_2(C_2, K^i) \qquad (5)$$

total equivalents of exchangeable sites per gram of exchanger. This approach can be further generalized to include subtler differences in sites, such as variations in aluminum ordering within a class of sites, by replacing the sum in eq 5 with the integral in eq 6, where $f(K)$ is a distribution function for the selectivity coefficient of the exchange.

$$\frac{q_2(C_2)}{Q} = \int \theta_2(C_2, K)\, f(K)\, dK \qquad (6)$$

The idea of expressing the heterogeneity of the exchanger's surface in terms of distribution function was previously presented.[8-10] As discussed by Sposito,[11] the form of eq 6 is completely general and can be used to derive any isotherm equation by substitution of the proper functional form for $f(K)$. Kinniburgh et al.[12] presented four of those functional forms in their derivation of a model for the exchange of divalent cations in ferrihydrite. The major advantages and disadvantages of eq 6 as a model for ion exchange have been reviewed.[13] The most attractive feature of isotherm equations of the form given by eq 6 is their applicability in describing ion-exchange data. The most important limitation of eq 6[13] is that it does not necessarily represent the actual mechanism for exchange. The underlying assumption in deriving eq 6 is that the exchanger is composed of independent classes of sites whose distribution is $f(K)$; all the sites exchange with the same function for the isotherm, namely $\theta_2$. The ability of eq 6 to describe ion exchange is contingent upon the validity of this assumption, which must be verified by auxiliary experiments before the use of eq 6 can be guaranteed to yield meaningful results.

Equation 6 is a Fredholm integral equation of the first kind (IFK). The mathematical techniques that have been used to "deconvolve" or find a solution for different types of IFKs have been reviewed.[14] Among the most successful techniques for solving IFKs is the method of regularization.[15,16] The unique aspect of the deconvolution method is that it is not necessary to make an assumption concerning the functional form of the distribution function to examine an isotherm. Consequently, the deconvolution of ion-exchange isotherms to obtain the selectivity coefficient distribution function $f(K)$ provides selectivities for specific sites not previously obtained.

Experiments to assess the physical significance of the results obtained from deconvolution are being conducted. Isotherms describing the exchange of $Cs^+$ with $Na^+$ in the synthetic zeolites Na–A and Na–Y are being measured and deconvolved. The areas under the peaks in the recovered distributions will be compared with the cation-site populations optained crystallographically. This set of experiments will validate the deconvolution technique and will provide selectivity coefficients specific to the different crystallographic sites in the zeolites.

The success of the technique of regularization in determining selectivity coefficient distributions from monovalent ion-exchange isotherms[1] does not ensure the successful deconvolution of multivalent isotherms. The reason for this is the increased complexity of the $\theta_2(C_2, K)$ function in eq 6 in the divalent and trivalent case. Analysis of eq 6 with other deconvolving techniques, such as the singular value decomposition approach,[14] indicates that the $\theta_2$ function in the divalent and trivalent case makes the system in eq 6 a very ill-posed problem, more so than in the monovalent case. Consequently, the deconvolution of multivalent isotherms required careful numerical verification.

## Technique

The regularization method chosen to effect deconvolution in this study was presented by Butler et al.[16] The method requires the solution $f(K)$ to minimize the functional given in eq 7. The

$$\Phi = \|q_2^{\exp} - q_2^{\text{calc}}\|^2 + \alpha\|f(K)\|^2 \qquad (7)$$

first term of the functional is the sum of squared residuals, based on the experimentally obtained data and the respective predictions from eq 6. The second term is the squared $L_2$-norm of $f(K)$ times a parameter $\alpha$, which provides smoothing by causing variations in $f(K)$ to be small.

In their scheme, Butler et al. develop the solution $f(K)$ subject to a nonnegativity constraint that forces $f(K)$ to be greater than or equal to zero. The calculation involves two major steps. First, the smoothing parameter $\alpha$ is fixed and the functional $\Phi$ is minimized after the experimentally obtained and calculated $q_2$ values have been transformed so that the sum of squared residuals becomes a weighted sum. The assigned weights are inversely proportional to the absolute standard deviations in the experimental measurements and are scaled so that the sum of the squares of the weights equals the number of measurements taken. The second step involves determination of the optimal value of the smoothing parameter $\alpha$ through the minimization of an auxiliary function $H(\alpha)$.

(8) Adamson, A. W. *Physical Chemistry of Surfaces*; Wiley: New York, 1982; p 372.
(9) Sposito, G. *Soil Sci. Soc. Am. J.* **1979**, *43*, 197.
(10) Sposito, G. *Soil Sci. Soc. Am. J.* **1980**, *44*, 652.
(11) Sposito, G. *The Surface Chemistry of Solids*; Oxford University Press: New York, 1984; Chapter 4.
(12) Kinniburgh, D. G.; Barker, J. A.; Whitfield, M. *J. Colloid Interface Sci.* **1983**, *95*, 370.
(13) Sposito, G. *CRC Crit. Rev. Environ. Control* **1985**, *15*, 1.
(14) Wing, M. G. *Los Alamos Nat. Lab.*, [*Rep.*] *LA (U.S.)* **1984**, *LA-UR-84 1234*.
(15) Groetsch, C. W. *The Theory of Tikhonov Regularization for Fredholm Equations of the First Kind*; Pitman Advanced Publishing: Boston, 1984.
(16) Butler, J. P.; Reeds, J. A.; Dawson, S. V. *SIAM J. Numer. Anal.* **1981**, *18*, 381.

The function $H(\alpha)$, which depends on the indeterminate error of each experimental measurement, represents the sum of squared deviations of the smoothed function $f(K)$ from the true distribution function. Because of the lack of knowledge concerning the exact magnitude and direction of the experimental errors, the auxiliary function $H(\alpha)$ is constructed so that the value of $\alpha$ it yields tends to oversmooth. Consequently, the optimal choice of $\alpha$ is larger in magnitude than the ideal $\alpha$ by an unknown amount.

The details of the computational procedure used for deconvolution of monovalent ion-exchange isotherms have been presented.[1] Extension of the published approach to the deconvolution of multivalent isotherms is immediate. Numerically, the only difference is the functional form of $\theta_2(C_2, K)$ used in eq 6. Consequently, the published algorithm[1] fully describes the procedure used for the numerical calculations.

The performance of regularization, as well as most other deconvolution techniques, is very sensitive to the distribution of the values of $C_2$ used for isotherm data acquisition. To collect data or use acquired data in the most judicious manner, Hanson's criterion[17] may be followed. As noted by Hanson, the best choice for the $N$ values of $C_2$ at which the measurements of $q_2$ are effected, within the limits $C_{2_{N+1}}$ and $C_{2_0}$, consists of the solutions to the equations of the form given by eq 8. This choice of $C_{2_i}$

$$q_2(C_{2_i}) = q_{2_0} + i\Delta q_2 \tag{8}$$

$$\Delta q_2 = (q_{2_{N+1}} - q_{2_0})/(N + 1) \qquad i = 1, ...,N$$

ensures that the values for $C_2$ are selected most densely where $q_2$ is changing most rapidly. The disadvantage to Hanson's criterion is that it requires an initial fitting of the experimental data as well as possible measurement of additional data at the values of $C_2$ that cause the most critical changes in $q_2$.

It is important to emphasize that, to apply the deconvolution numerical technique of regularization to isotherm data describing multivalent exchange, a careful accounting of the exchanging cations is necessary. For instance, the first step in collecting isotherm data in a system where the ingoing cation is divalent and the cation to be exchanged is monovalent should involve the measurement of possible over exchange. The details of the experiment to be performed will very depending on the system under consideration. To illustrate, over exchange in a system where $Ba^{2+}$ is exchanging with $Na^+$ in the zeolite Na–A could be studied by labeling the solid phase with $^{22}Na$ and equilibrating the labeled Na–A with solutions of various concentrations of $Ba^{2+}$ labeled with $^{133}Ba$. After equilibration, the two phases are separated and the measured ratio of the amount of Ba in the solid phase to the amount of Na that has abandoned the solid phase indicates the extent of over exchange taking place in this system. If over ion exchange is observed, then the isotherm data need to be collected by measuring the total amount of Ba in the solid phase as well as the amount of ingoing anions in the solid phase that have combined with $Ba^{2+}$ to achieve a one-to-one exchange with $Na^+$.

## Results and Discussion

*Computer-Generated Isotherms.* To test the performance of regularization in determining selectivity coefficient distributions, multivalent ion-exchange isotherms have been computer generated. This allows immediate comparison between the distributions used for data generation and the distributions recovered by the proposed deconvolving technique. The ion-exchange isotherms were generated by solving eq 6 in the forward direction. In the case of divalent exchange, the function $\theta_2$ used in eq 6 was defined as in eq 3; whereas, for trivalent exchange, the function $\theta_2$ was defined as in eq 4. To test how experimental errors in the data would affect the results and how the Butler, Reeds, and Dawson's (BRD) criterion for $\alpha$ should be applied, random errors were incorporated into the data used to recover the distributions. In the computer-generated isotherms, the total concentration $C_0$ was 0.1 N, the ratio of activity coefficients was 1.0, and the total equivalents of exchangeable sites per gram of exchanger $Q$ was 1.0.

(17) Hanson, R. J. *SIAM J. Numer. Anal.* **1971**, *8*, 616.

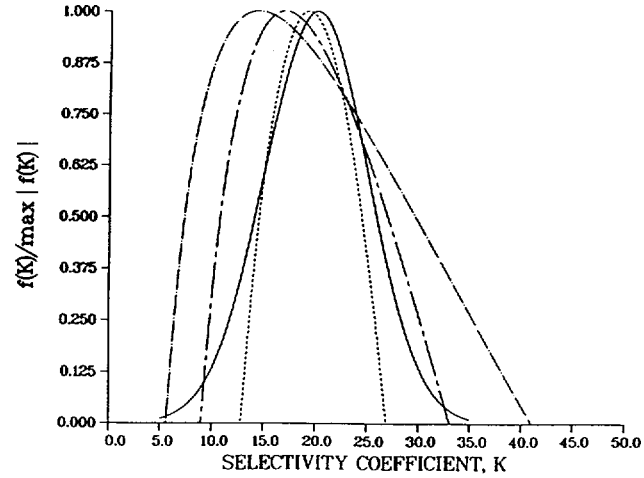


**Figure 1.** Unimodal distributions: actual (solid line), univalent case recovered from data with 5% error (broken line), divalent case recovered from data with 5% error (dashed line), trivalent case recovered from data with 5% error (dotted line).

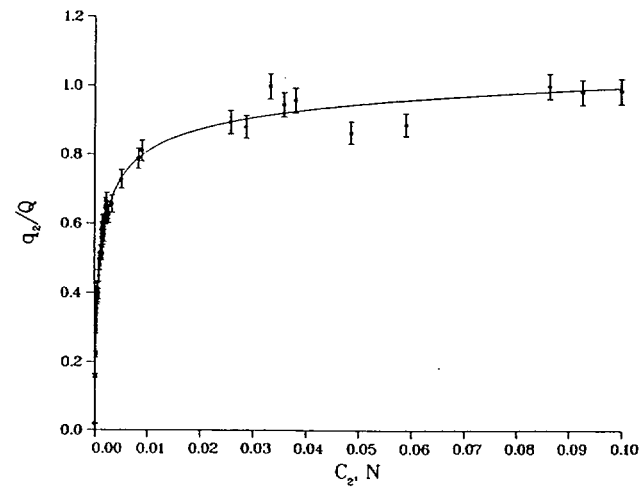


**Figure 2.** Divalent case—unimodal distribution: computer-generated data with 5% error (■), fit obtained from recovered distribution (solid line).

The first test case to be presented was performed with the unimodal, normal distribution of eq 9 for monovalent, divalent, and trivalent exchange. The monovalent case was included in this study only for comparison. The peak representing this distribution

$$f(K) = \frac{1.0}{12.5} \exp\left[-\frac{(K - 20.0)^2}{50.0}\right] \tag{9}$$

is shown in Figure 1 in an arbitrary scale because the values of the distribution have been divided by the maximum value of the distribution function $f(K)$ in the integration interval.

The 40 values of $C_2$ at which $q_2$ was evaluated were determined by applying Hanson's criterion to 40 initial data points generated from $C_2$ values equally spaced between $1.0 \times 10^{-5}$ and 0.1. The relative intermediate error imposed on the isotherm data was 5%, as illustrated by the magnitude of the error bars in Figure 2. Deconvolution was effected with 301 selectivity coefficient values equally spaced in the interval from 1.0 to 50.0. The optimal $\alpha$ occurred in the vicinity of one-tenth the BRD $\alpha$, as was empirically determined by Britten et al.[18] earlier. The recovered distributions for the monovalent, divalent, and trivalent case (using one-tenth of the BRD $\alpha$) are presented in Figure 1, where the $f(K)$ values have been divided by the maximum value of the recovered distributions. Figure 1 shows a decline in the quality of the recovered

(18) Britten, J. A.; Travis, B. J.; Brown, L. F. *Los Alamos Natl. Lab.*, [*Rep.*] *LA* (*U.S.*) **1983**, LA-UR-83 1654.

TABLE I: Unimodal Distributions

| | | recovered from data with 5% error | | |
|---|---|---|---|---|
| | actual | univalent | divalent | trivalent |
| median | 20.0 | 19.5 | 18.9 | 18.7 |
| mean | 20.0 | 19.6 | 19.3 | 19.6 |
| most probable $K$ | 20.0 | 19.1 | 16.8 | 14.2 |
| area | 1.0 | 1.0 | 1.0 | 1.0 |
| width at $f(K)/\max\lvert f(K)\rvert = 0.5$ | 11.8 | 10.0 | 16.2 | 22.4 |

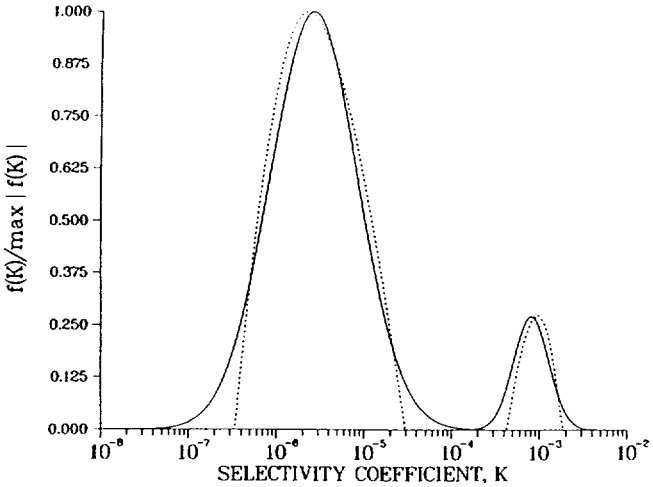


**Figure 3.** Divalent case—bimodal distributions: actual (solid line), recovered from data with absolute error 0.01 (broken line).

distribution as the complexity of $\theta_2(C_2, K)$ increases from the univalent to the trivalent case. The median, mean, most probable selectivity coefficient, area, and width at half-height for the actual as well as the recovered distributions are shown in Table I. Inspection of Table I indicates that, even in the worst case, that of the trivalent exchange, the results obtained by deconvolution provide a reasonably accurate estimate for the selectivity coefficient of the exchange. The fit shown in Figure 2 for divalent exchange was obtained by numerically integrating eq 6 with use of the recovered distribution obtained by deconvolution. Figure 2 shows the ability of the recovered distribution to fit the noisy isotherm data.

The second test to be presented was performed with the log-normal bimodal distribution[19] in eq 10 for divalent exchange. The peaks representing this distribution are shown in Figure 3, where the distribution values have been divided by the maximum value of $f(K)$ in the integration interval.

$$f(K) = \frac{0.05}{2.89K}\exp\left[-\frac{(\ln K + 11.51)^2}{2.65}\right] + \frac{0.95}{1.15K}\exp\left[-\frac{(\ln K + 6.91)^2}{0.42}\right] \quad (10)$$

The 40 values of $C_2$ at which $q_2$ was evaluated were determined by applying Hanson's criterion to 40 initial data points generated from $C_2$ values equally spaced between 0.05 and 0.1. The absolute indeterminate error imposed on the isotherm data was 0.01, which represents 2% of the average $q_2$ value. Deconvolution was effected with 301 selectivity coefficient values logarithmically distributed in the interval from $1.0 \times 10^{-8}$ to $1.0 \times 10^{-2}$. The recovered distribution using one-tenth the BRD $\alpha$ is shown in Figure 3, where the $f(K)$ values have been normalized as previously described. The median, mean, most probable selectivity coefficient, and area for each peak in the actual as well as the recovered distribution are shown in Table II.

The log-normal bimodal distribution used for the trivalent case is defined in eq 11. The peaks representing this distribution are

(19) Johnson, N. L.; Kotz, S. *Continuous Univariate Distribution-1*; Houghton Mifflin: Boston, 1970; p 112.

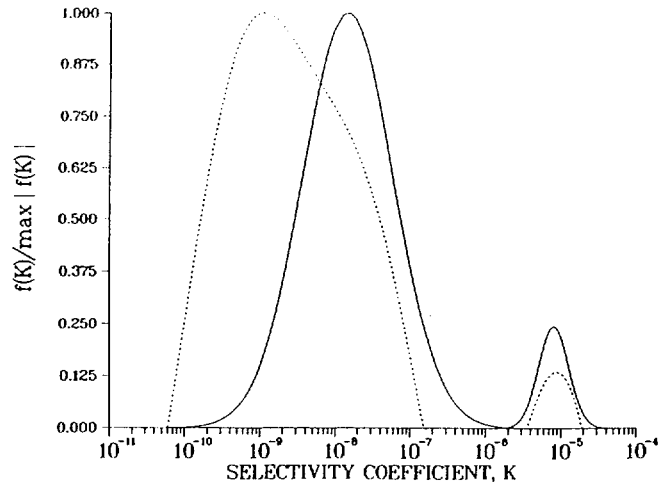


**Figure 4.** Trivalent case—bimodal log-normal distributions: actual (solid line), recovered from data with absolute error of 0.01 (broken line).

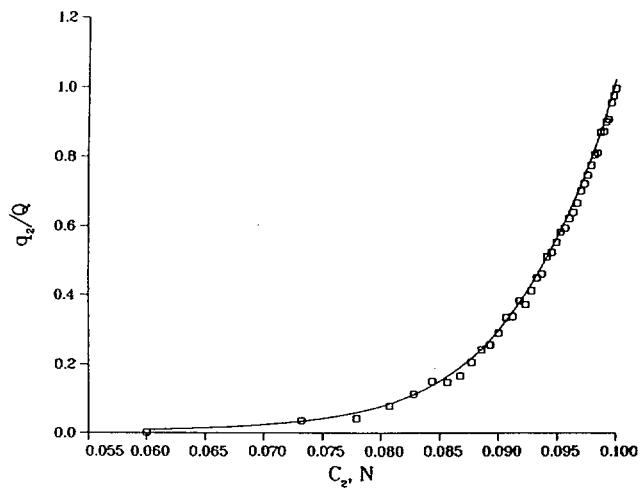


**Figure 5.** Trivalent case—bimodal log-normal distribution: computer-generated data with absolute error of 0.01 (□), fit obtained from recovered distribution (solid line).

shown in Figure 4, where the distribution values have been divided by the maximum value of $f(K)$ in the integration interval.

$$f(K) = \frac{0.05}{3.46K}\exp\left[\frac{-(\ln K + 16.12)^2}{3.82}\right] + \frac{0.95}{1.15K}\exp\left[\frac{-(\ln K + 11.51)^2}{0.42}\right] \quad (11)$$

The 40 values of $C_2$ at which $q_2$ was evaluated were determined by applying Hanson's criterion to 40 initial data points generated from $C_2$ values equally spaced between 0.06 and 0.1. The absolute indeterminate error imposed on the isotherm data was 0.01, which represents 2% of the average $q_2$ value. Deconvolution was effected with 351 selectivity coefficient values logarithmically distributed in the interval from $1.0 \times 10^{-11}$ to $1.0 \times 10^{-4}$. The recovered distribution using one-tenth the BRD $\alpha$ is shown in Figure 4, where the $f(K)$ values have been normalized as previously described. The median, mean, most probable selectivity coefficient, and area for each peak in the actual as well as the recovered distribution are shown in Table III. Inspection of the results obtained for the trivalent case indicates that the deconvolution of data with approximately 2% error can yield selectivity coefficient distributions that differ from the actual values by up to 1 order of magnitude. The main reason for the differences between the recovered and actual distributions is the ill-posed nature of deconvolution problems. Frequently, different $f(K)$ can give rise to very similar data; consequently, small variations in the isotherm data may cause different estimates of $f(K)$. This is illustrated by the perfect fit

**TABLE II: Divalent Case, Bimodal Distributions**

| | first peak | | second peak | |
|---|---|---|---|---|
| | actual | recd from data with abs error of 0.01 | actual | recd from data with abs error of 0.01 |
| median | $1.1 \times 10^{-5}$ | $7.9 \times 10^{-6}$ | $1.1 \times 10^{-3}$ | $1.1 \times 10^{-3}$ |
| mean | $1.9 \times 10^{-5}$ | $9.4 \times 10^{-6}$ | $1.1 \times 10^{-3}$ | $1.1 \times 10^{-3}$ |
| most probable $K$ | $2.8 \times 10^{-6}$ | $2.3 \times 10^{-6}$ | $8.1 \times 10^{-4}$ | $9.5 \times 10^{-4}$ |
| area | 0.05 | 0.05 | 0.95 | 0.97 |

**TABLE III: Trivalent Case, Bimodal Log-Normal Distributions**

| | first peak | | second peak | |
|---|---|---|---|---|
| | actual | recd from data with abs error of 0.01 | actual | recd from data with abs error of 0.01 |
| median | $1.2 \times 10^{-7}$ | $3.6 \times 10^{-8}$ | $1.1 \times 10^{-5}$ | $1.1 \times 10^{-5}$ |
| mean | $2.5 \times 10^{-7}$ | $4.4 \times 10^{-8}$ | $1.1 \times 10^{-5}$ | $1.0 \times 10^{-5}$ |
| most probable $K$ | $1.6 \times 10^{-8}$ | $1.2 \times 10^{-9}$ | $8.1 \times 10^{-6}$ | $8.9 \times 10^{-6}$ |
| area | 0.05 | 0.04 | 0.95 | 0.99 |

**TABLE IV: Trivalent Case, Bimodal Normal Distributions**

| | actual | | recd from data with abs error of 0.01 |
|---|---|---|---|
| | first peak | second peak | |
| median | 3.0 | 15.0 | 8.3 |
| mean | 3.0 | 15.0 | 9.3 |
| most probable $K$ | 3.0 | 15.0 | 3.9 |
| area | 0.4 | 0.6 | 1.0 |

to the original isotherm data shown in Figure 5, where the fit was obtained by numerical integration of eq 6 with the distribution obtained by deconvolution.

A drawback of the deconvolution technique is that it is not always able to resolve multiple closely positioned peaks. Physically, this would correspond to an exchanger with two or more very similar types of sites. The following test case further illustrates this point. The normal bimodal distribution used for data generation in the trivalent case is defined in eq 12. The peaks representing this distribution are shown in Figure 6, where the distribution values have been divided by the maximum value of $f(K)$ in the integration interval.

$$f(K) = \frac{0.4}{1.3}\exp\left[-\frac{(K-3.0)^2}{0.50}\right] + \frac{0.6}{5.0}\exp\left[-\frac{(K-15.0)^2}{8.0}\right] \quad (12)$$

The 40 values of $C_2$ at which $q_2$ was evaluated were determined by applying Hanson's criterion to 40 initial data points generated from $C_2$ values equally spaced between $1.0 \times 10^{-5}$ and 0.1. The absolute indeterminate error imposed on the isotherm data was 0.01, which represents 2% of the average $q_2$ value. Deconvolution was effected with 301 selectivity coefficient values uniformly distributed in the interval from 1.0 to 50.0. The recovered distribution using one-tenth the BRD $\alpha$ is shown in Figure 6, where the $f(K)$ values have been normalized as previously described. The median, mean, most probable selectivity coefficient, and area for each peak in the actual as well as the recovered distribution are shown in Table IV. Inspection of the results indicates that deconvolution was unable to resolve the two closely positioned peaks. Figure 7 further illustrates the ill-posed nature of this deconvolution problem, since the fit obtained by numerical integration of eq 6 with the broad unimodal distribution obtained from deconvolution is able to reproduce perfectly the shape of the original isotherm (generated with a bimodal distribution).

The accuracy of the results obtained from deconvolution decreases as the complexity of the $\theta_2$ function increases. Consequently, more precise isotherms need to be measured for trivalent than for divalent or monovalent[1] exchange before deconvolution is effected. To alleviate this problem, improvements to the numerical method of regularization will be attempted. As has been observed by these authors, the nonnegativity constraint of the regularization technique used in this study is vital to the success of deconvolution. Therefore, the incorporation of additional constraints into the regularization approach should improve the

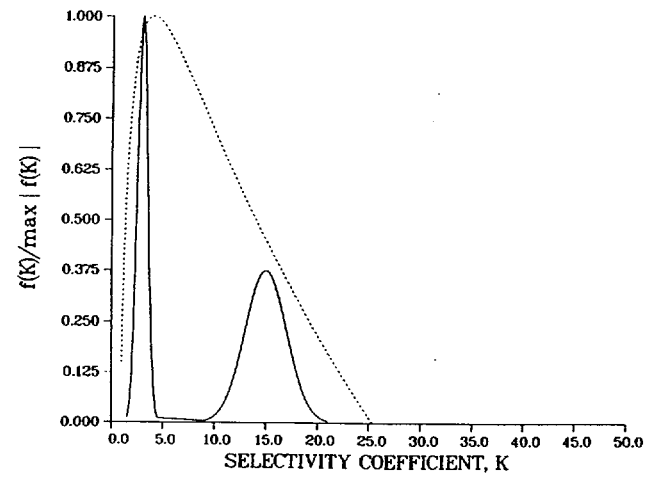


**Figure 6.** Trivalent case—bimodal normal distributions: actual (solid line), recovered from data with absolute error of 0.01 (broken line).

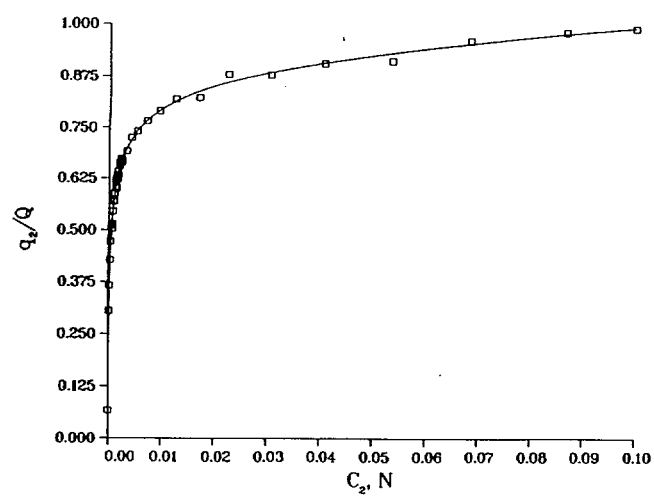


**Figure 7.** Trivalent case—bimodal normal distribution: computer-generated data with absolute error of 0.01 (□), fit obtained from recovered distribution (solid line).

results obtained by deconvolution. For instance, an additional constraint that could be imposed on the regularization approach deals with the maximum area under the peaks of the selectivity coefficient distribution. Inspection of eq 6 indicates that this area can never be greater than 1.

*Experimental Isotherm, Ca–Na Exchange in Zeolite A.* The deconvolution method was applied to real isotherm data presented by Wiers et al.[20] who described the exchange of $Ca^{2+}$ for $Na^+$

(20) Wiers, B. H.; Grosse, R. J.; Cilley, W. A. *Environ. Sci. Technol.* **1982**, *16*, 617.

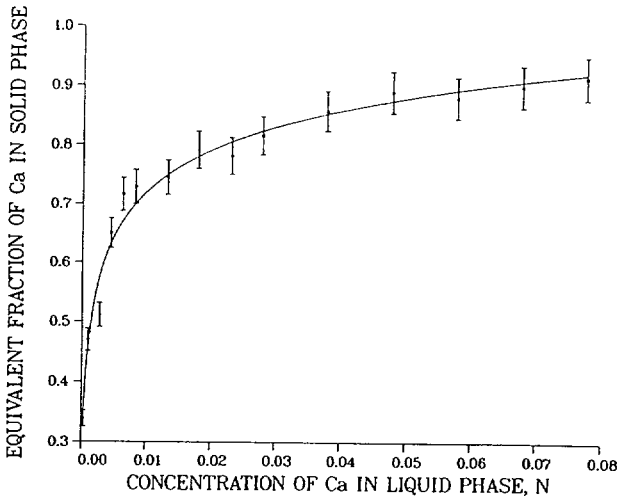


**Figure 8.** Ca–Na exchange in zeolite A: experimental data published by Wiers et al. (■), fit obtained from recovered distribution (solid line).

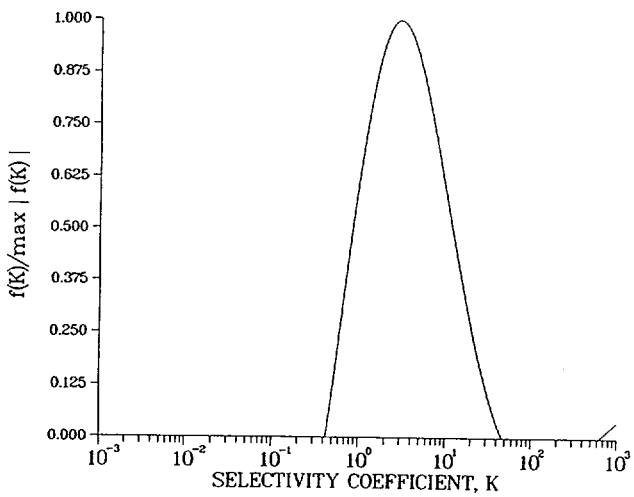


**Figure 9.** Recovered distribution from Ca–Na isotherm in zeolite A.

in the zeolite A. Wiers and co-workers kept a careful accounting of the exchanging cations in the measurement of this isotherm and observed no over exchange. The values published by Wiers for the equivalent fraction of Ca in the solid and liquid phase (columns 9 and 10 of Table I in ref 20), correspond to $q_{Ca}/Q$ and $C_{Ca}/C_0$, respectively. The total concentration of exchanging cations $C_0$ was 0.1 N. The values used for the ratio of activity coefficients $\gamma_{Na}{}^2/\gamma_{Ca}$ at each of the isotherm data points are listed in column 3 of Table II in ref 20. An indeterminate error of 4.5% was used to deconvolve Wiers' isotherm, as is illustrated by the magnitude of the error bars in Figure 8. Deconvolution was effected with 301 values logarithmically spaced in the interval from $1.0 \times 10^{-3}$ to $1.0 \times 10^{3}$. The recovered distribution, shown in Figure 9, yields a median of 9.13, a mean of 11.73, and a most probable selectivity coefficient of 2.80. The fit obtained by numerical integration of eq 6, with the recovered distribution, is shown in Figure 8. The recovered $f(K)$ fits Wiers' data within the relative indeterminate error estimated. There are two main problems with the application of the method to data obtained from the literature. The first is that the precision of the isotherm data is unknown; consequently, to apply the method, it is necessary to estimate the indeterminate error in the data. The second drawback is that Hanson's criterion for the selection of the data points cannot be applied. Figure 8 indicates the scarcity of data points in the region of rapid change in the isotherm. This lack of information results in the numerical error shown by the recovered distribution for values of the selectivity coefficient larger than $6 \times 10^2$.

The definition for selectivity coefficient used by Wiers et al.[20] differs from the definition given in this paper by a factor of two. Wiers and co-workers used molality in their definition of selectivity coefficient whereas normality is employed in this paper's definition. The range of selectivity coefficients reported by Wiers et al. is from 1.28 to 46.44, which is in good agreement with the range from 0.44 to 46.00 corresponding to the first and last nonzero values of the distribution recovered by deconvolution. The value of 2.81 reported by Wiers et al. for the equilibrium constant of the Ca–Na exchange in zeolite A agrees well with the value of 2.80 for the most probable selectivity coefficient obtained by deconvolution. Since the equilibrium constant for the exchange equals the selectivity coefficient times the ratio of activity coefficients of the exchanging cations in the solid phase, the observed agreement indicates a value very close to one for the ratio of activity coefficients in the solid phase.

The broadness of the peak in the recovered distribution shown in Figure 9 is consistent with the large range of selectivity coefficient values in the Kielland plot presented by Wiers et al. The selectivity coefficient distribution recovered by deconvolution could indicate the existence of one type of exchanging site for Ca in the zeolite A, where the Ca ions experience different steric and electronic environments. Alternatively, the lack of structure resolution in the recovered peak could be due to the small number of data points in the isotherm used for deconvolution. In the latter case, the recovered peak could contain multiple unresolved peaks corresponding to similar exchanging sites in the zeolite. The maximum number of Ca ions exchanged for Na ions, reported by Wiers et al. is 90%. Consequently, the absence of additional peaks in the recovered distribution for small selectivity coefficient values could be the result of the lack of information in the region from 90 to 100% Ca loading.

## Conclusions

Deconvolution of multivalent computer-generated ion-exchange isotherms has been effected by the method of regularization previously presented by Butler, Reeds, and Dawson. The method yields reasonable estimates for divalent or trivalent selectivity coefficients in different types of sites of an exchanger. The results reported show that the deconvolution of multivalent isotherms yields poorer results than the deconvolution of monovalent ones. In fact, the deconvolution of trivalent isotherms can yield values for the selectivity coefficients that differ from the actual values by up to 1 order of magnitude. Consequently, future work will involve the improvement of the performance of the numerical technique of regularization used for deconvolution.

The method of deconvolution has been tested with an experimentally obtained isotherm from the literature.[20] This isotherm reported by Wiers et al. describes the divalent exchange of $Ca^{2+}$ for $Na^+$ in zeolite A. Deconvolution was successfully effected with only 15 isotherm data points. The recovered selectivity coefficient distribution agrees well with the selectivity coefficient values determined by Wiers et al. The broadness of the peak in the selectivity coefficient distribution recovered by deconvolution indicates that the Ca ions experience many different environments in one type of exchanging site in the region from 0 to 90% Ca–Na exchange in zeolite A.

Exchangers, such as zeolites, can exhibit structural properties that prevent a multivalent cation from replacing multiple monovalent cations in the solid phase. Consequently, the multivalent cations may combine with anions such as hydroxyls existing either in solution or in the solid phase to accomplish a one-to-one exchange with monovalent cations. The extent to which secondary processes such as the one in eq 13 occur can be determined only by maintaining a careful accounting of the ions in solution as well as the exchanging ions in the solid phase.

$$M_1{}^+(s) + M_2{}^{z_2+}(aq) + (z_2 - 1)OH^- \rightleftharpoons M_1{}^+(aq) + [M_2(OH)_{(z_2-1)}]^+(s) \quad (13)$$

Complicated multivalent exchange, exhibiting over ion exchange, can still be modeled by an IFK for the primary exchange mechanism and Langmuir isotherms for the secondary processes. Numerically, there is no difference between deconvolving uncomplicated and complicated multivalent isotherms. The inde-

terminate errors in the complicated case, however, are bound to be larger since multiple measurements are often necessary to access the state of a particular exchanged ion. Consequently, deconvolution will yield poorer results, which may be improved only by improving the precision of the isotherm data obtained.

*Acknowledgment.* We thank B. J. Travis, W. L. Earl, B. R. Erdal, D. L. Bish, and J. H. Hall for helpful discussions. This research has been supported by the Nevada Nuclear Waste Storage Investigations Project, which is managed by the Yucca Mountain Project Office of the U.S. Department of Energy.

# Application of deconvolution to the analysis of univalent ion-exchange isotherms in zeolites X and Y

**Inés R. Triay and Robert S. Rundberg**
*Los Alamos National Laboratory, Los Alamos, NM, USA*

A numerical method of regularization has been used to effect the deconvolution of isotherms obtained from the literature describing the exchange of $Li^+$, $K^+$, and $Rb^+$ into the synthetic faujasites NaX and NaY. The obtained selectivity coefficient distributions fit the univalent isotherms used for deconvolution. The relative number of $K^+$ cations undergoing exchange with the obtained selectivity coefficients has been compared with published cation-site populations in K-X and K-Y, determined crystallographically.

**Keywords:** Deconvolution; isotherm; exchange; zeolite; faujasite; X; Y; selectivity

## INTRODUCTION

The structural effects on ion selectivities in the synthetic faujasites, Linde X and Y, have been studied using the method of deconvolution of ion-exchange isotherms[1] coupled with reported cation-site populations obtained by X-ray crystallography. This approach allows correlation of the exchangeable ion sites, the number and distribution of those sites, and the ion selectivities for each of those sites with structural differences in the exchanger.

The thermodynamics of ion exchange have been reviewed by Cremers.[2] The selectivity coefficient $K$ for the hypothetical monovalent ion-exchange process in Reaction (1a) is given by Equation (1b), where $a_1$ and $a_2$ are the activities in solution of the cation to be exchanged and the ingoing cation, respectively; $q_1$ and $q_2$ are the concentrations of these cations in the solid phase that are expressed as moles of cation per gram of exchanger:

$$M_1 - X + M_2^+ \rightleftharpoons M_1^+ + M_2 - X \tag{1a}$$

$$K = \frac{q_2 a_1}{q_1 a_2} \tag{1b}$$

As a result of mass balance considerations, Equation (1b) can be rewritten as Equation (2), where $Q$ is the total moles of exchangeable sites per gram of exchanger (ion-exchange capacity), $C_0$ is the total concentration of cations in the liquid phase, $C_2$ is the concentration of the ingoing cation, and $\gamma_1$ and $\gamma_2$ are the activity coefficients in the solution phase of the cation to be exchanged and the ingoing cation, respectively.

$$q_2 = \frac{KQ\gamma_2 C_2}{C_0\gamma_1 + (K\gamma_2 - \gamma_1)C_2} \tag{2}$$

The measured $K$ can vary with $q_2$ in reversible ion exchange even for cases where exchange is taking place in only one type of site. This is the result of nonideal mixing of the exchangeable sites. In addition, the measured $K$ can vary due to exchange taking place in different types of sites having different selectivities for the exchanging cation. Many authors have successfully described ion exchange in terms of multiple sites.[3–5] Consequently, one may consider a set of simultaneous equilibria as in Equation (3), where $X^1, X^2, \ldots, X^n$ represent different sites in the ion exchanger X.

$$M_1 - X^1 + M_2^+ \rightleftharpoons M_1^+ + M_2 - X^1 \tag{3a}$$

$$M_1 - X^2 + M_2^+ \rightleftharpoons M_1^+ + M_2 - X^2 \tag{3b}$$

$$\vdots$$

$$M_1 - X^n + M_2^+ \rightleftharpoons M_1^+ + M_2 - X^n \tag{3c}$$

The solid-phase concentration of cation $M_2^+$ in site $i$ is then given by Equation (4), and the total solid-phase concentration of $M_2^+$ is given by the sum in Equation (5):

$$q_2^i = \frac{K^i Q^i \gamma_2 C_2}{C_0\gamma_1 + (K^i\gamma_2 - \gamma_1)C_2} \tag{4}$$

Address reprint requests to Dr. Triay at the Los Alamos National Laboratory, Los Alamos, NM 87545, USA
Received 1 June 1988

© 1989 Butterworth Publishers

$$q_2 = \sum_{i=1}^{n} q_2^i = \sum_{i=1}^{n} \frac{K^i Q^i \gamma_2 C_2}{C_0\gamma_1 + (K^i\gamma_2 - \gamma_1)C_2} \quad (5)$$

This approach can be further generalized to include subtler differences in sites by replacing the sum in Equation (5) with the integral Equation (6), where $f(K)$ is a distribution function for the selectivity coefficient of the exchange:

$$q_2(C_2) = \int q_2(C_2, K) f(K)\, dK \quad (6)$$

The idea of expressing the heterogeneity of the exchanger in terms of a distribution function has been previously presented.[6–10]

Equation (6) is a Fredholm Integral Equation of the First Kind (IFK). Many numerical techniques[11–13] have been used to 'deconvolve' or find a solution for different types of IFKs. These numerical techniques allow the solution of the IFK without any a priori assumption concerning the functional form of the solution. Consequently, the unique feature of the deconvolution method is that no assumptions are made about the number of peaks and/or shape of the selectivity coefficient distributions to be obtained.

## TECHNIQUE

The computational procedure used for deconvolution of ion-exchange isotherms has been published.[1] The regularization method chosen to effect deconvolution was presented by Butler, Reeds, and Dawson (BRD).[13] The method requires the solution, $f(K)$, to minimize the functional given in Equation (7). The first term of the functional is the sum of squared residuals, based on the experimentally obtained data and the respective predictions from Equation (6). The second term is the squared $L_2$-norm of $f(K)$ times a parameter $\alpha$, which provides smoothing by causing variations in $f(K)$ to be small:

$$\Phi = \| q_2^{\text{exp}} - q_2^{\text{calc}} \|^2 + \alpha \| f(K) \|^2 \quad (7)$$

In their scheme, Butler *et al.*[13] develop the solution, $f(K)$, subject to a nonnegativity constraint that forces $f(K)$ to be greater than or equal to zero. The calculation involves two major steps: Firt, the smoothing parameter $\alpha$ is fixed and the functional $\Phi$ is minimized after the experimentally obtained and calculated $q_2$ values have been transformed so that the sum of squared residuals becomes a weighted sum. The assigned weights are inversely proportional to the absolute standard deviations in the experimental measurements and are scaled so that the sum of the squares of the weights equals the number of measurements taken. The second step involves determination of the optimal value of the smoothing parameter $\alpha$ through the minimization of an auxiliary function $H(\alpha)$.[1,13]

The function $H(\alpha)$, which depends on the indeterminate error of each experimental measurement, represents the sum of squared deviations of the smoothed function $f(K)$ from the true distribution function. Because of the lack of knowledge concerning the exact magnitude and direction of the experimental errors, the auxiliary function $H(\alpha)$ is constructed so that the value of $\alpha$ that it yields tends to oversmooth. Consequently, the determined $\alpha$ is larger in magnitude than the ideal $\alpha$ by an unknown amount.

Application of the BRD criterion to the deconvolution of isotherms has been investigated by deconvolving computer-generated isotherms.[1] These numerical studies indicate that the ideal $\alpha$ occurs in the vicinity of one-tenth the BRD $\alpha$, as was previously observed by Britten *et al.*[14] Therefore, the selectivity coefficient distributions to be reported were obtained by using one-tenth the BRD $\alpha$. The results of the numerical tests also showed that regularization can successfully deconvolve monovalent ion-exchange isotherms with up to 10% indeterminate errors.

The deconvolution method was applied to isotherm data published by Sherry,[15] who described the exchange of $Li^+$, $K^+$, and $Rb^+$ into the synthetic faujasites NaX and NaY. To employ Sherry's values directly, deconvolution was effected by using the mole fraction of the cations in the solid phase (e.g., $q_{Li}/Q$), which amounted to dividing both sides of Equation (6) by $Q$ before the method was applied. The total concentration was 0.1 N, the temperature was 25°C, and the ratios of activity coefficients were obtained from the literature.[16] All isotherms were deconvolved using a small number of selectivity coefficient values in the interval of integration from $1.0 \times 10^{-5}$ to 100.0. The position of the peaks in the selectivity coefficient distributions, recovered from these preliminary calculations, was used to redefine the interval of integration to be used for each isotherm as well as the distribution of the deconvolution values in the integration interval. Numerical studies investigated the result of underestimating the magnitude of the indeterminate errors in the data used for deconvolution. In all cases studied, when the error in the generated isotherm data exceeded the error used for deconvolution by more than 1%, the function $H(\alpha)$ would not minimize. Consequently, the magnitude of the indeterminate errors used for deconvolution of Sherry's isotherms was estimated by systematically decreasing the relative indeterminate errors until regularization was unable to find an optimal $\alpha$ corresponding to a minimum in the auxiliary function $H(\alpha)$. The computational parameters used to recover the selectivity coefficient distributions to be presented were compiled in *Table 1*.

## RESULTS AND DISCUSSIONS

The recovered selectivity coefficient distributions obtained from deconvolution of Sherry's isotherms[15] are shown in *Figures 1–6*, where the distribution values have been divided by the maximum value of $f(K)$ in the integration interval. The fits shown in *Figures 7–12* were obtained by numerically integrat-

**Table 1** Computational parameters for deconvolution of ion-exchange isotherms

| Isotherm | Relative indeterminate error (%) | No. of points in integration interval | Integration interval |
|---|---|---|---|
| Li-Na-X | 8.0 | 501 | $10^{-5}$–$10^{0}$ |
| Li-Na-Y | 10.0 | 501 | $10^{-5}$–$10^{0}$ |
| K-Na-X | 4.0 | 701 | $10^{-5}$–$10^{2}$ |
| K-Na-Y | 5.5 | 701 | $10^{-5}$–$10^{2}$ |
| Rb-Na-X | 4.0 | 701 | $10^{-5}$–$10^{2}$ |
| Rb-Na-Y | 4.0 | 551 | $10^{-1}$–$10^{2}$ |

**Table 2** Recovered selectivity coefficient distribution from Li-Na-X isotherm

| | |
|---|---|
| Median | 0.21 |
| Mean | 0.21 |
| Most probable *K* | 0.21 |
| Total area | 0.85 |

**Table 3** Recovered selectivity coefficient distribution from Li-Na-Y isotherm

| | |
|---|---|
| Median | 0.19 |
| Mean | 0.19 |
| Most probable *K* | 0.16 |
| Total area | 0.69 |

**Table 4** Recovered selectivity coefficient distribution from K-Na-X isotherm

| | First peak | Second peak | Third peak |
|---|---|---|---|
| Median | 0.10 | 1.3 | 15.6 |
| Mean | 0.12 | 1.3 | 16.2 |
| Most probable *K* | 0.05 | 1.3 | 16.3 |
| Total area | 0.47 | 0.45 | 0.20 |
| Relative area | 0.42 | 0.41 | 0.18 |

ing Equation (6) using the recovered distributions. In all cases studied, the recovered $f(K)$ fits Sherry's data within the estimated relative indeterminate error, which is illustrated by the magnitude of the error bars in *Figures 7–12*. The median, mean, most probable selectivity coefficient, and area for each of the peaks in the distributions are presented in *Tables 2–7*.

Because the distribution of ions over the different

**Table 5** Recovered selectivity coefficient distribution from K-Na-Y isotherm

| | First peak | Second peak | Third peak |
|---|---|---|---|
| Median | 0.06 | 2.3 | 12.3 |
| Mean | 0.06 | 2.4 | 12.4 |
| Most probable *K* | 0.04 | 2.1 | 12.7 |
| Total area | 0.38 | 0.41 | 0.29 |
| Relative area | 0.35 | 0.38 | 0.27 |
| Relative cation-site population[3] | 0.35 | 0.37 | 0.28 |

**Table 6** Recovered selectivity coefficient distribution from Rb-Na-X isotherm

| | First peak | Second peak | Third peak |
|---|---|---|---|
| Median | 0.31 | 1.9 | 26.7 |
| Mean | 0.37 | 1.9 | 26.4 |
| Most probable *K* | 0.09 | 1.5 | 26.2 |
| Total area | 0.21 | 0.30 | 0.17 |
| Relative area | 0.31 | 0.45 | 0.25 |

**Table 7** Recovered selectivity coefficient distribution from Rb-Na-Y isotherm

| | First peak | Second peak |
|---|---|---|
| Median | 1.5 | 10.4 |
| Mean | 1.5 | 10.4 |
| Most probable *K* | 1.5 | 10.4 |
| Total area | 0.29 | 0.41 |
| Relative area | 0.42 | 0.58 |

zeolite sites is influenced by the affinity of the sites for the ions as well as by the hydration properties of the ions,[17] it is difficult to assign the selectivity coefficients in the recovered distribution to any one process. However, the intent of the development of the deconvolution method for the analysis of isotherms was to design a technique capable of determining selectivity coefficients corresponding to distinct sites in the exchanger. Consequently, the correspondence between the peaks in the recovered selectivity coefficient distributions and the different crystallographic sites in the exchanger will be examined by comparing the areas of the peaks in the

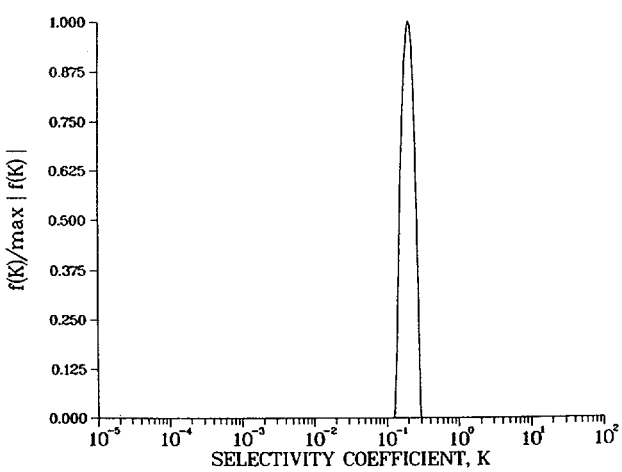


**Figure 1.** Recovered distribution from Li-Na-X isotherm

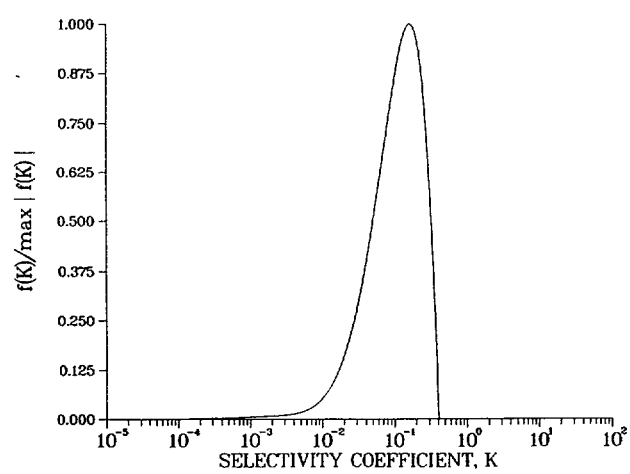


**Figure 2** Recovered distribution from Li-Na-Y isotherm

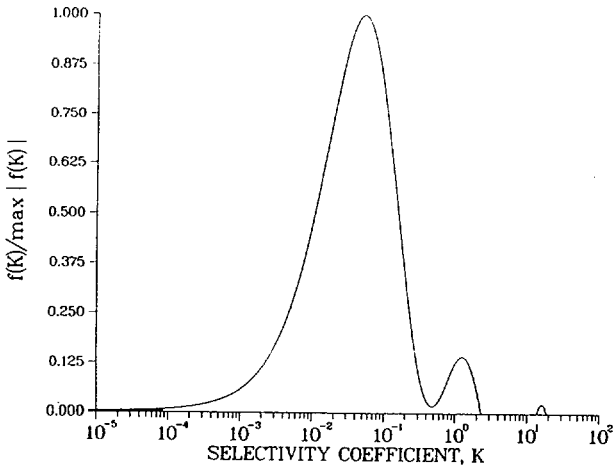


**Figure 3** Recovered distribution from K-Na-X isotherm

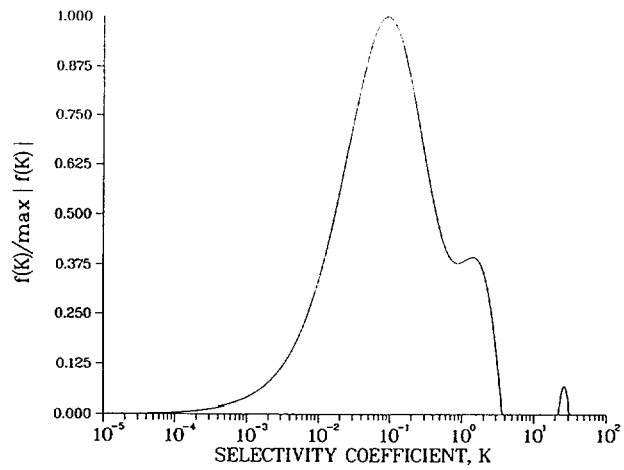


**Figure 5** Recovered distribution from Rb-Na-X isotherm

distributions with available crystallographic data on the cation-site populations in zeolites X and Y.[18]

As was previously noted by Sherry,[15] there are 85 sodium ions in the unit cell of Na-X: 16 in either the sodalite cages or the hexagonal prisms (site I′ and site I, respectively), 32 in the large cavities in the plane of the six tetrahedra connecting the supercages and the sodalite cages (site II), and 37 in either crystallographically equivalent sites or in constant motion within the supercage (site III). The number of exchangeable sites in the larger cavities is 81% of the total exchangeable sites. The area under the selectivity distribution curve obtained from deconvolution of the Li-Na-X isotherm corresponds to 85% of the cation-exchange capacity. Thus, it is conceivable that the remaining 15% of the lithium cations are being excluded from the smaller sodalite cages or hexagonal prisms. The fact that there is only one peak in the recovered distribution from deconvolution indicates that the difference in selectivity between lithium and sodium is not very large among the rest of the sites.This similarity results from the large hydration number of both ions, which would probably make them energetically insensitive to the structure surrounding the large cavities. The selectivity coefficient of 0.18 read from the flat portion (lithium mole fraction from 0.0 to 0.4) of Sherry's Kielland plot for Li-Na-X (Ref. 15) is in good agreement with the value of 0.21 for the selectivity obtained from deconvolution. The nonlinear shape of the Kielland plot at larger lithium mole fractions is consistent with the finite width observed in the recovered selectivity distribution. The discrepancy between the current results and those previously reported[1] for Li-Na-X is a result of the difference in the magnitude of the indeterminate error used for deconvolution. In the previous paper,[1] a relative error of 10% was used to effect deconvolution, whereas in the present work, an error of 8% was used. The authors believe that the current results are slightly more accurate, since the 10% error previously used was a very conservative estimate made by visual inspection of Sherry's[15] data.

The unit cell of Na-Y has 50 sodium cations,[15] 16 in site I or I′, and the rest in the large cages. Consequently, 32% of the cations are located in either the sodalite cages or the hexagonal prisms and 68% of the cations are located in the larger cages. The area of the selectivity coefficient distribution recovered from deconvolution of the Li-Na-Y isotherm corresponds to 69% exchange, indicating that the exchange of $Li^+$

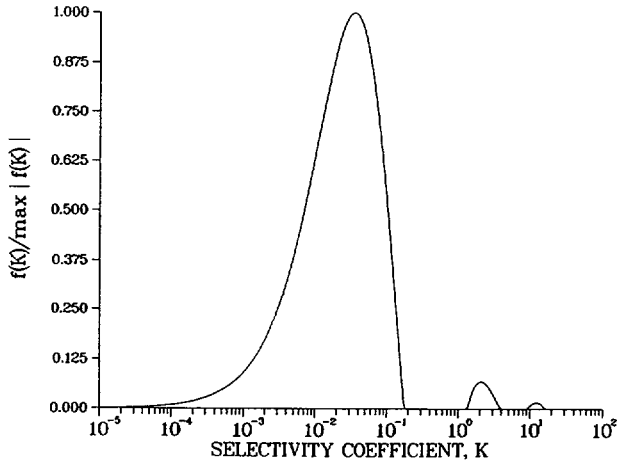


**Figure 4** Recovered distribution from K-Na-Y isotherm

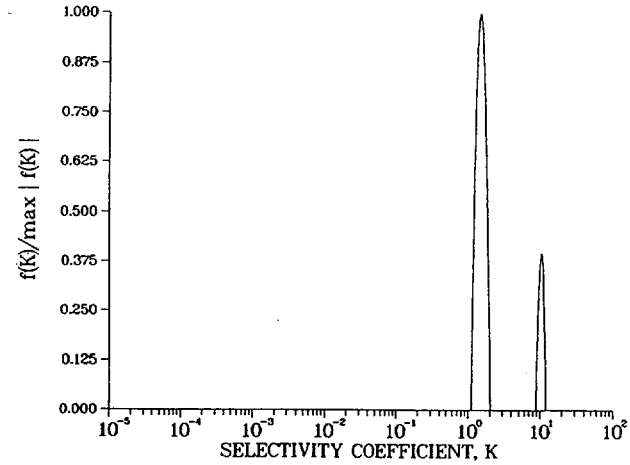


**Figure 6** Recovered distribution from Rb-Na-Y isotherm

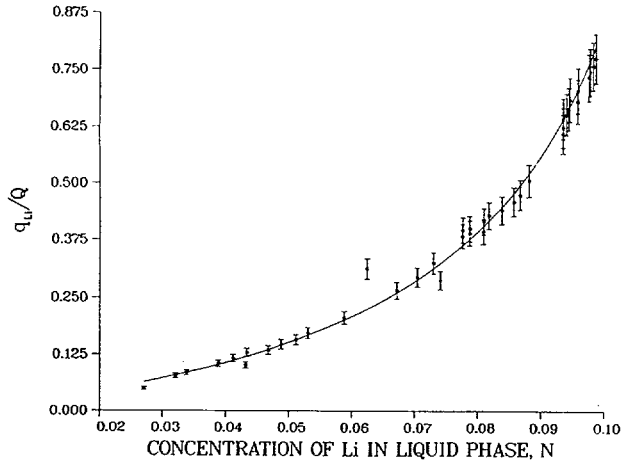


**Figure 7** Experimental data presented by Sherry[15] for Li-Na-X (■); fit obtained from recovered distribution (solid line)

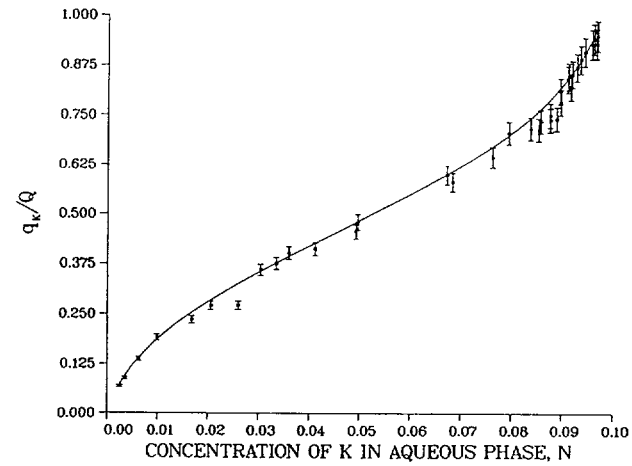


**Figure 9** Experimental data presented by Sherry[15] for K-Na-X (■); fit obtained from recovered distribution (solid line)

for $Na^+$ in zeolites X and Y is very similar. As in Na-X, the lithium cations in Na-Y appear to be excluded from the smaller cages. The similarity in the position of the peaks in the recovered distributions from Li-Na-X and Li-Na-Y isotherms suggests that the larger cavities exhibit similar selectivities for $Li^+$ over $Na^+$ in zeolites X and Y. The broader distribution recovered from the Li-Na-Y isotherm is in agreement with the increased nonlinearity in the shape of the Kielland plot[15] resulting from the Li-Na-Y data.

The cation site populations for K-X and K-Y (Ref. 19) have been published. According to Mortier and Bosmans,[19] K-X has 19% of the potassium cations in sites I and I′, 27% in site II, and 54% in site III. K-Y has 28% of the ptoassium cations in site I′, 37% in site II, and 35% in site III. Inspection of *Tables 4* and *5* indicates that the relative areas under the peaks of the selectivity coefficient distributions agree with crystallographic data for K-Y but not for K-X. However, the relative areas under the peaks recovered from the K-Na-X isotherm, reported by Sherry,[15] agree with the site population for Na-X (19% of $Na^+$ in sites I and I′, 38% in site II, and 43% in site III). There are two obvious sources of error in the comparisons made. The K-X and K-Y analyzed by Mortier and Bosmans[19] do not have exactly the same number of extraframework cations as do the Na-X and Na-Y used by Sherry.[15] The total area under the peaks of the recovered selectivity coefficient distributions for K-X and K-Y is approximately 1.1, which indicates that the estimation of the indeterminate errors used for deconvolution caused an error of at least 10%.

Correlation of the results from deconvolution with the available crystallographic data indicates that the smaller cages in the zeolites X and Y are selective for $K^+$ over $Na^+$. According to Sherry,[15] the extraframework cations need to totally or partially dehydrate in order to enter the smaller cages. Consequently, exchange of $K^+$ for $Na^+$ involves dehydration of the $K^+$ ions as well as rehydration of the $Na^+$ being released into the solution phase. A possible explanation for the results obtained is that less energy is required for dehydration of the $K^+$ ions than is recovered when the $Na^+$ ions are rehydrated. The hydration energies of the exchanging cations calcu-

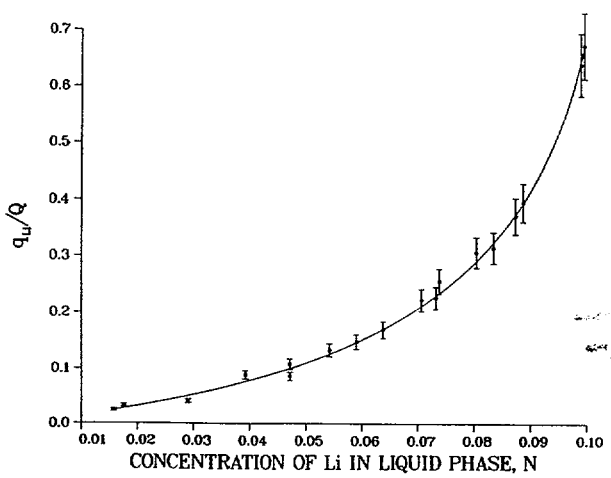


**Figure 8** Experimental data presented by Sherry[15] for Li-Na-Y (■); fit obtained from recovered distribution (solid line)

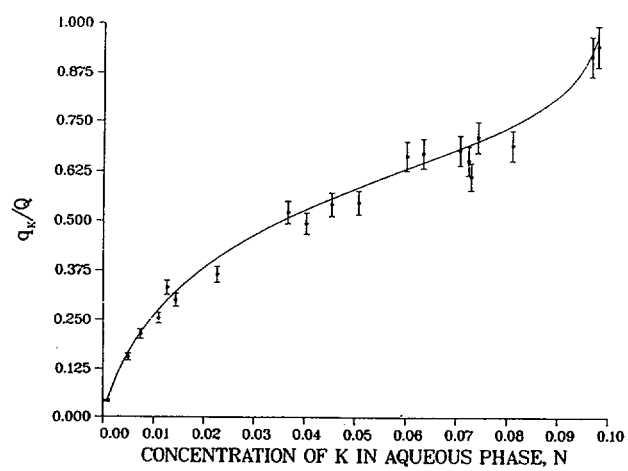


**Figure 10** Experimental data presented by Sherry[15] for K-Na-Y (■); fit obtained from recovered distribution (solid line)

lated using the Latimer equation[20] are consistent with this rationale.

The best-fit curve shown in Sherry's data[15] for Rb-Na-X is extrapolated over the range 0.094–0.10 N. The assumed intercept at 0.10 N corresponds to approximately 81% exchange as determined from crystallographic data combined with the assumption that the $Rb^+$ is excluded from the sodalite cages. When the arguments of Hanson are used,[21] the absence of data points in this important region of rapid change prevents deconvolution from yielding accurate results. Inspection of the recovered distribution from the Rb-Na-Y isotherm indicates the exclusion of the $Rb^+$ ions from 30% of the exchangeable sites. This would be consistent with Sherry's observation concerning the exclusion of $Rb^+$ from the 16 extraframework positions in the hexagonal prisms or sodalite cages of the Linde zeolite.

Experiments to further assess the physical significance of the results obtained using the method of deconvolution are being carried out. Isotherms describing the exchange of $Cs^+$ with $Na^+$ in the synthetic zeolites NaA and NaY are being measured and deconvolved. The areas under the peaks in the recovered distributions will be compared with the cation site populations obtained crystallographically. Although it has been previously noted[1] that the width of the peaks in the recovered selectivity coefficient distributions could be an artifact of the numerics, the physical meaning of the width of the peaks should be closely related to the degree of nonideality of mixing of the exchangeable sites. Future efforts will be devoted to the study of this potential correspondence.

## CONCLUSIONS

The numerical technique of regularization with nonnegativity constraints has been employed to deconvolve isotherm data presented by Sherry,[15] describing the exchange of $Li^+$, $K^+$, and $Rb^+$ for $Na^+$ in both Linde X and Y. The recovered selectivity coefficient distributions were used to generate fits for the original isotherm data. The obtained fits reproduced the shape of the original data quite well. The areas under the peaks of the recovered selectivity coefficient distributions were correlated with available crystallographic data obtained from the literature. The agreement between the peak areas and the cation-site populations seems to indicate that deconvolution yields selectivity coefficients that correspond to exchange in the different crystallographic sites of a zeolite. These site-specific selectivities are not obtainable with any other technique. Consequently, the method of deconvolution coupled with crystallographic analyses will become a unique and powerful technique for the study of ion exchange in relatively rigid exchangers such as zeolites.

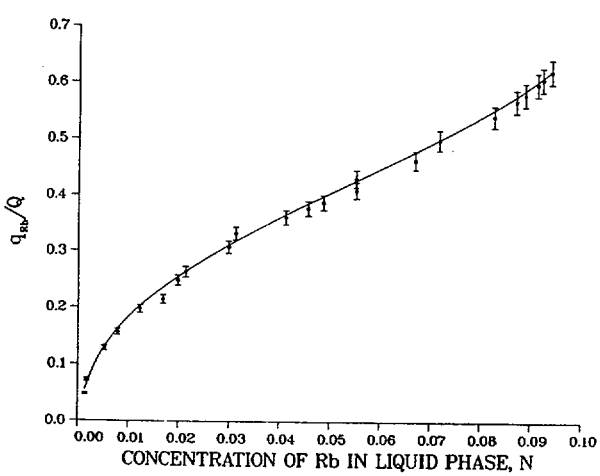


**Figure 11** Experimental data presented by Sherry[15] for Rb-Na-X (■); fit obtained from recovered distribution (solid line)

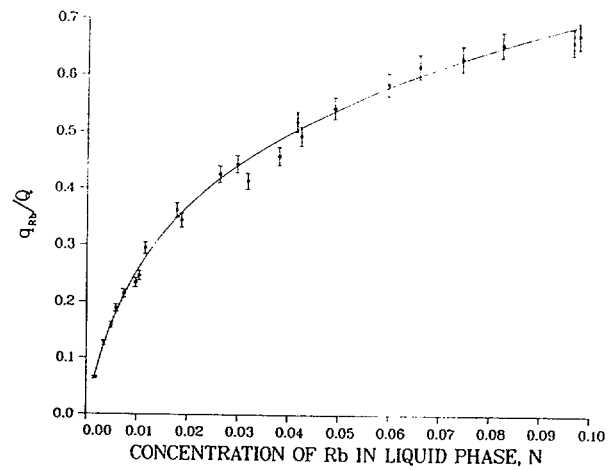


**Figure 12** Experimental data presented by Sherry[15] for Rb-Na-Y (■); fit obtained from recovered distribution (solid line)

## ACKNOWLEDGEMENTS

The authors thank B.J. Travis, B.R. Erdal, D.L. Bish, and J.H. Hall for helpful discussions. This research has been supported by the Nevada Nuclear Waste Storage Investigations (NNWSI) Project, as part of the Civilian Radioactive Waste Management Program. The NNWSI Project is managed by the Waste Management Project Office of the U.S. Department of Energy, Nevada Operations Office.

## REFERENCES

1 Triay, I.R. and Rundberg, R.S. *J. Phys. Chem.* 1987, 5269
2 Cremers, A. in *Molecular Sieves – II* (Ed. J.R. Katzer) American Chemical Society, Washington, DC, 1977, p. 179
3 Barrer, R.M. and Klinowski, J. *J. Chem. Soc., Faraday Trans. 1* 1972, **68**, 73
4 Barrer, R.M. and Munday, B.M. *J. Chem. Soc. A* 1971, 2914
5 Brouwer E., Baeyens B., Maes A. and Cremers, A. *J. Phys. Chem.* 1983, **87**, 1213
6 Adamson, A.W. *Physical Chemistry of Surfaces*, John Wiley & Sons, New York, 1982, p. 372
7 Sposito, G. *Soil Sci. Soc. Am. J.* 1979, **43**, 197
8 Sposito, G. *Soil Sci. Soc. Am. J.* 1980, **44**, 652
9 Sposito, G. *The Surface Chemistry of Soils*, Oxford University Press, Inc., New York, 1984, Chap. 4
10 Kinniburgh, D.G., Barker, J.A. and Whitfield, M. *J. Coll. Interface Sci.* 1983, **95**, 370
11 Wing, M.G. *Los Alamos National Laboratory Report*, LA-UR-84 1234, Los Alamos, NM, 1984

12 Groetsch, C.W. *The Theory of Tikhonov Regularization for Fredholm Equations of the First Kind*, Pitman Advanced Publishing Program, Boston, 1984
13 Butler, J.P., Reeds, J.A. and Dawson, S.V. *SIAM J. Numer. Anal.* 1981, **18**, 381
14 Britten, J.A., Travis, B.J. and Brown, L.F. *Los Alamos National Laboratory Report*, LA-UR-83 1654, Los Alamos, NM, 1983
15 Sherry, H.S. *J. Phys. Chem.* 1966, **70**, 1158
16 Harned, H.S. and Owen, B.B. *The Physical Chemistry of Electrolytic Solutions*, Reinhold Publishing Co., New York, 1958, p. 731
17 Uytterhoeven, J.B. in *Proceedings of the Sixth International Zeolite Conference* (Eds. D. Olson and A. Bisio) Butterworths, Guildford, UK, 1984, p. 49
18 Mortier, W.J. *Compilation of Extra Framework Sites in Zeolites*, Butterworths, Guildford, UK, 1982, p. 19
19 Mortier, W.J. and Bosmans, H.J. *J. Phys. Chem.* 1971, 3327
20 Moore, W.J. *Physical Chemistry*, Prentice-Hall, Englewood Cliffs, NJ, 1972, p. 430
21 Hanson, R.J. *SIAM J. Numer. Anal.* 1971, **8**, 616

# RADIONUCLIDE MIGRATION AS A FUNCTION OF MINERALOGY

Inés R. TRIAY, Alan J. MITCHELL, Martin A. OTT
Los Alamos National Laboratory
INC-11, MS J514
Los Alamos, NM 87545
(505) 665-1755

## ABSTRACT

The migration of radionuclides is studied as a function of mineralogy utilizing batch sorption and column experiments. The transport behavior of alkaline, alkaline-earth, and transition metals and actinide species is studied in pure mineral separates. The solid phases utilized for these investigations are silicates, alumino-silicates, carbonates, and metal oxides and oxyhydroxides. The results of this effort are utilized to aid in the elucidation of the dominant chemical mechanisms of radionuclide migration; the prediction of radionuclide transport in conditions similar to those expected at the candidate high-level nuclear waste repository site at Yucca Mountain, Nevada; and the identification of materials that act as natural geological barriers or that can be utilized as strong sorbers in engineered barriers.

## INTRODUCTION

An effort has been initiated to study the migration of radionuclides in mineral phases that can play an important role at the candidate high-level nuclear waste repository site at Yucca Mountain. The radionuclides in this effort are simple cations (strontium, barium, and cesium species), anions (pertechnetate), and actinides [Np(V), Pu(IV), Pu(VI), and Am(III) species]. The water utilized to prepare the radionuclide solutions is water from the well J-13 at the Nevada Test Site. This water is thought to be representative of the groundwater in the candidate site at Yucca Mountain. The solid phases for this study are silicates (quartz and cristobalite), feldspars, a zeolite (clinoptilolite), a clay mineral (montmorillonite), calcite, an iron oxide (hematite), an iron oxyhydroxide (goethite), a manganese oxide (hollandite), and a manganese oxyhydroxide (romanechite).

Batch sorption experiments are utilized to determine the partition of radionuclides between the solid and solution phase. Previous sorption studies[1] indicate that simple cations such as $Sr^{+2}$, $Ba^{+2}$, and $Cs^{+}$ sorb strongly to aluminosilicates such as clays and zeolites via a mechanism of ion exchange. However, ion exchange does not play a significant role in the sorption of actinides under near neutral pH. Beall and Allard[2] report that three major factors control actinide sorption under environmental conditions: pH (for hydrolyzable ions), surface chemisorption reactions for minerals that contain strong complexing ions, and redox reactions. Dran et al.[3] studied the sorption of actinide analogues on granite minerals utilizing MeV ion beam techniques. Two retention mechanisms were found to dominate the sorption of transuranium analogues, namely incorporation within hydrosilicates and precipitation of secondary crystalline phases.

Sanchez et al.[4] studied the adsorption of Pu(IV) and Pu(V) on goethite. Analysis of the data obtained with the triple layer model[4] predicted that four hydrolytic species of Pu(IV), namely $Pu(OH)^{+3}$, $Pu(OH)_2^{+2}$, $Pu(OH)_3^{+}$, and $Pu(OH)_4$ adsorb on the goethite surface. Technetium (one of the longest lived radionuclides) is assumed to be transported as pertechnetate in the subsurface. Consequently, it has the potential to travel at a faster rate than the average groundwater velocity due to charge and size exclusion effects. Bondietti and Francis[5] postulate that current risk assessments that consider Tc and Np potentially capable of migrating unretarded from high-level radioactive waste repositories as $TcO_4^-$ and $NpO_2^+$ may be overestimating their potential hazard to the public. Their study[5] points out that the Fe(II) in many subsurface waters may maintain Tc and Np in less soluble oxidation states such as $TcO_2$ and $NpO_2$.

In the present studies, the batch sorption results will be tested under flowing conditions utilizing column experiments. One of the most important aspects of this effort is that column experiments are sensitive to multiple species present in solution (as is expected in the case of actinides), and formation of colloidal suspensions (such as in the case of Pu and Am). Consequently, comparison of the column studies with the batch sorption investigations is expected to provide new and significant information for radionuclide migration as a function of speciation for important mineral phases.

## EXPERIMENTAL

The zeolite phase being utilized in these studies is a natural clinoptilolite sample that was purified to eliminate the smectite fraction using the method of Chipera and Bish.[6] The clay is a natural montmorillonite sample. Two calcite samples are being utilized, one synthetic and one natural. The hematite and goethite utilized are synthetic samples. The hollandite and romanechite used are natural samples. The purity of the minerals was determined by powder pattern x-ray diffraction and elemental chemical analysis. All solid phases utilized were found to be at least 99% pure. Efforts to obtain and analyze the purity of quartz, cristobalite, and feldspar are under way.

All solutions being utilized were prepared with water from the well J-13 of the Nevada Test Site. The measured pH of the J-13 water was 7.9; the chemical composition of J-13 water has been reported.[1] Solutions to study the behavior of alkaline and alkaline-earth metals were prepared by adding a spike (less than $10^{-6}$ M in concentration) of $^{85}Sr$, $^{137}Cs$, and $^{133}Ba$ to J-13 water; the pH of this solution is 7.7. Np(V) was prepared in acidic solution by dissolution of $NpO_2$, followed by adjustment to the +4 oxidation sate and purification by ion exchange. An aliquot of the acidic $^{237}Np(V)$ solution was added to J-13 water to yield a solution with a Np concentration of $5 \times 10^{-6}$ M and a pH of 7.6. The colloidal $^{239}Pu(IV)$ in J-13 water utilized was prepared by diluting an acidic solution of Pu(IV). The resulting pH of the colloidal Pu(IV) solution is 7.5; the Pu molarity is $1 \times 10^{-6}$. The size of Pu(IV) colloids suspended in J-13 is in the range between 50 and 400 nm.[7] A stock solution of $^{241}Am(III)$ was prepared by dissolving $AmO_2$ in 9 M HCL. Aliquots of Am(III) stock solutions are added to J-13 water to yield solutions with a pH of 7.5.

The batch sorption experiments consist of pretreating 1 g of pure mineral with 20 ml of J-13 water by agitating the phases for 14 days and separating the phases by centrifugation. The pretreated solid phase is then equilibrated with 20 ml of the solution containing the radionuclide(s) of interest in J-13 water. This equilibration step is followed by separating the phases by centrifugation, determining the amount of radionuclide(s) left in solution after equilibration, and determining a sorption coefficient for the radionuclide(s) sorbed onto the solid phase by comparing the amount of radionuclide(s) in the solution phase initially and after equilibration.

The definition of sorption coefficient, $K_d$, is given in the following equation:

$$K_d = \frac{\text{radionuclide concentration in solid phase}}{\text{radionuclide concentration in solution phase}},$$

at equilibrium. (1)

The assumption that equilibrium is attained during the experiments conducted is inherent in the definition of $K_d$. There is no evidence to prove or disprove this assumption. If equilibrium is not attained in the sorption equilibration step of these experiments, the value of $K_d$'s reported should be used as distribution coefficients for the radionuclide between the solid and solution phases only under the set of experimental conditions specified.

In Equation 1, the concentration in the solid phase is expressed as moles per gm and the concentration in the liquid phase is expressed as moles per ml.

The transport experiments consist of eluting the solutions containing the radionuclides studied through columns made of crushed minerals. The amount of radionuclides eluted through the columns is measured as a function of time. The resulting elution curves are used to obtain the retardation factors, $R_f$, of the radionuclides in each type of column. The free column volume is determined utilizing tritiated water. The retardation factor is given by the ratio of the velocity of water through the column (measured with tritiated water) to the migration velocity of the radionuclide. The porosity of the column was determined by dividing the free column volume by the total column volume. The total volume of the columns utilized is 4.2 $cm^3$ and the flow velocity is 158 m/y.

The retardation factors obtained under flowing conditions and the sorption coefficients obtained using batch sorption techniques are being compared on the basis of the following equation:

$$K_d = (R_f - 1)\,\varepsilon/\rho \quad . \qquad (2)$$

where $\rho$ is the bulk column density and $\varepsilon$ the column porosity.[8]

The amount of radionuclide in solution for column and batch sorption work was determined using radioanalytical techniques. Strontium, cesium, and barium were studied together, and the solution was analyzed for each element using gamma-ray spectrometry. Each actinide was studied separately, and the solutions were analyzed using liquid scintillation counting.

## RESULTS AND DISCUSSION

The preliminary results obtained indicate three main mechanisms for the retardation of radionuclides in the types of solid mineral phases

studied: cation exchange, surface complexation, and physical adsorption. The sorption coefficients obtained by batch sorption techniques for Sr, Cs, and Ba in the various mineral phases under study are given in Table 1. The sorption equilibration time for the experiments in Table 1 was 21 days. Strontium, cesium, and barium exist as simple cations in J-13 water and sorb via an ion exchange mechanism in zeolites and clays. The high degree of sorption of these cations in these exchangers (that abound at Yucca Mountain) indicates that naturally occurring minerals constitute an important geological barrier for Sr, Cs, and Ba. Comparison of the results obtained by batch sorption techniques with those obtained using column experiments shows good agreement for Sr, Cs, and Ba in the minerals studied to date using column techniques (synthetic calcite and hematite).

**Table 2:** Sorption Coefficients for Np in Pure Minerals

| Mineral | Kd (ml/g) Np* | Np† | pH |
|---|---|---|---|
| synthetic calcite | $1.4\times10^{1}$ | $1.2\times10^{1}$ | 8.1 |
| calcite (Mexico) | $2.4\times10^{2}$ | $6.5\times10^{2}$ | 8.1 |
| montmorillonite (AZ) | $6.3\times10^{1}$ | $4.7\times10^{1}$ | 8.1 |
| clinoptilolite (ID) | | $2.7\times10^{1}$ | 8.0 |
| synthetic hematite | $3.3\times10^{3}$ | $3.2\times10^{3}$ | 8.0 |
| synthetic goethite | $1.8\times10^{5}$ | $1.1\times10^{5}$ | 8.4 |
| hollandite (NM) | $1.2\times10^{3}$ | $1.1\times10^{3}$ | 8.1 |
| romanechite (AZ) | $3.8\times10^{2}$ | $3.9\times10^{2}$ | 8.1 |

*Sorption Equilibration Time = 21 days
†Sorption Equilibration Time = 124 days

**Table 1:** Sorption Coefficients for Sr, Cs, and Ba in Pure Minerals

| Mineral | Kd (ml/g) Sr | Cs | Ba | pH |
|---|---|---|---|---|
| synthetic calcite | $4.0\times10^{-1}$ | $3.3\times10^{-1}$ | $7.7\times10^{-1}$ | 7.9 |
| calcite (Mexico) | $5.7\times10^{0}$ | $1.3\times10^{0}$ | $5.0\times10^{0}$ | 8.0 |
| montmorillonite (AZ) | $1.4\times10^{3}$ | $1.4\times10^{3}$ | $1.7\times10^{3}$ | 8.0 |
| synthetic hematite | $2.4\times10^{1}$ | $4.0\times10^{-2}$ | $1.3\times10^{2}$ | 8.0 |
| synthetic goethite | $1.2\times10^{3}$ | $3.1\times10^{0}$ | $1.3\times10^{4}$ | 8.4 |
| hollandite (NM) | $5.5\times10^{1}$ | $1.9\times10^{0}$ | $9.7\times10^{3}$ | 8.0 |
| romanechite (AZ) | $6.2\times10^{1}$ | $6.8\times10^{0}$ | $2.2\times10^{4}$ | 8.1 |

The sorption coefficients for Np(V) in pure mineral separates have been compiled in Table 2. All metal oxides and oxyhydroxides utilized were found to be strong sorbers of Np in J-13 water. The mechanism responsible for this strong Np retardation seems to be surface complexation. Calcite has been found to be a moderately strong sorber for Np in J-13 water. The higher sorption of the natural calcite as opposed to the synthetic calcite can be explained in terms of surface area of the minerals. The natural calcite has a surface area a factor of 3 higher than the synthetic one. Clinoptilolite and montmorillonite are poor Np sorbers. Although Np(V) exists at least partially as the neptunyl cation in J-13 water, one possible explanation of these results is that the neptunyl cation is too large to fit in the cation exchange sites and dehydration of the neptunyl cation to replace the resident exchangable cations is energetically unfavorable.

The retardation behavior of Am(III) seems relatively independent of mineralogy. In fact, previous observations indicate that Am can adsorb onto non-geologic media.[9] Most of the observations made seem to indicate that surface coprecipitation or physical adsorption are responsible for the retardation behavior of Am. The correlation of Am retardation with the surface area of the minerals utilized is underway. This correlation is expected to aid in the elucidation of the mechanism(s) responsible for the retardation of Am. As in the case of Np, Am does not seem to sorb via a cation exchange mechanism for exchangers such as clinoptilolite and montmorillonite. This result has been verified using initial Am concentrations as low as $10^{-11}$ M. Comparison of the Am retardation results obtained using extremely small Am concentrations with those obtained at larger concentration levels will confirm the presence/absence of Am surface co-precipitates.

Plutonium retardation is extremely sensitive to the oxidation-reduction potential of the water utilized. Pu(IV) exists mainly in colloidal form in J-13 water and can be excluded due to its size from the column's pores. This indicates that Pu(IV) has the potential of traveling in the subsurface faster than the average groundwater. Pu(V) and Pu(VI) can act as ionic species in J-13 water. However, preliminary results indicate that Pu sorption kinetics are relatively slow; consequently, this needs to be taken into account when comparisons between column and batch sorption experiments are made.

Preliminary results describing the elution of Pu(IV) colloid in J-13 water through columns of synthetic calcite and hematite can be seen in Figures 1 and 2. In these figures, $A/A_t$ refers to the sum of Pu activity eluted divided by the total activity of Pu injected into the column. In the synthetic calcite column, less than 2% of the Pu eluted before the

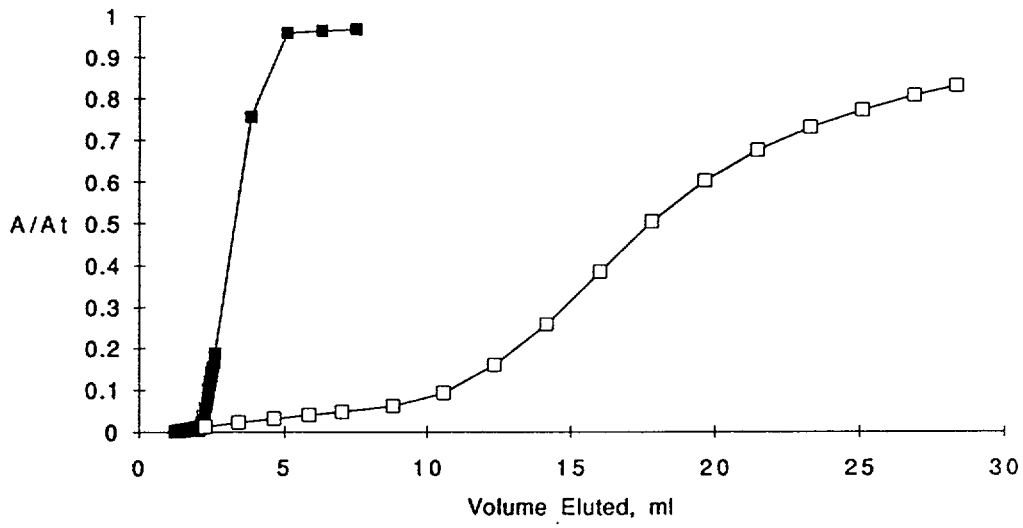


Figure 1: Tritiated Water (filled squares) and Pu(IV) Colloid in J-13 Water (open squares) Eluted Through Synthetic Calcite

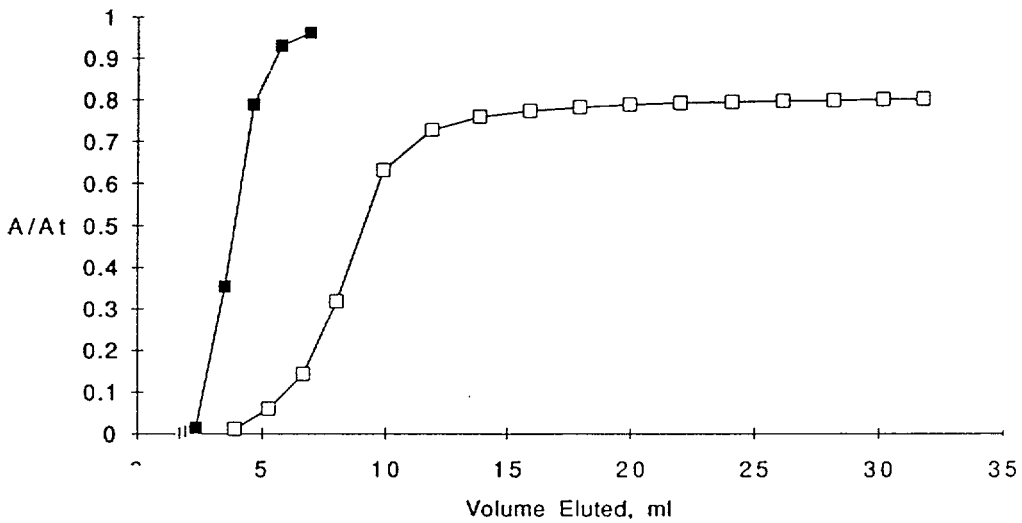


Figure 2: Tritiated Water (filled squares) and Pu(IV) Colloid in J-13 Water (open squares) Eluted through Synthetic Hematite

tritium front. In the case of synthetic hematite, there was no Pu elution before tritium was eluted. The sorption coefficients calculated for Pu(IV) colloid determined from the column experiments are 5 ml/g for synthetic calcite and 1 ml/g for synthetic hematite. Since the Pu used is colloidal in nature, these results need to be compared with results obtained using the same minerals and well-characterized synthetic colloids in order to determine whether the retardation observed is due to filtration or to an actual chemical interaction between Pu and the solid phase.

The results that have been obtained to date are still under analysis, and their interpretation should point to the studies that need to be effected in order to further elucidate radionuclide retardation as a function of mineralogy. The computer code EQ3 is being employed to determine the speciation of Np, Am, and Pu in J-13 water at room temperature.

## CONCLUSIONS

The prediction of the radionuclide release rates to the accessible environment in the candidate high-level nuclear waste repository depends strongly on the interaction of the radionuclides with the minerals that exist at Yucca Mountain. The type of retardation information to be utilized in performance assessment calculations depends on our knowledge of migration mechanisms. The fact that the column work being performed is capable of shedding new light on the interaction of the different actinide species with solid

phases of interest makes this work essential to the safety objectives of a repository. Because the transport experiments being performed in this effort will utilize pure mineral phases and well-characterized solution phases (containing actinides in known oxidation states), this work will be instrumental in deciding the types of parameters that must be monitored in transport calculations. For instance, for Np sorption, pH seems to be an extremely dominant factor. In the case of Pu retardation, the oxidation state of Pu (and consequently the Eh of the solution) dominate the Pu migration behavior.

Although it is difficult to foresee the prediction of radionuclide migration in Yucca Mountain tuffs considering solely the information obtained from experiments using the pure minerals that constitute the whole rock, the experiments being performed in this study will provide an excellent means of making predictions (probably within an order of magnitude of the real values) for the sorption parameters for radionuclides in tuff that can be utilized in transport calculations. The work described will aid in the elucidation of the retardation mechanisms as a function of mineralogy. Identifying and understanding these retardation mechanisms is extremely important to the safety objectives of a repository. The efforts discussed also provide a means of identifying materials that act as natural barriers or can be utilized for engineered barriers to ensure public safety. For instance, iron oxides and oxyhydroxides such as hematite and goethite, even if found at the trace level at Yucca Mountain, can significantly retard the migration of Np. These materials can also be used in engineered barriers to further retard the transport of actinide species in a repository.

## ACKNOWLEDGMENTS

The authors wish to acknowledge P. Palmer and D. Hobart, who prepared all the actinide solutions utilized in this effort. This work was supported by the Yucca Mountain Site Characterization Project Office as part of the Civilian Radioactive Waste Management Program. This Project is managed by the U.S. Department of Energy, Yucca Mountain Project. The data reported can be found in laboratory notebook TWS-INC-9/88-6.

## REFERENCES

1. K. THOMAS, Los Alamos National Laboratory LA-10960-MS (December 1987).

2. G. W. BEALL, B. ALLARD, "Sorption of Actinides from Aqueous Solutions Under Environmental Conditions," In *Proceedings of a Symposium on Adsorption from Aqueous Solutions*, Plenum Press, New York, 1981.

3. J. DRAN, G. DELLA MEA, A PACCAGNELLA, J. PETIT, M. MENAGER. Radiochimica Acta **44/45**, 299 (1988).

4. A. SANCHEZ, J. MURRAY, T. SIBLEY. Radiochimica Acta **49**, 2297 (1985).

5. E. BONDIETTI, C. FRANCIS. Science **203**, 1337 (1979).

6. S. CHIPERA, D. BISH. Clinoptilolite/Smectite Assemblages, 36th Annual Clay Minerals Conference, Socorro, NM, October 18-22, 1987.

7. J. THOMPSON. Journal of Radioanalytical and Nuclear Chemistry **130**, 353 (1989).

8. J. RELYEA. Radioactive Waste Management and the Nuclear Fuel Cycle **3**, 151 (1982).

9. I. TRIAY, A. MEIJER, M. CISNEROS, G. MILLER, A. MITCHELL, M. OTT, D. HOBART, P. PALMER, R. PERRIN, R. AGUILAR, "Sorption of Am in Tuff and Pure Minerals Using Synthetic and Natural Groundwaters," Accepted for publication in Radiochimica Acta.

J. Phys. Chem. 1987, 91, 5269-5274



# Determination of Selectivity Coefficient Distributions by Deconvolution of Ion-Exchange Isotherms

**Inés R. Triay and Robert S. Rundberg***

*Los Alamos National Laboratory, Los Alamos, New Mexico 87545* *(Received: January 5, 1987)*

The behavior of monovalent ion-exchange isotherms has been mathematically described by a Fredholm integral equation of the first kind (IFK). A numerical technique of regularization applied to deconvolute the IFK yielded the selectivity coefficient distributions from the ion-exchange isotherms. Regularization has successfully recovered normal and log-normal unimodal and bimodal distributions from computer-generated isotherms. This method has also been used to deconvolute ion-exchange isotherms obtained from the literature.

## Introduction

A fundamental understanding of the ion-exchange properties of polyelectrolytes, synthetic zeolites, and naturally occurring minerals is of great interest. Methods to predict these properties can support the application of exchange behavior of different materials to problems such as separation, strategic recovery, or sorption of radionuclides in geologic media. The properties and applications of zeolites, which constitute a very important class of ion exchangers, have been reviewed.[1-3] Synthetic and natural zeolites may be used as adsorbents, catalysts, or ion exchangers. Present as well as potential ion-exchange applications of zeolites include regenerative and nonregenerative processes such as ammonium and metal removal from waste water, radioisotope removal and storage, detergent building, artificial-kidney dialysate regeneration, ruminant feeding of nonprotein nitrogen, and ion-exchange fertilizing. The most common experimental technique used to study the ability of substances to act as ion exchangers is the measurement of ion-exchange isotherms. The ion-exchange isotherm is the equilibrium solid-phase concentration of a given ion as a function of the aqueous-phase concentration when the temperature and ionic strength are held constant. The solid-phase concentration increases with aqueous-phase concentration until the exchangeable sites are saturated, provided the structure of the ion exchanger does not change as the adsorbed ions are replaced. The point of saturation is determined by the ion-exchange capacity. If some assumptions are made about the activity coefficients of adsorbed cations, net free energies of exchange can be determined from the ion-exchange isotherm. As will be shown in this paper, if the shape of the ion-exchange isotherm is assumed to result from the simultaneous equilibria of cations in solution with different exchange sites in the solid phase, the ion-exchange isotherm yields information on exchangeable ion sites, the number and distribution of those sites, and the ion selectivities for each of those sites. Differences in the ion selectivities or net free energies of exchange for the various possible sites should result from structural differences in the sites. These differences lead to both steric and Coulombic effects. For example, a large, hydrated cation may have to lose waters of hydration before it is adsorbed in the smaller sodalite cage in the zeolite Linde A, whereas dehydration could be unnecessary when the larger supercage is considered. The structure surrounding the aluminum anion positions in a zeolite may hinder the approach of cations, resulting in unfavorable Coulombic interactions. The relative location of aluminum anions could lead to the crowding of large cations in some configurations. Ion-exchange isotherms might be used to study these structural effects.

The thermodynamic formalism for ion exchange has been reviewed by Cremers;[4] consequently, only the essentials necessary for the deconvolution method will be given here. The selectivity coefficient, $K$, for the hypothetical monovalent ion-exchange

(1) Cremers, A. Presented at the Workshop on Experimental Methodologies in Radionuclide Sorption Studies, OECD, Paris, June 1983.

(2) Breck, D. W. In *Potential Uses of Natural and Synthetic Zeolites in Industry*; Townsend, R. P., Ed.; The Chemical Society, Burlington House: London, 1979; p 391.

(3) "Zeolites for Industry", symposium organized by the SCI and the British Zeolites Association; *Chem. Ind. (London)* 1984, 237.

(4) Cremers, A. In *Molecular Sieves*; Katzer, James R., Ed.; American Chemical Society: Washington, DC, 1977; Vol. II, p 179.

0022-3654/87/2091-5269$01.50/0 © 1987 American Chemical Society

process in reaction 1a is given by eq 1b, where $a_1$ and $a_2$ are the activities in solution of the cation to be exchanged and the ingoing cation, respectively; $q_1$ and $q_2$ are the concentrations of these cations in the solid phase that are expressed as moles of cation per gram of exchanger.

$$M_1 - X + M_2^+ \rightleftharpoons M_1^+ + M_2 - X \quad (1a)$$

$$K = \frac{q_2 a_1}{q_1 a_2} \quad (1b)$$

As a result of mass balance considerations, eq 1b can be rewritten as eq 2, where $Q$ is the total moles of exchangeable sites per gram of exchanger (ion-exchange capacity), $C_0$ is the total concentration of cations in the liquid phase, $C_2$ is the concentration of the ingoing cation, and $\gamma_1$ and $\gamma_2$ are the activity coefficients in the solution phase of the cation to be exchanged and the ingoing cation, respectively.

$$q_2 = \frac{KQ\gamma_2 C_2}{C_0\gamma_1 + (K\gamma_2 - \gamma_1)C_2} \quad (2)$$

The measured $K$ will vary with $q_2$ in reversible monovalent ion exchange because of the heterogeneity of the adsorbent's surface. In light of the evidence that ions in ion exchangers (such as zeolites) may experience different crystallographic environments, Barrer and Klinowski[5] have examined the theoretical basis for ion exchange involving several groups of homogeneous sites in the exchanger. Among the authors who have successfully analyzed ion exchange in terms of different types of sites, Barrer and Munday[6] interpreted exchange isotherms in the zeolite K–F by assuming two types of sites, and Brouwer, Baeyens, Maes, and Cremers[7] described the exchange of cesium and rubidium ions in illite clay in terms of three kinds of sites. Consequently, one may consider a set of simultaneous equilibria as in eq 3 where $X^1, X^2, ..., X^n$ represent different sites in the ion exchanger X.

$$M_1 - X^1 + M_2^+ \rightleftharpoons M_1^+ + M_2 - X^1 \quad (3a)$$

$$M_1 - X^2 + M_2^+ \rightleftharpoons M_1^+ + M_2 - X^2 \quad (3b)$$

$$\vdots$$

$$M_1 - X^n + M_2^+ \rightleftharpoons M_1^+ + M_2 - X^n \quad (3c)$$

The solid-phase concentration of the cation $M_2^+$ in site $i$ is then given by eq 4, and the total solid-phase concentration of $M_2^+$ is given by the sum in eq 5.

$$q_2^i = \frac{K^i Q^i \gamma_2 C_2}{C_0\gamma_1 + (K^i\gamma_2 - \gamma_1)C_2} \quad (4)$$

$$q_2 = \sum_{i=1}^{n} q_2^i = \sum_{i=1}^{n} \frac{K^i Q^i \gamma_2 C_2}{C_0\gamma_1 + (K^i\gamma_2 - \gamma_1)C_2} \quad (5)$$

This approach can be further generalized to include subtler differences in sites, such as variations in aluminum ordering within a class of sites, by replacing the sum in eq 5 with the integral in eq 6, where $f(K)$ is a distribution function for the selectivity coefficient of the exchange.

$$q_2(C_2) = \int q_2(C_2,K)\, f(K)\, dK \quad (6)$$

The idea of expressing the heterogeneity of the adsorbent's surface in terms of a distribution function has been previously presented by Adamson[8] for the net free energy of adsorption of nonelectrolytes. Sposito[9,10] has derived a generalized form of eq 6, intended for cation exchange, by integrating over a continuum of Langmuir equations. As previously discussed by Sposito,[11] the form of eq 6 is completely general and can be used to derive any isotherm equation by substitution of the proper functional form for $f(K)$. Kinniburgh et al.[12] have presented four of those functional forms in their derivation of a model for the exchange of divalent cations in ferrihydrite. The model was derived by assuming a distribution of exchange sites obeying a competitive Langmuir isotherm. The result of integration over all sites was equated to four different composite isotherms, including the discrete-site Langmuir, the generalized Freundlich, the Langmuir–Freundlich, and the Tóth isotherm. Each of the composite isotherms considered yielded a different functional form for $f(K)$ whose parameters were determined by fitting the composite isotherms to the experimental data. The major advantages and disadvantages of using eq 6 as a model for ion exchange have been reviewed.[13] The most attractive feature of isotherm equations of the form given by eq 6 is their applicability in describing ion-exchange data. Kinniburgh[14] has reported several general purpose isotherms (multisite Langmuir, Tóth, and the modified Dubinin–Radushkevich) which are well-suited to fit exchange data obtained by using heterogeneous exchangers. This was exemplified by the success of these isotherm equations in fitting experimental data describing the adsorption of P and K by soils, Na–Cu exchange in montmorillonite, and Zn adsorption by ferrihydrite. The most important limitation of eq 6[13] is that it does not necessarily represent a chemical model for exchange. The underlying assumption in deriving eq 6 is that the exchanger is composed of independent classes of sites whose distribution is $f(K)$. The ability of eq 6 to describe ion exchange is contingent upon the validity of this assumption which must be verified by auxiliary experiments before the use of eq 6 can be guaranteed to yield meaningful results. The model for ion exchange proposed in eq 6 could not be used to analyze isotherms that show maxima and minima resulting from metastability or side processes such as hydrolysis of the solid phase[5] because descriptions for these phenomena are not incorporated in the model.

Equation 6 is a Fredholm integral equation of the first kind (IFK). The mathematical techniques that have been used to "deconvolute" or find a solution for different types of IFKs have been reviewed.[15] Among the techniques that have been most successfully used to solve IFKs is the method of regularization.[16] Regularization is a numerical technique that stabilizes the "deconvolution" by introducing a smoothing function to the fitting process. Recently, modifications to regularization have received considerable attention.[17] In fact, regularization with proper modifications has been recently used[18] to effect the calculation of surface site energy distributions from gas adsorption isotherms. This problem is analogous to the one posed when selectivity coefficient distributions are desired from ion-exchange isotherms because the competition between ions for fixed ionic sites is similar to the competition between neutral species for adsorption sites. The unique aspect of the deconvolution method is that it is not necessary to make an assumption concerning the functional form of the distribution function to examine an isotherm. Consequently, the deconvolution of ion-exchange isotherms to obtain the selectivity coefficient distribution function, $f(K)$, provides selectivities for specific sites not previously obtained.

## Technique

The regularization method chosen to effect deconvolution in this study was presented by Butler, Reeds, and Dawson.[17] The

(5) Barrer, R. M.; Klinowski, J. *J. Chem. Soc., Faraday Trans. I* **1972**, *68*, 73.
(6) Barrer, R. M.; Munday, B. M. *J Chem. Soc. A* **1971**, 2914.
(7) Brouwer, E.; Baeyens, B.; Maes, A.; Cremers, A. *J. Phys. Chem.* **1983**, *87*, 1213.
(8) Adamson, A. W. *Physical Chemistry of Surfaces*; Wiley: New York, 1982; p 372.
(9) Sposito, G. *Soil Sci. Soc. Am. J.* **1979**, *43*, 197.
(10) Sposito, G. *Soil Sci. Soc. Am. J.* **1980**, *44*, 652.
(11) Sposito, G. *The Surface Chemistry of Soils*; Oxford University Press: New York, 1984; Chapter 4.
(12) Kinniburgh, D. G.; Barker, J. A.; Whitfield, M. *J. Colloid Interface Sci.* **1983**, *95*, 370.
(13) Sposito, G. *CRC Crit. Rev. Environ. Control* **1985**, *15*, 1.
(14) Kinniburgh, D. G. *Environ. Sci. Technol.* **1986**, *20*, 895.
(15) Wing, M. G. Report LA-UR-84 1234; Los Alamos National Laboratory: Los Alamos, NM, 1984.
(16) Groetsch, C. W. *The Theory of Tikhonov Regularization for Fredholm Equations of the First Kind*; Pitman Advanced Publishing Program: Boston, 1984.
(17) Butler, J. P.; Reeds, J. A.; Dawson, S. V. *SIAM J. Numer. Anal.* **1981**, *18*, 381.
(18) Britten, J. A.; Travis, B. J.; Brown, L. F. Report LA-UR-83; Los Alamos National Laboratory: Los Alamos, NM, 1983.

method requires the solution, $f(K)$, to minimize the functional given in eq 7. The first term of the functional is the sum of squared residuals, based on the experimentally obtained data and the respective predictions from eq 6. The second term is the squared $L_2$-norm of $f(K)$ times a parameter $\alpha$, which provides smoothing by causing variations in $f(K)$ to be small.

$$\Phi = \|q_2^{\text{exptl}} - q_2^{\text{calcd}}\|^2 + \alpha \|f(K)\|^2 \quad (7)$$

In their scheme, Butler et al. develop the solution, $f(K)$, subject to a nonnegativity constraint that forces $f(K)$ to be greater than or equal to zero. The calculation involves two major steps. First, the smoothing parameter $\alpha$ is fixed and the functional, $\Phi$, is minimized after the experimentally obtained and calculated $q_2$ values have been transformed so that the sum of squared residuals becomes a weighted sum. The assigned weights are inversely proportional to the absolute standard deviations in the experimental measurements and are scaled so that the sum of the squares of the weights equals the number of measurements taken. The second step involves determination of the optimal value of the smoothing parameter $\alpha$ through the minimization of an auxiliary function, $H(\alpha)$. The details of the computational procedure used for regularization are included in the Appendix.

The function $H(\alpha)$, which depends on the indeterminate error of each experimental measurement, represents the sum of squared deviations of the smoothed function $f(K)$ from the true distribution function. Because of the lack of knowledge concerning the exact magnitude and direction of the experimental errors, the auxiliary function, $H(\alpha)$, is constructed so that the value of $\alpha$ it yields tends to oversmooth. Consequently, the optimal choice of $\alpha$ is larger in magnitude than the ideal $\alpha$ by an unknown amount.

It is important to understand the need for an optimal amount of smoothing in a deconvolution method such as regularization. The function of the smoothing parameter, $\alpha$, is to provide a natural band-pass for this system, which prevents the researcher from obtaining more information from deconvolution than the indeterminate error (noise) in his data permits—in accordance with Shannon's information theory.[19]

The performance of regularization, as well as most other deconvolution techniques, is very sensitive to the distribution of the values of $C_2$ used for isotherm data acquisition. To collect data or use acquired data in the most judicious manner, one may follow Hanson's criterion.[20] As noted by Hanson, the best choice for the $N$ values of $C_2$ at which the measurements of $q_2$ are effected, within the limits $C_{2_{N+1}}$ and $C_{2_0}$, consists of the solutions to the equations of the form given by eq 8. This choice of $C_{2_i}$ ensures that the values for $C_2$ are selected most densely where $q_2$ is changing most rapidly. The disadvantage to Hanson's criterion is that it requires an initial fitting of the experimental data as well as possible measurement of additional data at the values of $C_2$ that cause the most critical changes in $q_2$.

$$q_2(C_{2_i}) = q_{2_0} + i\Delta q_2, \quad \Delta q_2 = (q_{2_{N+1}} - q_{2_0})/(N+1) \qquad i = 1, ..., N \quad (8)$$

## Results and Discussion

*Computer-Generated Isotherms.* To test the performance of regularization in determining selectivity coefficient distributions, ion-exchange isotherms have been computer generated. This allows immediate comparison between the distributions used for data generation and the distributions recovered by using the proposed deconvoluting technique. The ion-exchange isotherms were generated by solving eq 6 in the forward direction. To test how experimental errors in the data would affect the results and how the Butler, Reeds, and Dawson (BRD) criterion for $\alpha$ should be applied, random errors were incorporated into the data used to recover the distributions. In the computer-generated isotherms, the total concentration, $C_0$, was 0.1 N, the ratio of activity coefficients was 1.0, and the total moles of exchangeable sites per gram of exchanger, $Q$, was 1.0.

(19) Shannon, C. E. *Bell Syst. Tech. J.* **1948**, *27*, 379, 623.
(20) Hanson, R. J. *SIAM J. Numer. Anal.* **1971**, *8*, 616.

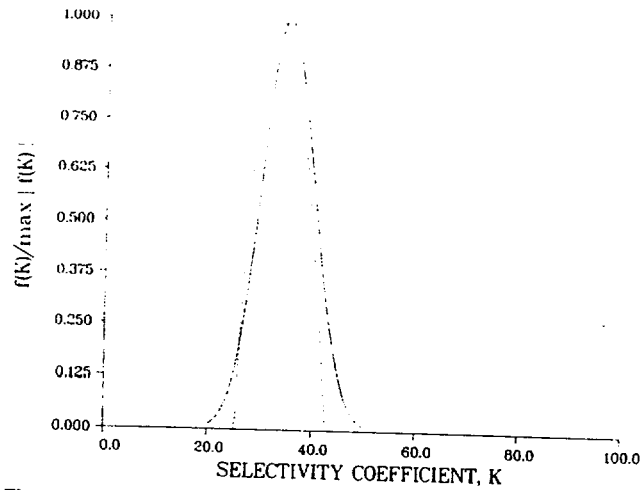


**Figure 1.** Unimodal distributions: actual (solid line); recovered from data with absolute indeterminate error of 0.06 (broken line).

**TABLE I: Unimodal Distributions**

| | actual | recovd from data with abs indeterminate error of 0.06 |
|---|---|---|
| median | 35.0 | 33.8 |
| mean | 35.0 | 33.9 |
| most probable $K$ | 35.0 | 33.0 |
| area | 1.00 | 1.00 |

The first test case to be presented was performed by using the unimodal, normal distribution in eq 9. The interval of integration used in eq 6 to generate the isotherms was from 20.0 to 50.0. The peak representing this distribution is shown in Figure 1 in an arbitrary scale because the values of the distribution have been divided by the maximum value of the distribution function, $f(K)$, in the integration interval.

$$f(K) = \frac{1.0}{12.5} \exp\left[-0.5\left(\frac{K - 35.0}{5.0}\right)^2\right] \quad (9)$$

The 40 values of $C_2$ at which $q_2$ was evaluated were determined by applying Hanson's criterion to 40 initial data points generated from $C_2$ values equally spaced between $5.0 \times 10^{-4}$ and 0.1. The absolute indeterminate error imposed on the isotherm data was 0.06, which represents 10% of the average $q_2$. Deconvolution was effected with 301 selectivity coefficient values equally spaced in the interval from 1.0 to 100.0. The optimal $\alpha$ occurred in the vicinity of one-tenth the BRD $\alpha$, as was empirically determined by Britten et al.[18] earlier. The recovered distribution using one-tenth of the BRD $\alpha$ is presented in Figure 1, where the $f(K)$ values have been divided by the maximum value of the recovered distribution. The median, mean, most probable selectivity coefficient, and area for the actual as well as the recovered distribution are shown in Table I.

The second test was performed using the log-normal bimodal distribution[21] in eq 10. The interval of integration for the first peak in the distribution was from $1.0 \times 10^{-3}$ to 1.0; the interval of integration for the second peak was from 0.1 to 100.0. The peaks representing this distribution are shown in Figure 2, where the distribution values have been divided by the maximum value of $f(K)$ in the integration interval.

$$f(K) = \frac{0.1}{1.73\,K} \exp\left[-0.5\left(\frac{\ln(K) + 2.30}{0.69}\right)^2\right] + \frac{0.9}{1.73K} \exp\left[-0.5\left(\frac{\ln(K) - 2.30}{0.69}\right)^2\right] \quad (10)$$

The 40 values of $C_2$ at which $q_2$ was evaluated were determined by applying Hanson's criterion to 40 initial data points generated

(21) Johnson, N. L.; Kotz, S. *Continuous Univariate Distribution*; Houghton Miffin: Boston, 1970; Vol. 1, p 112.

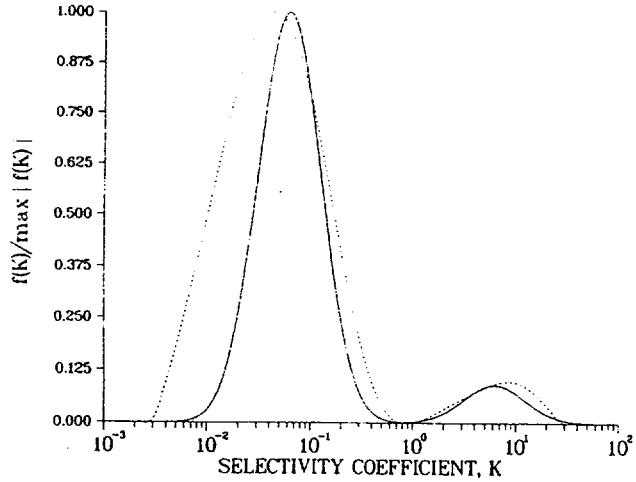


**Figure 2.** Bimodal distributions: actual (solid line); recovered from data with 2% relative indeterminate error (broken line).

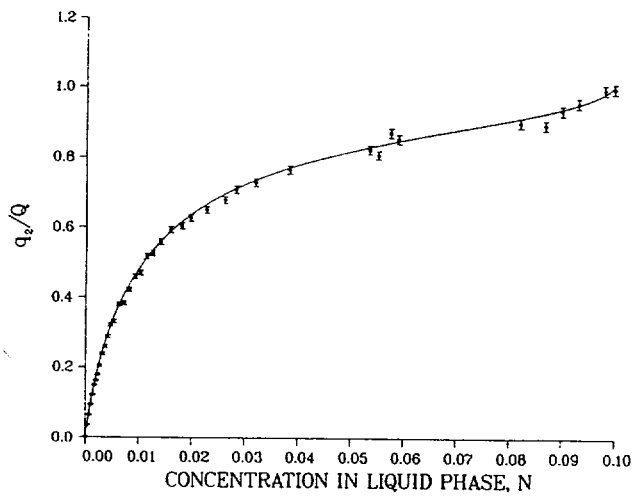


**Figure 3.** Computer-generated data with 2% relative indeterminate error (■); fit obtained from recovered distribution (solid line).

**TABLE II: Bimodal Distributions**

| | first peak | | second peak | |
|---|---|---|---|---|
| | actual | recovd from data with 2% rel indeterminate error | actual | recovd from data with 2% rel indeterminate error |
| median | 0.10 | 0.12 | 10.0 | 12.2 |
| mean | 0.10 | 0.27 | 10.0 | 12.0 |
| most probable $K$ | 0.06 | 0.05 | 6.2 | 8.2 |
| area | 0.10 | 0.11 | 0.90 | 0.89 |

from $C_2$ values equally spaced between $1.0 \times 10^{-5}$ and 0.1. The relative indeterminate error imposed on the isotherm data for the case using the bimodal distribution was 2%. Deconvolution was effected with 101 selectivity coefficient values logarithmically distributed in the interval from $1.0 \times 10^{-3}$ to 100.0. The recovered distribution using one-tenth the BRD $\alpha$ is shown in Figure 2, where the $f(K)$ values have been normalized as previously described. The median, mean, most probable selectivity coefficient, and area for each peak in the actual as well as the recovered distribution are shown in Table II. The fit shown in Figure 3 was obtained by numerically integrating eq 6 using the recovered bimodal distribution from the isotherm data with 2% error.

The main reason for the differences between the recovered and actual distributions is the ill-posed nature of deconvolution problems. Frequently, different $f(K)$ can give rise to very similar data; consequently, small variations in the isotherm data may cause different estimates of $f(K)$. This results from the attenuation of high-frequency components in the actual $f(K)$ in their contribution

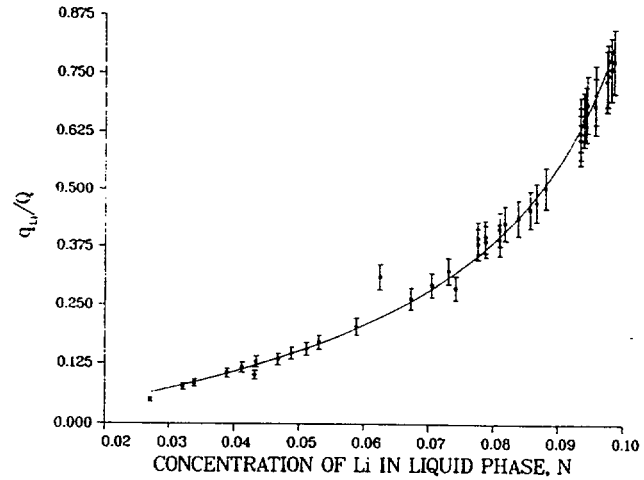


**Figure 4.** Experimental data presented by Sherry for LiNa–X (■); fit obtained from recovered distribution (solid line).

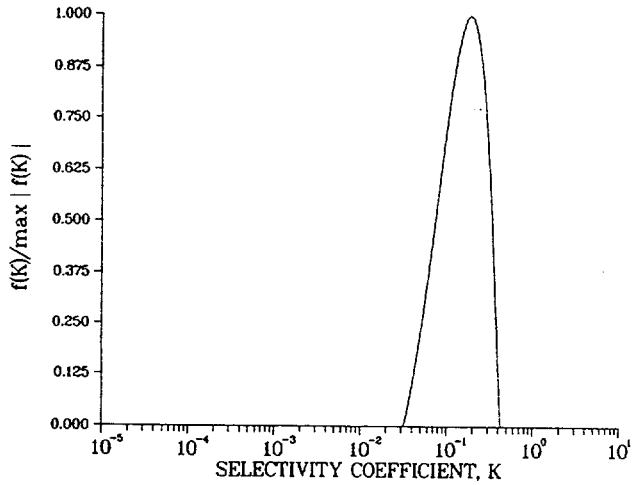


**Figure 5.** Recovered distribution from LiNa–X isotherm.

to the isotherm data, because of the smoothing effect of the $q_2(C_2,K)$ function. The broadening that may be observed in some recovered distributions is obviously an artifact of the numerical method that results from the nature of the function used to determine the optimal smoothing parameter, $\alpha$. Normally, the oversmoothing is accentuated as the indeterminate errors in the data increase. In all cases studied, the areas under the peaks for the recovered distributions reproduce a almost perfectly the areas under the peaks in the actual distributions, as is illustrated in Tables I and II. Although the choice for the optimal smoothing parameter as one-tenth of the BRD $\alpha$ is slightly less conservative than the one suggested by Butler et al.,[17] the nature of $q_2(C_2,K)$ in eq 6 hinders fitting of the noise in the isotherm, and allows the researcher to make a more realistic, yet safe, choice of $\alpha$.

*Experimental Isotherm, Zeolite X.* The method was applied to real isotherm data previously presented by Sherry,[22] who described the exchange of Li cations into the Linde Na–X type of synthetic faujasite. To employ Sherry's values directly, deconvolution was effected by using the mole fraction of $Li^+$ in the solid phase ($q_{Li}/Q$), which amounted to dividing both sides of eq 6 by $Q$ before the method was applied. An indeterminate error of 10% was used to deconvolute Sherry's isotherm, as is illustrated by the magnitude of the error bars in Figure 4. The total concentration was 0.1 N, the temperature was 25 °C, and the ratio of activity coefficients, $\gamma_{Li}/\gamma_{Na}$, was 1.036.[23] Deconvolution was effected with 301 values logarithmically spaced in the interval from $1.0 \times 10^{-5}$ to 10.0. The recovered distribution, shown in Figure 5,

(22) Sherry, H. S. *J. Phys. Chem.* **1966**, *70*, 1158.
(23) Harned, H. S.; Owen, B. B. *The Physical Chemistry of Electrolytic Solutions*; Reinhold: New York, 1958; p 731.

yields a median of 0.22, a mean of 0.21, and a most probable selectivity coefficient of 0.19. The fit obtained by numerical integration of eq 6, using the recovered distribution, is shown in Figure 4. The recovered $f(K)$ fits Sherry's data within the relative indeterminate error estimated. There are two main problems with the application of the method to data obtained from the literature. The first is that the precision of the isotherm data is unknown; consequently, to apply the method, it is necessary to estimate the indeterminate error in the data. The second drawback is that Hanson's criterion for the selection of the data points cannot be applied. Therefore, future work will include the remeasurement of isotherm data with a smaller indeterminate error, followed by deconvolution using Hanson's criterion for the choice of data points.

The recovered distribution shown in Figure 5 cannot be immediately compared to the standard net free energy for the Li–Na exchange previously calculated by Sherry, who employed the method of Gaines and Thomas.[24] Sherry reported a single net standard free energy for the Li–Na exchange, whereas the deconvolution method emphasizes the heterogeneity of the exchange process, which leads to a distribution. More important is the fact that the conversion of selectivity coefficients to equilibrium constants (which yield standard net free energies) necessitates the evaluation of surface activity coefficients that are not easily obtainable. Qualitatively, however, our distribution agrees with previous observations[22,25,26] concerning the endothermicity of the Li–Na exchange in zeolites X and Y from consideration of the large hydration sphere of $Li^+$. Because the distribution of ions over the different zeolite sites is influenced by the affinity of the sites for the ions as well as by the hydration properties of the ions,[27] it is impossible to assign the selectivity coefficients in the recovered distribution to any one process without the aid of other tools such as crystallographic studies and molecular modeling.[28,29]

## Conclusions

The application of the deconvolution method to computer-generated isotherms has demonstrated that the differences in the selectivities for ion exchange caused by structural differences in the ion-exchange sites can be determined from ion-exchange isotherms with realistic random Gaussian errors. The advantage of the deconvolution method is that no assumptions are made about the number of peaks and/or shape of the selectivity coefficient distribution. The peaks observed from deconvoluting an isotherm do not necessarily correspond to different crystallographic sites, but to differences in selectivity that result from steric or Coulombic effects on the ion–site interactions.

An underlying assumption in the use of simultaneous equilibria to describe ion exchange is that the functional form of the concentration dependence of the surface activity coefficients does not cause anomalous peaks in the recovered distribution function. This assumption is supported by both experimental and theoretical evidence[30,31] and by the relatively narrow, nearly Gaussian peak obtained from deconvolution of the Li–Na exchange isotherm for zeolite X.

As was previously noted by Sherry,[22] there are 85 sodium ions in the unit cell of Na–X: 16 in either the sodalite cages or the hexagonal prisms, 32 in the large cavities in the plane of the 6 tetrahedra connecting the supercages and the sodalite cages, and 37 either in crystallographically equivalent sites or in constant motion within the supercage. The number of exchangeable sites in the larger cavities is 81% of the total exchangeable sites. The area under the selectivity distribution curve obtained from deconvolution corresponds to 87% of the cation-exchange capacity. Thus, it is conceivable that the remaining 13% of the Li cations are being excluded from the smaller sodalite cages or hexagonal prisms. The selectivity distribution function showed no evidence of another peak corresponding to Li exchange into the smaller cavities. This observation is consistent with two different rationales. Either the selectivity for the smaller sites is so small that it is impossible to fill those sites at the ionic strength used by Sherry (0.1 N) or the lithium cations cannot enter the sodalite cages for kinetic reasons. The latter possibility is supported by the measurements of Barrer and Falconer,[30] who observed a selectivity coefficient of 0.47 for Li over Na in basic sodalite at a temperature of 85 °C. The fact that there is only one peak in the recovered distribution from deconvolution indicates that the difference in selectivity between lithium and sodium is not very large. This similarity results from the large hydration number of both ions, which would probably make them energetically insensitive to the structure surrounding the large cavities.

The selectivity coefficient of 0.18 read from the flat portion (lithium mole fraction from 0.0 to 0.4) of Sherry's Kielland plot[22] is in good agreement with the value of 0.19 for the most probable selectivity obtained from deconvolution. The nonlinear shape of the Kielland plot at larger lithium mole fractions is consistent with the finite width observed in the selectivity distribution by the authors of this paper. The distribution function recovered by using deconvolution does not show a peak for the lower selectivity sites. Consequently, the recovered distribution cannot be used to apply the method of Gaines and Thomas, which necessitates the extrapolation of the Kielland plot to the end member Li–X.

Because the method of Gaines and Thomas only allows determination of the overall net free energy of exchange, the net free energy for specific sites is currently unobtainable. However, if some reasonable assumptions were made concerning the concentration dependence of surface activity coefficients, the deconvolution of net free energies of exchange for individual sites would be possible. Using probes sensitive to the chemical environment, such as NMR, in conjunction with the deconvolution of isotherms would allow the generation of Kielland plots for individual sites, thus fully characterizing the exchange process.

In addition to zeolites, the deconvolution method could be directly applied to any ion exchanger including polyelectrolytes such as cation- and anion-exchange resins, clays, and macromolecules. The method is not restricted to ion-exchange equilibria. In addition to the aforementioned extension of the method to gas adsorption,[18] it is possible to use deconvolution to study surface adsorption of organics.

The method presented here can only be applied to monovalent ion-exchange isotherms. The reason for this limitation arises from the behavior of higher charge ions during exchange.[32] For instance, divalent cations can combine with monovalent anions in solution to replace a single monovalent cation in a zeolite; the extent to which this process takes place can only be determined experimentally. This dichotomy in the behavior of polyvalent ions complicates the experimental procedures used to obtain isotherm data. The deconvolution of polyvalent ion-exchange isotherms is the subject of a future work.

## Summary

Deconvolution of computer-generated ion-exchange isotherms has been effected by using the method of regularization previously presented by Butler, Reeds, and Dawson. The major drawback of this technique is that the optimal value of the smoothing parameter used for regularization tends to oversmooth and causes broadening of the recovered distribution. Although a criterion to choose the optimal amount of smoothing is vital to prevent the researcher from obtaining more information than the indeterminate error in his data permits, the lack of knowledge about the

(24) Gaines, G. L.; Thomas, H. C. *J. Chem. Phys.* **1953**, *21*, 714.
(25) Barrer, R. M.; Rees, L. V. C.; Shamsuzzoha, M. *J. Inorg. Nucl. Chem.* **1966**, *28*, 629.
(26) Barrer, R. M.; Davies, J. A.; Rees, L. V. C. *J. Inorg. Nucl. Chem.* **1968**, *30*, 3333.
(27) Uytterhoeven, J. B. In *Proceedings of the Sixth International Zeolite Conference*; Olson, D., Bisio, A., Eds.; Butterworths: Trowbridge, England, 1984; p 49.
(28) Wright, P. A.; Thomas, J. M.; Cheetham, A. K.; Nowak, A. K. *Nature (London)* **1985**, *318*, 611.
(29) Ramdas, S.; Thomas, J. M.; Betteridge, P. W.; Cheetham, A. K.; Davies, E K. *Angew. Chem., Int. Ed. Engl.* **1984**, *23*, 671.
(30) Barrer, R. M.; Falconer, J. D. *Proc. R. Soc. London, A* **1956**, *236*, 227.
(31) Kielland, J. *J. Soc. Chem. Ind. London* **1935**, *54*, 232T.
(32) Barrer, R. M. *J. Chem. Soc.* **1950**, 2343.

exact magnitude of the indeterminate errors causes the value of the optimal choice of the smoothing parameter to be larger than its ideal value. Nevertheless, the method has successfully recovered normal and log-normal, unimodal and bimodal selectivity coefficient distributions from isotherm data. Although deconvolution may cause broadened distributions, the areas under the peaks in the recovered distributions from isotherm data with up to 10% indeterminate errors are almost identical with the actual areas. The success of the deconvolution method is most sensitive to the choice of data points and the indeterminate errors in the data. The optimal distribution of the isotherm data points can be determined by using Hanson's criterion.

Sherry's experimentally obtained isotherm describing the exchange of Li cations into the Linde Na–X faujasite has been deconvoluted by using regularization. The recovered distribution fits Sherry's data within the relative indeterminate error estimated to effect deconvolution. Because the distribution of exchanged ions in the solid phase is influenced by the selectivity of sites for the ions as well as the hydration properties of the ions, the selectivity coefficients obtained by deconvolution of ion-exchange isotherms will complement data from crystallographic studies and molecular modeling. Consequently, future work will include correlation of the data obtained by deconvolution with zeolite crystallographic data, NMR data, and modeling of the solvation and exchange processes.

*Acknowledgment.* We thank W. L. Earl, B. R. Erdal, D. L. Bish, and J. H. Hall for helpful discussions. This research has been supported by the Nevada Nuclear Waste Storage Investigations Project, U.S. DOE.

## Appendix

*Computational Procedure.* The numerical problem to be solved is given by eq 11 where the $N + 2$ values of $q_{2_i}^w$ correspond to

$$q_{2_i}^w = w_i q_2(C_{2i}) = \int_D q_2^w(C_{2i},K)\, f(K)\, dK + \epsilon_i \qquad i = 0, ..., N + 1 \quad (11)$$

the weighted experimental measurements of $q_2$ taken at the various concentrations, $C_{2_i}$. It is assumed that each experimentally obtained value is the sum of the integral in eq 11 and an indeterminate error, $\epsilon_i$. Since the exact magnitude of each inndeterminate error is unknown, when an absolute indeterminate error is suspected, $\epsilon_i$ is simply the standard deviation of the isotherm experiment, whereas when a relative indeterminate error is suspected, e.g., 5%, $\epsilon_i$ is a function of the specific experimental value, e.g., 5% $q_2(C_{2_i})$. The weight of each experimental quantity, $w_i$, is a function of the indeterminate error $\epsilon_i$, as shown in eq 12; the function $q_2^w(C_{2_i},K)$, given by eq 13, is directly proportional to $w_i$.

$$w_i = \frac{1}{\epsilon_i}\left[(N+2)\left(\sum_{i=0}^{N+1}\frac{1}{\epsilon_i^2}\right)^{-1}\right]^{1/2} \quad (12)$$

$$q_2^w(C_{2_i},K) = \frac{w_i K Q \gamma_2 C_{2_i}}{C_0\gamma_1 + (K\gamma_2 - \gamma_1)C_{2_i}} \quad (13)$$

In this procedure $\alpha$ is varied systematically and for each fixed $\alpha$ an optimal vector $f(K)$ is found. The optimal $f(K)$ is given by the dot product of $q_2^w(C_2,K)$ and a vector, **V**, which should satisfy eq 14 as closely as computationally feasible. The matrix **U** has $(N + 2) \times (N + 2)$ entries which are given by eq 15, where $D$ is the domain of $q_2^w(C_2,K)\cdot\mathbf{V} > 0$; **I** represents the identity matrix.

$$(\mathbf{U} + \alpha\mathbf{I})\mathbf{V} = q_2^w \quad (14)$$

$$U_{i,j} = \int_D q_2^w(C_{2_i},K) q_2^w(C_{2_j},K)\, dK \quad (15)$$

The optimal **V** is found by minimizing the function $\psi$, given by eq 16, where † denotes the transpose. The first derivative of $\psi$ is given by the vector $\psi'$ and the second derivative is given by the matrix $\psi''$. The algorithm to find the optimal **V** proceeds on the basis of a pure Newton search with the direction, $\delta$, given by eq 19. The search is arbitrarily terminated when the value of $\sigma$, given by eq 20, is less than or equal to $10^{-6}$.

$$\psi = 0.5\mathbf{V}^\dagger(\mathbf{U} + \alpha\mathbf{I})\mathbf{V} - \mathbf{V}\cdot q_2^w \quad (16)$$

$$\psi'_i = \frac{\partial\psi}{\partial V_i} = \sum_{j=0}^{N+1}(\mathbf{U} + \alpha\mathbf{I})_{ij}V_j - q_{2_i}^w \quad (17)$$

$$\psi''_{ij} = \frac{\partial^2\psi}{\partial V_i\,\partial V_j} = (\mathbf{U} + \alpha\mathbf{I})_{ij} \quad (18)$$

$$\delta = (\psi'')^{-1}\psi' \quad (19)$$

$$\sigma = \frac{\|(\mathbf{U} + \alpha\mathbf{I})\mathbf{V} - q_2^w\|}{\|q_2^w\|} \quad (20)$$

In order to find the optimal smoothing parameter, the function $H(\alpha)$ (given by eq 21) is calculated at each given $\alpha$. The optimum value of $\alpha$, according to Butler et al.,[17] corresponds to the minimum of the function $H(\alpha)$.

$$H(\alpha) = q_2^{w\dagger}\mathbf{TUT}q_2^w - q_2^{w\dagger}Tq_2^w + 2\,\|\mathbf{V}\|(N+2)\left(\sum_{i=0}^{N+1}\frac{1}{\epsilon_i^2}\right)^{-1/2} \quad (21)$$

$$\mathbf{T} = (\mathbf{U} + \alpha\mathbf{I})^{-1} \quad (22)$$

The details of the algorithm used for the implementation of the computational procedure follow. The FORTRAN code used to effect the deconvolution of monovalent ion-exchange isotherms is available upon request to the authors.

## Algorithm

1. Set $\alpha_0 = \alpha_{max}$.
2. Calculate $\mathbf{U} + \alpha\mathbf{I}$ assuming $q_2^w(C_2,K)\cdot\mathbf{V} > 0$.
3. Set $\mathbf{V}^0 = \mathbf{T}q_2^w$.
4. Calculate $q_2^w(C_2,K)\cdot\mathbf{V}^0$.
5. Calculate $(\mathbf{U} + \alpha\mathbf{I})$ subject to $q_2^w(C_2,K)\cdot\mathbf{V}^0 > 0$.
6. Calculate **T**, $\psi'(\mathbf{V}^0)$, and $\delta$.
7. Calculate $\psi(\mathbf{V}^0)$.
8. Set $i\mathrm{exp} = 0$.
9. Set $\mathbf{V}^1 = \mathbf{V}^0 - 0.5^{i\mathrm{exp}}\,\delta$.
10. Set $i\mathrm{exp} = i\mathrm{exp} + 1$.
11. Calculate $\psi(\mathbf{V}^1)$.
12. If $\psi(\mathbf{V}^1) > \psi(\mathbf{V}^0)$, go to step 9; else, set $\mathbf{V}^0 = \mathbf{V}^1$.
13. Calculate $q_2^w(C_2,K)\cdot\mathbf{V}^0$.
14. Calculate $\sigma$.
15. If $\sigma > 10^{-6}$, to to step 5.
16. Set $f(K) = \max\{0, q_2^w(C_2, K)\cdot\mathbf{V}^0\}$.
17. If $\alpha_0 = \alpha_{max}$, calculate $H(\alpha_0)$, set $\alpha_1 = \alpha_0 - 0.1\alpha_0$, and go to step 5.
18. Calculate $H(\alpha_1)$.
19. If $\alpha_1 \le \alpha_{min}$, stop.
20. Set $\alpha_0 = \alpha_1$.
21. Set $\alpha_1 = \alpha_0 - 0.1\alpha_0$.
22. Go to step 5.